

MASTER THESIS

DARK MATTER IN SUPERSYMMETRIC
INVERSE-SEESAW MODELS

YANG LIU

SUPERVISOR: PROF. DR. WERNER POROD

UNIVERSITÄT WÜRZBURG, THEORETICAL PHYSICS II

Abstract

The lightest right-handed neutrino in keV range and sneutrino dark matter are studied in two models: the supersymmetric minimal inverse-seesaw model and the B-L supersymmetric standard model *BLSSM*. Numerical calculations show that the first model is excluded for keV range sterile neutrino dark matter if sterile neutrinos are produced by Shi-Fuller mechanism, and sneutrino dark matter is overproduced. The model BLSSM is then studied. In this model the annihilation of the lightest right-handed sneutrinos is mediated by a singlet Higgs and produces lightest sterile neutrinos. This Higgs-funnel can effectively reduce the relic density of sneutrinos. Numerical calculations show that there exists regions in parameter space where the sneutrino relic density is consistent with the astronomical observations and allowed by collider experiments.

Zusammenfassung

In dieser Arbeit werden zwei supersymmetrische Modelle untersucht: zum einen ein Modell beruhend auf einem effektiven minimalen Inverse-Seesaw-Mechanismus, zum anderen das um eine zusätzliche Eichgruppe $U(1)_{B-L}$ erweiterte supersymmetrische Standardmodell *BLSSM*. In diesen Modellen sind sowohl das leichteste rechtshändige Neutrino (mit Masse im keV-Bereich) als auch das leichteste Sneutrino potentialle Kandidaten für dunkle Materie. Die numerischen Ergebnisse zeigen, dass das minimale Inverse-Seesaw-Modell ausgeschlossen ist, wenn die rechtshändigen Neutrinos durch den Shi-Fuller Mechanismus erzeugt werden. Weiterhin ist auch der Beitrag des Sneutrinos zur dunklen Materie zu groß um die beobachtete Dichte erklären zu können. Das Modell ist somit ausgeschlossen, selbst wenn jeweils nur ein Kandidat einen Beitrag zur dunklen Materiedichte liefert.

Im BLSSM gibt es zwei neue Higgsbosonen unter der neuen Eichgruppe $U(1)_{B-L}$, die Singletts unter der SM-Eichgruppe sind. Der Beitrag des Sneutrinos zur dunklen Materiedichte kann durch den Higgs-Funnel mit dem leichtesten Singlett reduziert werden. Numerische Analysen zeigen, dass Bereiche im Parameterraum existieren, in welchen die beobachtete dichte der dunklen Materie durch rechtshändigen Sneutrinos erklärt werden kann. Diese Bereiche sind nicht durch Beschleunigerexperimenten eingeschränkt.

Contents

1	Introduction	3
2	Supersymmetry	5
2.1	Motivation	5
2.2	SUSY Algebra	6
2.2.1	Anti-symmetric (Grassman) Algebra	6
2.2.2	Majorana Spinor	8
2.2.3	Supersymmetry Algebra	9
2.3	Superfield	10
2.3.1	SUSY Transformations	10
2.3.2	Chiral Superfield	11
2.3.3	Vector Superfield	11
2.4	SUSY Invariant Lagrangian	12
2.4.1	Chiral Superfield	12
2.4.2	Vector Superfield	13
2.5	Breaking SUSY	15
2.6	MSSM	16
2.6.1	Higgs Sector	19
2.6.2	Neutralino and Chargino	20
2.6.3	Sfermions	22
3	Neutrino Physics	23
3.1	Neutrino Mixing and Oscillation	23
3.2	Seesaw I Mechanism	26
3.3	Inverse-Seesaw Mechanism	27
4	The Models	28
4.1	Minimal Inverse-Seesaw	28
4.2	Neutrino Interactions	30
4.3	BLSSM	34
5	Dark Matter	37
5.1	Production Mechanism and Relic Density	37
5.2	Detection	42

6	Analytical Calculations of the Decay Widths	44
6.1	Three-body-decay	44
6.2	Total decay width of three-body decay	51
6.3	Loops	52
7	Numerical Results Model I	60
7.1	Neutrino Decay	60
7.2	Sneutrino Relic Density	65
8	Numerical Results Model II	67
9	Conclusion and Outlook	76

1 Introduction

Dark matter DM has long been postulated to explain the non-baryonic missing mass observed in the nearby galaxies. Different objects are suggested to explain the observed relic density. Among them the beyond standard model BSM particles are promising dark matter candidates. Once they are found, it will provide strong signal for new physics. One type of very frequently studied BSM model is supersymmetric models, especially the minimal supersymmetric extension of standard model, the MSSM. The lightest supersymmetric particle LSP is protected by R-parity which makes it the most stable supersymmetric particle, thus neutral LSP is naturally good dark matter candidate.

Another particle that points exactly to new physics is neutrino. As is observed in neutrino experiments (KamLand, Kamiokande etc.), the three standard model SM neutrinos are mixed which can be achieved by assuming neutrinos are massive. Models such as seesaw mechanism provide good explanations of the origin and smallness of neutrino masses, which is usually done by introducing the right-handed neutrinos (also called *sterile neutrinos*) that are missing in SM into neutrino sector. The sterile neutrino interact only weakly and can be another good DM candidate.

In this thesis, sterile neutrino and right-handed sneutrino DM in supersymmetric minimal inverse-seesaw model are first studied. The numerical results show that both scenarios give overproduced dark matter and they are therefore excluded by astronomical observations. The same sectors of B-L supersymmetric standard model $BLSSM$ is then probed where a Higgs funnel is available to reduce the relic density. A second numerical test confirms this assumption and shows that there exist certain regions in parameter space where the relic density can be fine-tuned to fit the observation results.

The contents are structured as follows. In chapter 2 the supersymmetry theory is reviewed. The neutrino physics and mass models are introduced in chapter 3. The models are discussed in chapter 4. Chapter 5 is a brief review of dark matter over the topics that is related to this thesis. After the theory part follows the analytical calculations of the decay processes which is given in chapter 6 and numerical results that are shown in chapter 7 and 8. In the end the conclusion and the outlook is

drawn and discussed in chapter 9.

2 Supersymmetry

This chapter is a review of the basics of supersymmetry theory. The References[28, 4, 11, 13, 31, 2] are used while writing this review. The contents are structured in this way: first the motivation of SUSY is given at the beginning, then mathematical preparations are made which will be useful in the discussion of SUSY algebra in section 2.2.3 and superfield formalism in chapter 2.3. Using the superfield we will see how to construct a SUSY and gauge invariant Lagrangian in section 2.4. The SUSY breaking is briefly discussed in section 2.5, after that the simplest SUSY model *MSSM* is elaborated in 2.6.

Motivation

The *standard model*, *SM* describes the properties and interactions of elementary particles well and successfully, but there still remains some problems that are beyond the scope of SM. First and the most famous one is the *hierarchy problem*, which points out that the Higgs boson in SM will receive large loop corrections that strongly depends on the Planck scale $\sim 10^{18}$ GeV. The Higgs mass in SM is fine-tuned to fit to the electroweak scale, where the fine-tuning precision is about the order 10^{-28} . This is because the Higgs boson mass is not protected by any symmetry in SM. The second problem is the gauge unification problem. Large effort is invested in the past decades to find the *Grand Unified Theory*, *GUT*, which is supposed to unify the three gauge couplings. But this is not achievable within SM. The third problem is related to cosmology. SM fails to give good explanation of baryon asymmetry and to provide good candidates of *Dark Matter*. All these problems SM encountered are indicating that SM must be extended.

It was first pointed out by R. Haag, J.Lopuszański and M. Sohnius that *Supersymmetry*, *SUSY* is the only non-trivial extension of space-time symmetry beyond SM. This symmetry, being able to transform the fermions into bosons and vice versa, guarantees that the particles within one *Supermultiplet* have same masses, which protects the Higgs mass. Even more, it provides a solution to the hierarchy problem.

To look into details how SUSY solves the hierarchy problem, consider the 1-loop corrections of the Higgs mass that arise from coupling to fermions and scalar bosons respectively. The fermion Lagrangian is $-\lambda_f H \bar{f} f$, and the 1-loop correction is [28]

$$\Delta m_H^2 = -\frac{|\lambda_f|^2}{8\pi^2} \Lambda_{UV}^2 + \dots, \quad (2.1.1)$$

where Λ_{UV}^2 is the ultra-violet cut-off in regularization. Similarly one can write down the 1-loop correction of a Higgs couples to the scalar field with Lagrangian equal to $-\lambda_s |H|^2 |S|^2$ [28]:

$$\Delta m_H^2 = \frac{\lambda_s}{16\pi^2} \Lambda_{UV}^2 + \dots \quad (2.1.2)$$

If we compare the two corrections we may notice that the first terms of the two corrections have the same form and opposite signs. They can be cancelled out if a fermion is accompanied with two scalars and the coupling of the fermion and the scalars are the same. This is exactly the case in SUSY, since fermions and bosons within one supermultiplet have the same coupling, same masses and degrees of freedom.

Minimal Supersymmetric Standard Model, MSSM allows gauge coupling unification at the scale 10^{16} GeV, it also provides promising candidates for dark matter, the *Lightest Supersymmetric Particle, LSP*. Being protected by the R-parity of MSSM, the LSP are stable states. Together with the fact that SUSY particles must be heavy, these properties make neutral LSP an ideal candidate for dark matter, specially the cold dark matter, which is favoured by the current standard model of Cosmology, the Λ CDM. All in all, it is worth treating SUSY seriously as the right direction leading to new physics.

SUSY Algebra

Anti-symmetric (Grassman) Algebra

The Grassmann variables are anti-commuting variables, they fulfill the relation:

$$\theta_i \theta_j = -\theta_j \theta_i. \quad (2.2.1)$$

This follows that θ_i^2 and higher orders are vanished in expansions. The integration of Grassmann variables works in the same way as ordinary differentiation. If we define a function f as a function of Grassmann variable θ

$$f(\theta) = f_0 + f_1 \theta, \quad (2.2.2)$$

then the integration and differentiation rules are:

$$\int d\theta f(\theta) = f_1 = \frac{d}{d\theta} f(\theta). \quad (2.2.3)$$

It follows that the following relations also valid:

$$\int d\theta = 0 \quad \int d\theta f(\theta + \theta') = \int d\theta f(\theta) = f_1. \quad (2.2.4)$$

The delta function acting in the integral is defined as:

$$\int d\theta \delta(\theta - \theta') f(\theta) = f(\theta'), \quad (2.2.5)$$

it has the same result as directly replacing the delta function with $\theta - \theta'$, thus we can conclude that

$$\delta(\theta - \theta') = \theta - \theta'. \quad (2.2.6)$$

The Grassmann variable is frequently used in supersymmetry when constructing theories with superspace formalism as superspace coordinates. It is thus important to note the following integration and differentiation rules of Grassmann variables since these will be often encountered when discussing the SUSY Lagrangian and action.

Two Grassman variables θ_α and $\bar{\theta}^{\dot{\alpha}}$ are need for the formalisation in the theory below. If we consider different Grassmann variables, the differentiation rules are:

$$\frac{d\theta_a}{d\theta_b} = \delta_{ab} \quad \frac{d\theta_a}{d\bar{\theta}^b} = 0 \quad \frac{d\bar{\theta}^{\dot{a}}}{d\bar{\theta}^{\dot{b}}} = \delta_{\dot{a}\dot{b}}. \quad (2.2.7)$$

For integration the $d^2\theta$ is defined as

$$d^2\theta = -\frac{1}{4} d\theta^\alpha d\theta^\beta \epsilon_{\alpha\beta} \quad d^2\bar{\theta} = -\frac{1}{4} d\bar{\theta}_{\dot{\alpha}} d\bar{\theta}_{\dot{\beta}} \epsilon^{\dot{\alpha}\dot{\beta}}, \quad (2.2.8)$$

then the integrations with respect to these elements are just

$$\int d^2\theta \theta\theta = 1 \quad \int d^2\bar{\theta} \bar{\theta}\bar{\theta} = 1. \quad (2.2.9)$$

When performing the integrations eq. (2.2.9) to superfields, this is equivalent to take the factor in front of the corresponding superspace coordinates. Also it is worth noticing that the integrals disappear when integrating over total derivatives w.r.t. the superspace coordinates.

Majorana Spinor

Majorana particles are fermions whose anti-particles are themselves. This name was given due to the Italian physicist Ettore Majorana who first proposed this concept in 1937. Absent in the standard model, Majorana particles are now widely studied in different BSM models and they also provide a good explanation to the neutrino masses.

By definition, Majorana spinors means:

$$\psi = \psi^c = C^{-1}\bar{\psi}^T, \quad (2.2.10)$$

where the matrix $C = i\gamma_2\gamma_0$ is the charge conjugation matrix. This condition is called reality/Majorana condition. Satisfying the reality condition, the Majorana field is[30]:

$$\psi(x) = \sum_s \int_p (a_s(p)u_s(p)e^{-ip\cdot x} + a_s^\dagger(p)v_s(p)e^{ip\cdot x}), \quad (2.2.11)$$

with the spinors u, v satisfying:

$$u_s(p) = v_s^c(p). \quad (2.2.12)$$

Recall that the Weyl representation is:

$$\gamma^\mu = \begin{pmatrix} 0 & \sigma^\mu \\ \bar{\sigma}^\mu & 0 \end{pmatrix} \quad \gamma_5 = \begin{pmatrix} -1_2 & 0 \\ 0 & 1_2 \end{pmatrix}, \quad (2.2.13)$$

where $\sigma^\mu = (1_2, \sigma^i)$ with σ^i the Pauli matrices. In Weyl representation the reality condition requires:

$$\psi = \begin{pmatrix} \psi_L \\ \psi_R \end{pmatrix} = C^{-1}\bar{\psi}^T = -i\gamma_2\gamma_0\gamma_0\psi^* = \begin{pmatrix} i\sigma_2\psi_R \\ -i\sigma_2\psi_L \end{pmatrix}. \quad (2.2.14)$$

This means that one can write down a Majorana spinor using only left-handed 2-component spinor with the right-handed part substituted by $-i\sigma_2\psi_L^*$, i.e.

$$\psi_M = \begin{pmatrix} \psi_L \\ -i\sigma_2\psi_L^* \end{pmatrix}. \quad (2.2.15)$$

For 2-spinors, the notation from Bailin and Love[4] are used, where

$$\psi_L = \chi_\alpha \quad \psi_R = \bar{\chi}^{\dot{\alpha}}. \quad (2.2.16)$$

The bar represents the hermitian conjugation of the spinors, which is defined as:

$$(\chi_\alpha)^\dagger = \chi_\alpha^* = \bar{\chi}_{\dot{\alpha}} \quad (\bar{\chi}^{\dot{\alpha}})^\dagger = (\bar{\chi}^{\dot{\alpha}})^* = \chi^\alpha. \quad (2.2.17)$$

The indices can be raised and lowered like Lorentz indices using the matrix ϵ :

$$\begin{aligned}\epsilon_{\alpha\beta} &= \epsilon_{\dot{\alpha}\dot{\beta}} = -i\sigma_2 & \epsilon^{\alpha\beta} &= \epsilon^{\dot{\alpha}\dot{\beta}} = i\sigma_2 \\ \chi^\alpha &= \epsilon^{\alpha\beta}\chi_\beta & \bar{\chi}_{\dot{\alpha}} &= \epsilon_{\dot{\alpha}\dot{\beta}}\bar{\chi}^{\dot{\beta}},\end{aligned}\tag{2.2.18}$$

and note that

$$\chi\chi = \chi^\alpha\chi_\alpha \quad \bar{\chi}\bar{\chi} = \bar{\chi}_{\dot{\alpha}}\bar{\chi}^{\dot{\alpha}}.\tag{2.2.19}$$

With these relations, one can write down the mass part of the Lagrangian density for two component Majorana spinors:

$$\frac{1}{2}M\bar{\psi}_M\psi_M = \frac{1}{2}M(\bar{\chi}\bar{\chi} + \chi\chi).\tag{2.2.20}$$

Supersymmetry Algebra

The supersymmetry algebra can have N sets of generators. The one with $N = 1$ generator is the *supersymmetry algebra*, the rests are called *extended supersymmetry algebras*. Here we only discuss the $N = 1$ scenario, which is also the scenario that MSSM is based on.

The operator P^2 is the Casimir operator, which means that all the states within one irreducible representation share the same mass. The generator \mathcal{Q}_a , also called supercharge, is the conserved charge of supersymmetry, it has the following (anti-)commutation relations[28]:

$$\begin{aligned}\{\mathcal{Q}_\alpha, \mathcal{Q}_\beta\} &= \{\bar{\mathcal{Q}}_\alpha, \bar{\mathcal{Q}}_\beta\} = 0 \\ \{\mathcal{Q}_\alpha, \bar{\mathcal{Q}}_{\dot{\alpha}}\} &= -2\sigma_{\alpha\dot{\alpha}}^\mu P_\mu \\ [\mathcal{Q}_\alpha, P^\mu] &= [\bar{\mathcal{Q}}_{\dot{\alpha}}, P^\mu] = 0.\end{aligned}\tag{2.2.21}$$

When acting on the massless states, only two states maintain the same supersymmetric representation, i.e. $|p, s\rangle$ and $|p, s - \frac{1}{2}\rangle$. These two states form a *supermultiplet* which contains one complex boson and one Weyl fermion, it is a irreducible representation of supersymmetry. When $s = \frac{1}{2}$, this is called *chiral supermultiplet*. Chiral supermultiplet contains one fermion and its Supersymmetric partner, *sfermion*, which is a spin-0 particle and the name was added with a s because it is a scalar boson. Similarly for $s = 1$ the two states form a *vector supermultiplet*, it contains a vector boson and a fermion which is called (take photon as an example) *Photino*, the *-ino* added at the end is used to mark the fermionic superpartners. Note that, when $s = 2$ the two fields are graviton and gravitino.

The above discussion is only for massless states, the case for massive states is a little bit more complicated. It generates spin- $s + \frac{1}{2}$, s and $s - \frac{1}{2}$ mutiplets and

contains totally $2(2s + 1)$ fermions(bosons)[4].

Superfield

Supersymmetry can be more conveniently expressed in superfield formalism, where component fields from supermultiplets are written compactly as an object called *superfield*, *sfield*, which is defined on the extended space, the *superspace*, with space-time coordinate x^μ and four additional anti-symmetric coordinates θ^α and $\bar{\theta}_{\dot{\alpha}}$. The chiral and the vector superfields are obtained by acquiring certain constraints on the general superfield. A general form of superfield is[28]:

$$S(x, \theta, \bar{\theta}) = a + \theta\xi + \bar{\theta}\bar{\xi} + \theta\theta b + \bar{\theta}\bar{\theta}c + \bar{\theta}\bar{\sigma}^\mu\theta v_\mu + \bar{\theta}\bar{\theta}\theta\eta + \theta\theta\bar{\theta}\bar{\theta}\zeta + \theta\theta\bar{\theta}\bar{\theta}d, \quad (2.3.1)$$

every component in front of the superspace coordinates is a function of x^μ , all the higher terms vanished because the coordinates θ and $\bar{\theta}$ are anti-symmetric.

SUSY Transformations

The SUSY transformations on superspace are defined as[28]:

$$\hat{Q}_\alpha = i\frac{\partial}{\partial\theta^\alpha} - (\sigma^\mu\bar{\theta})_\alpha\partial_\mu \quad \hat{Q}^{\dagger\dot{\alpha}} = i\frac{\partial}{\partial\bar{\theta}^{\dot{\alpha}}} - (\bar{\sigma}^\mu\theta)^{\dot{\alpha}}\partial_\mu. \quad (2.3.2)$$

These operators also follow the same (anti-)commutation relations as eq. (2.2.21). When acting on a superfield, the SUSY transformations can be viewed as translations in superspace[28]:

$$\begin{aligned} \sqrt{2}\delta_\epsilon S &= -i(\epsilon\hat{Q} + \bar{\epsilon}\hat{Q}^\dagger)S \\ &= S(x^\mu + i\epsilon\sigma^\mu\bar{\theta} + i\bar{\epsilon}\bar{\sigma}^\mu\theta, \theta + \epsilon, \bar{\theta} + \bar{\epsilon}) - S(x^\mu, \theta, \bar{\theta}). \end{aligned} \quad (2.3.3)$$

Under SUSY transformations, every component of the field S also transforms differently. The complete transformations can be found in [28]. Note that the d -term is a space-time total derivative under SUSY transformations.

The SUSY chiral covariant derivatives are defined as:

$$\begin{aligned} D_\alpha &= \frac{\partial}{\partial\theta^\alpha} - i(\sigma^\mu\bar{\theta})_\alpha\partial_\mu & D^\alpha &= -\frac{\partial}{\partial\theta_\alpha} + i(\bar{\theta}\bar{\sigma}^\mu)^\alpha\partial_\mu, \\ \bar{D}^{\dot{\alpha}} &= \frac{\partial}{\partial\bar{\theta}^{\dot{\alpha}}} - i(\bar{\sigma}^\mu\theta)^{\dot{\alpha}}\partial_\mu & \bar{D}_{\dot{\alpha}} &= -\frac{\partial}{\partial\bar{\theta}^{\dot{\alpha}}} + i(\theta\sigma^\mu)_{\dot{\alpha}}\partial_\mu, \end{aligned} \quad (2.3.4)$$

they anti-commute with SUSY transformations therefore are useful in defining the chiral superfield.

Chiral Superfield

The chiral superfield is defined using chiral covariant derivative:

$$\bar{D}_{\dot{\alpha}}\Phi = 0. \quad (2.3.5)$$

To solve this equation, define

$$y^{\mu} = x^{\mu} + i\bar{\theta}\bar{\sigma}^{\mu}\theta, \quad (2.3.6)$$

using the new coordinate y^{μ} the chiral covariant derivatives are

$$\begin{aligned} D_{\alpha} &= \frac{\partial}{\partial\theta^{\alpha}} - 2i(\sigma^{\mu}\bar{\theta})_{\alpha}\frac{\partial}{\partial y^{\mu}} & D^{\alpha} &= -\frac{\partial}{\partial\theta_{\alpha}} + 2i(\bar{\theta}\bar{\sigma}^{\mu})^{\alpha}\frac{\partial}{\partial y^{\mu}} \\ \bar{D}^{\dot{\alpha}} &= \frac{\partial}{\partial\bar{\theta}^{\dot{\alpha}}} & \bar{D}_{\dot{\alpha}} &= -\frac{\partial}{\partial\bar{\theta}_{\dot{\alpha}}}. \end{aligned} \quad (2.3.7)$$

This means, when applying the condition eq. (2.3.5) to the general superfield eq. (2.3.1), the terms involving $\bar{\theta}$ don't contribute, the general chiral superfield is therefore:

$$\begin{aligned} \Phi &= \phi(y) + \sqrt{2}\theta\psi(y) + \theta\theta F(y) \\ &= \phi(x) + i\bar{\theta}\bar{\sigma}^{\mu}\theta\partial_{\mu}\phi(x) + \frac{1}{4}\theta\theta\bar{\theta}\bar{\theta}\partial_{\mu}\partial^{\mu}\phi(x) + \sqrt{2}\theta\psi(x) \\ &\quad - \frac{i}{\sqrt{2}}\theta\theta\bar{\theta}\bar{\sigma}^{\mu}\partial_{\mu}\psi(x) + \theta\theta F(x). \end{aligned} \quad (2.3.8)$$

This superfield contains one scalar ϕ , one fermion ψ and one auxiliary field F . Note that F is total space-time derivative and it plays an important role in spontaneous SUSY breaking. The multiplication of chiral superfields results in chiral superfields, this enables the superpotential formalisation.

Vector Superfield

The condition imposed on vector superfield is

$$V = V^*. \quad (2.3.9)$$

Define the following component fields with the ones in eq. (2.3.1)

$$\eta_{\alpha} = \lambda_{\alpha} - \frac{i}{2}(\sigma^{\mu}\partial_{\mu}\bar{\xi})_{\alpha} \quad v_{\mu} = A_{\mu} \quad d = \frac{1}{2}D + \frac{1}{4}\partial_{\mu}\partial^{\mu}a, \quad (2.3.10)$$

the vector superfield is then

$$\begin{aligned}
 V = & a + \theta\xi + \bar{\theta}\bar{\xi} + \theta\theta b + \bar{\theta}\bar{\theta}b^* + \bar{\theta}\bar{\sigma}^\mu\theta A_\mu + \bar{\theta}\bar{\theta}\theta(\lambda - \frac{i}{2}\sigma^\mu\partial_\mu\bar{\xi}) \\
 & + \theta\theta\bar{\theta}(\bar{\lambda} - \frac{i}{2}\bar{\sigma}^\mu\partial_\mu\xi) + \theta\theta\bar{\theta}\bar{\theta}(\frac{1}{2}D + \frac{1}{4}\partial_\mu\partial^\mu a).
 \end{aligned}
 \tag{2.3.11}$$

One thing to point out here is, when performing SUSY transformations to the vector fields, the D -term transforms into a total derivative of space-time coordinate x^μ , and it is the factor of the element $\theta\theta\bar{\theta}\bar{\theta}$. This fact will be used when deriving the SUSY invariant Lagrangian. Also one can show that, the component fields a , b and ξ can be gauged away when considering the *Wess-Zumino gauge*, where the vector superfield reduces to

$$V = \bar{\theta}\bar{\sigma}^\mu\theta A_\mu + \bar{\theta}\bar{\theta}\theta\lambda + \theta\theta\bar{\theta}\bar{\lambda} + \frac{1}{2}\theta\theta\bar{\theta}\bar{\theta}D.
 \tag{2.3.12}$$

This contains a vector field A_μ , a fermion field λ and an auxiliary field D , where D is implemented under the same consideration as the F field, and it will also be important in SUSY breaking.

SUSY Invariant Lagrangian

The action \mathcal{S}

$$\mathcal{S} = \int dx^\mu \int d^2\theta d^2\bar{\theta} S(x^\mu, \theta, \bar{\theta}),
 \tag{2.4.1}$$

is automatically invariant under SUSY transformations for any superfield $S(x^\mu, \theta, \bar{\theta})$ that is a combination of chiral and vector superfields. For SUSY invariant Lagrangian \mathcal{L} the terms that satisfy this condition are the F -term of chiral superfield and D -term of vector superfield. Note that the F -term must be added with an hermitian conjugation part to guarantee that the action is real.

Chiral Superfield

To construct kinetic and interaction terms between chiral component fields, consider the terms $\Phi_i^*\Phi_j$, $\Phi_i\Phi_j$ and $\Phi_i\Phi_j\Phi_k$, take the D - or F -terms respectively. The $\Phi_j^*\Phi_j$ transforms as a vector field, the corresponding D -term is

$$[\Phi_j^*\Phi_j]_D = F_j^*F_j - \partial^\mu\phi_j^*\partial_\mu\phi_j + i\bar{\psi}_j\bar{\sigma}^\mu\partial_\mu\psi_j + \text{total derivative}.
 \tag{2.4.2}$$

The other two combinations can be summarised as the *superpotential* W

$$W = \frac{1}{2}M^{ij}\Phi_i\Phi_j + \frac{1}{6}y^{ijk}\Phi_i\Phi_j\Phi_k. \quad (2.4.3)$$

Since the multiplication of chiral fields results in chiral field, the F -term of the Superpotential is then the part that contributes to the Lagrangian. Sum up the terms in the above discussion, the Lagrangian of chiral supermultiplets is

$$\mathcal{L}_{chiral} = [\Phi_j^*\Phi_j]_D + [W]_F + h.c.. \quad (2.4.4)$$

The auxiliary field F can be eliminated using its equation of motion, it shows that

$$F_j = -W_j^* = \frac{\delta W^*}{\delta \Phi_j}. \quad (2.4.5)$$

The scalar potential of the chiral superfield is:

$$\mathcal{V}(\phi, \phi^*) = F^*F. \quad (2.4.6)$$

Vector Superfield

In the abelian case, the field strength superfields are defined as

$$\mathcal{W}_\alpha = -\frac{1}{4}\bar{D}\bar{D}D_\alpha V \quad \bar{\mathcal{W}}_{\dot{\alpha}} = -\frac{1}{4}DD\bar{D}_{\dot{\alpha}}V. \quad (2.4.7)$$

Express the vector sfield in Wess-Zumino gauge (see eq.2.3.12) with coordinate y^μ :

$$V(y^\mu, \theta, \bar{\theta}) = \bar{\theta}\bar{\sigma}^\mu\theta A_\mu + \bar{\theta}\bar{\theta}\theta\lambda + \theta\theta\bar{\theta}\bar{\lambda} + \frac{1}{2}\theta\theta\bar{\theta}\bar{\theta}D, \quad (2.4.8)$$

the field strength sfield is then

$$\mathcal{W}_\alpha(y, \theta, \bar{\theta}) = \lambda_\alpha + \theta_\alpha D + \frac{i}{2}(\sigma^\mu\bar{\sigma}^\nu\theta)_\alpha F_{\mu\nu} + i\theta\theta(\sigma^\mu\partial_\mu\bar{\lambda})_\alpha. \quad (2.4.9)$$

The F -term of $[\mathcal{W}\mathcal{W}]_F$ contributes to the Lagrangian:

$$\int d^4x \mathcal{L} = \int d^4x \frac{1}{4}[\mathcal{W}\mathcal{W}]_F + h.c. = \int d^4x \left[\frac{1}{2}D^2 + i\bar{\lambda}\bar{\sigma}^\mu\partial_\mu\lambda - \frac{1}{4}F^{\mu\nu}F_{\mu\nu} \right]. \quad (2.4.10)$$

Now add the $U(1)$ gauge transformation

$$\Phi_j \rightarrow e^{2igq_j\Omega}\Phi_j \quad \Phi^{*j} \rightarrow \Phi^{*j}e^{-2igq_j\Omega^*}, \quad (2.4.11)$$

where Ω is a non-dynamical chiral superfield and q_j is the $U(1)$ charge. The chiral interaction term $[\Phi^{*j}\Phi_j]_D$ is not gauge invariant, this is compensated by adjusting the Lagrangian to

$$[\Phi^{*j}e^{2gq_jV}\Phi_j]_D, \quad (2.4.12)$$

with the vector sfield V transforms as

$$V \rightarrow V + i(\Omega^* - \Omega) \quad (2.4.13)$$

under the general gauge transformation. In Wess-Zumino gauge

$$[\Phi^{*j}e^{2gq_jV}\Phi_j]_D = F^{*j}F_j - \nabla_\mu\phi^{*j}\nabla^\mu\phi_j + i\bar{\psi}^j\bar{\sigma}^\mu\nabla_\mu\psi_j - \sqrt{2}gq_j(\psi^{*j}\psi_j\lambda + \bar{\lambda}\bar{\psi}^j\phi_j) + gq_j\phi^{*j}\phi_j D. \quad (2.4.14)$$

The Lagrangian for Abelian gauge theory is then

$$\mathcal{L}_{Abelian} = [\Phi^{*j}e^{2gq_jV}\Phi_j]_D + (W_F(\Phi_j) + h.c.) + \frac{1}{4}([\mathcal{W}\mathcal{W}]_F + h.c.). \quad (2.4.15)$$

The same procedure can be generalised to non-Abelian gauge theory as

$$\begin{aligned} \Phi_j &\rightarrow e^{2ig\Omega^a T^a} \Phi_j = (e^{i\Omega})_j^k \Phi_k \\ \mathcal{L} &= [\Phi^{*j}(e^{2gT^a V^a})_j^k \Phi_k]_D = [\Phi^{*j}(e^V)_j^k \Phi_k]_D, \end{aligned} \quad (2.4.16)$$

where T^a is the generator of the gauge group and g is the gauge coupling. Substitute V with V_{WZ} , this term is

$$\begin{aligned} [\Phi^{*j}(e^V)_j^k \Phi_k]_D &= F^{*j}F_j - \nabla_\mu\phi^{*j}\nabla^\mu\phi_j + i\bar{\psi}^j\bar{\sigma}^\mu\nabla_\mu\psi_j \\ &\quad - \sqrt{2}g(\psi^{*j}T^a\psi_j)\lambda - \sqrt{2}f\bar{\lambda}(\bar{\psi}^j T^a\phi_j) + g(\phi^{*j}T^a\phi_j)D^a. \end{aligned} \quad (2.4.17)$$

The non-Abelian field strength sfield is defined as

$$\mathcal{W}_\alpha = -\frac{1}{4}\bar{D}\bar{D}(e^{-V}D_\alpha e^V) = 2gT^a\mathcal{W}_\alpha^a, \quad (2.4.18)$$

where \mathcal{W}_α^a is the field strength sfield in adjoint representation. The SUSY and gauge invariant quantity is

$$\begin{aligned} \frac{1}{2g^2} \text{Tr}[\mathcal{W}^\alpha\mathcal{W}_\alpha]_F &= [\mathcal{W}^{a\alpha}\mathcal{W}_\alpha^a]_F \\ &= D^a D^a + 2i\lambda^a\sigma^\mu\nabla_\mu\bar{\lambda}^a - \frac{1}{2}F^{a\mu\nu}F_{\mu\nu}^a + \frac{i}{4}\epsilon^{\mu\nu\rho\sigma}F_{\mu\nu}^a F_{\rho\sigma}^a, \end{aligned} \quad (2.4.19)$$

and the Lagrangian for non-Abelian gauge theory is

$$\mathcal{L} = \frac{1}{4}[\mathcal{W}^{a\alpha}\mathcal{W}_{a\alpha}]_F + h.c. + [\Phi^{*j}(e^{2gT^a V^a})_j^k \Phi_k]_D + (W_F + h.c.), \quad (2.4.20)$$

with the scalar potential

$$\mathcal{V}(\phi_j, \phi^{*j}) = F^{*j}F_j + \frac{1}{2}\sum_a D^a D^a = W^{*j}W_j + \frac{1}{2}\sum_a g^2(\phi^{*j}T^a\phi_j)^2. \quad (2.4.21)$$

Breaking SUSY

The preservation of SUSY indicates SM particles have same masses as their superpartners. Since such particles are until now not detected in any experiments, SUSY must be broken. From first intuition one would expect that SUSY gets broken spontaneously as what was happened in SM. This is equivalent to say that the vacuum is not invariant under SUSY transformation, $Q|0\rangle \neq 0$. Since the Hamiltonian takes the form

$$H = \frac{1}{4}(Q_1\bar{Q}_1 + \bar{Q}_1Q_1 + Q_2\bar{Q}_2 + \bar{Q}_2Q_2), \quad (2.5.1)$$

this means that the vacuum should have positive energy $\langle 0|H|0\rangle > 0$. Therefore the SUSY scalar potential in eq. (2.4.21) should also have positive value in vacuum. This demands that the F and/or D field should acquire a non-vanishing value in the vacuum. These two scenarios are called *F-type SUSY breaking* and *D-type SUSY breaking* respectively.

To break SUSY with F field, one can add a linear term to the superpotential. This method was first brought up by L. O’Raifeartaigh where the superpotential is taken to be [1]

$$W = m\phi_1\phi_2 + g\phi_2(\phi_3^2 - M^2). \quad (2.5.2)$$

The F_i field equals to $(\frac{\partial W}{\partial \phi_i})^\dagger$, substitute W with eq. (2.5.2) one gets

$$F_1^\dagger = -m\phi_3 \quad F_2^\dagger = -g(\phi_3^2 - M^2) \quad F_3^\dagger = -m\phi_1 - 2\phi_2\phi_3. \quad (2.5.3)$$

F_1 and F_2 can not be zero simultaneously, SUSY is thus broken if one choose

$$\langle 0|F_1|0\rangle = \langle 0|F_3|0\rangle = 0, \quad \langle 0|F_2|0\rangle \neq 0. \quad (2.5.4)$$

F_2 can be chosen freely and this is called a *flat direction* of the scalar potential, and breaking SUSY results in a massless fermion called *goldstino*. This scenario seems to provide a good opportunity to break SUSY spontaneously, but it dose have its only defect. According to *Nelson-Seiberg theorem*, if the SUSY is broken by the F field, then the R -symmetry should also be broken otherwise the gaugino masses can not be explained. If R -symmetry is broken, then a *R-axion* will be generated which is in turn also hard to find in experiments. This theorem rules out F -type SUSY breaking in the visible sector.

The same trick can be done to the gauge sector by adding a linear part κD to the Lagrangian, as indicated by P. Fayet and J. Iliopoulos, where D contains only the

$U(1)$ part, we then arrive at the D -type SUSY breaking. The D part of scalar potential becomes[28]

$$V = \kappa D - \frac{1}{2}D^2 - gD \sum_i q_i |\phi_i|^2. \quad (2.5.5)$$

The equation of motion of the D field is therefore

$$D = \kappa - g \sum_i q_i |\phi_i|^2. \quad (2.5.6)$$

Suppose that the scalars ϕ_i have the masses m_i , the scalar potential then becomes

$$V = \sum_i |m_i|^2 |\phi_i|^2 + \frac{1}{2}(\kappa - g \sum_i q_i |\phi_i|^2)^2, \quad (2.5.7)$$

this term clearly can not be zero, SUSY is therefore broken. But just like the F -type breaking, this mechanism is also not applicable for visible sector. First this mechanism only applies to the abelian gauge field, for non-abelian gauge theories a Fayet-Iliopoulos term is not allowed. Second if the $U(1)$ gauge breaks in this way, it then indicates that the scalar will get mass $|m_i|^2 - gq_i\kappa$ where their fermion partners will have mass $|m_i|^2$, i.e. the SUSY scalars will be lighter than their fermion partners, which is against the experimental observations[28]. In MSSM, the SUSY breaking terms are added to the Lagrangian density to break SUSY explicitly. Also the breaking terms are taken to break SUSY *softly*, which means they will break SUSY without introducing any more divergences and thus MSSM still solves the hierarchy problem[3]. The explicit form of soft breaking terms will be given in the chapter 2.6.

MSSM

Minimal Supersymmetric Standard Model, MSSM expands the particles of SM into supermultiplets which contain both SM particles and their superpartners, and the Higgs sector is also extended to two Higgs doublets and Higgsino doublets. To illustrate this idea in detail, take the left-handed lepton of the first generation as an example

$$\begin{aligned} l_1 &= \begin{pmatrix} \nu_e \\ e \end{pmatrix} e_R^* \\ \tilde{l}_1 &= \begin{pmatrix} \tilde{\nu}_e \\ \tilde{e} \end{pmatrix} \tilde{e}_R^*, \end{aligned} \quad (2.6.1)$$

the supermultiplet L and E contains

$$\begin{aligned}\hat{L}_1 &= \begin{pmatrix} L_{\nu_e} \\ L_e \end{pmatrix}, & \hat{\tilde{E}}_1, \\ L_{\nu_e} \supset (\nu_e, \tilde{\nu}_e), & L_e \supset (e, \tilde{e}), & \hat{\tilde{E}}_1 \supset (e_R, \tilde{e}_R).\end{aligned}\tag{2.6.2}$$

The same form is applied to every other family of lepton and quark.

In SM, the charge conjugate higgs field ϕ^c couples to the up-type right chiral quarks to give them masses, but this is not the case in MSSM, since such a field will not be allowed. In stead, two higgs doublets are needed in MSSM to couple to the down- and up-type quarks:

$$H_d = \begin{pmatrix} H_d^0 \\ H_d^- \end{pmatrix} \quad H_u = \begin{pmatrix} H_u^+ \\ H_u^0 \end{pmatrix},\tag{2.6.3}$$

and two higgsino doublets

$$\tilde{H}_d = \begin{pmatrix} \tilde{H}_d^0 \\ \tilde{H}_d^- \end{pmatrix} \quad \tilde{H}_u = \begin{pmatrix} \tilde{H}_u^+ \\ \tilde{H}_u^0 \end{pmatrix}\tag{2.6.4}$$

are employed to solve the chiral anomaly. Also the SM gauge bosons have superpartners, called *gauginos*. As we will see in the coming section, after higgs bosons acquired vevs, the gauginos and higgsinos will mix to form *charginos* and *neutralinos*. The full superfield content is given in table 2.1.

The MSSM Lagrangian density is

$$\mathcal{L}_{MSSM} = \mathcal{L}_{SUSY} + \mathcal{L}_{SOFT},\tag{2.6.5}$$

where

$$\begin{aligned}\mathcal{L}_{SOFT} &= -\frac{1}{2}(M_3\tilde{g}^\alpha \cdot \tilde{g}^\alpha + M_2\tilde{W}^\alpha \cdot \tilde{W}^\alpha + M_1\tilde{B} \cdot \tilde{B} + h.c.) \\ &\quad - m_{\tilde{Q}_{ij}}^2 \tilde{Q}_i^\dagger \cdot \tilde{Q}_j - m_{\tilde{U}_{ij}}^2 \tilde{U}_i^\dagger \tilde{U}_j - m_{\tilde{D}_{ij}}^2 \tilde{D}_i^\dagger \tilde{D}_j \\ &\quad - m_{\tilde{L}_{ij}}^2 \tilde{L}_i^\dagger \cdot \tilde{L}_j - m_{\tilde{E}_{ij}}^2 \tilde{E}_i^\dagger \tilde{E}_j \\ &\quad - m_{H_u}^2 H_u^\dagger \cdot H_u - m_{H_d}^2 H_d^\dagger \cdot H_d - (bH_u \cdot H_d + h.c.) \\ &\quad - a_u^{ij} \tilde{U}_i \tilde{Q}_j \cdot H_u + a_d^{ij} \tilde{D}_i \tilde{Q}_j \cdot H_d + a_e^{ij} \tilde{E}_i \tilde{L}_j \cdot H_d + h.c.\end{aligned}\tag{2.6.6}$$

is the soft breaking terms added to break SUSY explicitly by introducing gaugino masses $M_{1,2,3}$, scalar squared-masses m^2 and the scalar coupling a^{ij} . The SUSY part is[11]

$$\mathcal{L}_{SUSY} = \mathcal{L}_g + \mathcal{L}_M + \mathcal{L}_H,\tag{2.6.7}$$

Names		spin 0	spin $\frac{1}{2}$	$(SU(3)_c, SU(2)_L, U(1)_y)$
squarks, quarks	\hat{Q}	$(\tilde{u}_L, \tilde{d}_L)$	(u_L, d_L)	$(3, 2, \frac{1}{6})$
	\hat{U}	\tilde{u}_R^*	u_R^\dagger	$(\bar{3}, 1, -\frac{2}{3})$
	\hat{D}	\tilde{d}_R^*	u_R^\dagger	$(\bar{3}, 1, \frac{1}{3})$
sleptons, leptons	\hat{L}	$(\tilde{\nu}, \tilde{e}_L)$	(ν, e_L)	$(1, 2, -\frac{1}{2})$
	\hat{E}	\tilde{e}_R^*	e_R^\dagger	$(1, 1, 1)$
	Higgs, higgsinos	\hat{H}_u	(H_u^+, H_u^0)	$(\tilde{H}_u^+, \tilde{H}_u^0)$
\hat{H}_d		(H_d^0, H_d^-)	$(\tilde{H}_d^0, \tilde{H}_d^-)$	$(1, 2, -\frac{1}{2})$
Names		spin $\frac{1}{2}$	spin 1	$(SU(3)_c, SU(2)_L, U(1)_y)$
gluino, gluon		\hat{g}	\hat{g}	$(8, 1, 0)$
winos, W bosons		\hat{W}^\pm, \hat{W}^0	\hat{W}^\pm, \hat{W}^0	$(1, 3, 0)$
binos, B bosons		\hat{B}^0	\hat{B}^0	$(1, 1, 0)$

Table 2.1: The full superfield content in MSSM. Table taken from P. Martin *A Supersymmetry Primer*[28]. Hat $\hat{}$ marks supermultiplets.

where

$$\mathcal{L}_g = \frac{1}{4} \int d^2\theta (\hat{W}_g^{a\alpha} \hat{W}_{g\alpha}^a + \vec{\hat{W}}_W^\alpha \cdot \vec{\hat{W}}_{W\alpha} + \hat{W}_Y^\alpha \hat{W}_{Y\alpha}) + h.c. \quad (2.6.8)$$

is the pure gauge part of the Lagrangian density, W represent three field strength superfields of each gauge group.

$$\begin{aligned} \mathcal{L}_M = \int d^4\theta \left[\hat{L}_i^\dagger e^{(g_2 \hat{V}^W \cdot \vec{\tau} - g_Y \hat{V}^Y)} \hat{L}_i + \hat{E}_i^\dagger e^{2g_Y \hat{V}^Y} \hat{E}_i + \hat{U}_i^\dagger e^{(g_s \hat{V}_g^\alpha \lambda^\alpha - \frac{4}{3} g_Y \hat{V}^Y)} \hat{U}_i \right. \\ \left. + \hat{D}_i^\dagger e^{(g_s \hat{V}_g^\alpha \lambda^\alpha + \frac{2}{3} g_Y \hat{V}^Y)} \hat{D}_i + \hat{Q}_i^\dagger e^{(g_s \hat{V}_g^\alpha \lambda^\alpha + 2g_2 \hat{V}^W \cdot \vec{\tau} + \frac{1}{3} g_Y \hat{V}^Y)} \hat{Q}_i \right] \end{aligned} \quad (2.6.9)$$

is the matter part of the Lagrangian density. The V is the gauge supermultiplet, λ^a represents 8 Gell-Mann matrices, τ is the usual Pauli matrices. The Higgs part is

$$\mathcal{L}_H = \int d^4\theta \left[\sum_p \hat{H}_p^\dagger e^{(g_2 \hat{V}^W \cdot \vec{\tau} + (-1)^n g_Y \hat{V}^Y)} \hat{H}_p + W_{MSSM} \delta^{(2)}(\bar{\theta}) + W_{MSSM}^\dagger \delta^{(2)}(\theta) \right] \quad (2.6.10)$$

where p is the summation over up- ($n=2$) and down-type ($n=1$) Higgs doublets. The superpotential is

$$W_{MSSM} = \mu \hat{H}_u \cdot \hat{H}_d - \hat{U} Y_u \hat{Q} \cdot \hat{H}_u - \hat{D} Y_d \hat{Q} \cdot \hat{H}_d - \hat{E} Y_e \hat{L} \cdot \hat{H}_d. \quad (2.6.11)$$

Higgs Sector

The scalar potential of Higgs sector is

$$V_H = \frac{1}{8}(g_Y^2 + g_2^2)(|H_u|^2 - |H_d|^2)^2 + \frac{g_2^2}{2}|H_u^\dagger H_d|^2 + |\mu|^2(|H_u|^2 + |H_d|^2) + m_1^2|H_d|^2 + m_2^2|H_u|^2 + (B_\mu H_u \cdot H_d + h.c.). \quad (2.6.12)$$

By letting Higgs acquire vevs

$$\langle H_d \rangle = \frac{1}{\sqrt{2}} \begin{pmatrix} v_1 \\ 0 \end{pmatrix} \quad \langle H_u \rangle = \frac{1}{\sqrt{2}} \begin{pmatrix} 0 \\ v_2 \end{pmatrix}, \quad (2.6.13)$$

the electroweak symmetry will be broken spontaneously. The expressions of W and Z bosons are altered due to the two Higgs doublets as

$$M_W = \frac{g_2}{2}(v_1^2 + v_2^2)^{\frac{1}{2}}, \quad M_Z = \frac{(g_2^2 + g_Y^2)^{\frac{1}{2}}}{2}(v_1^2 + v_2^2)^{\frac{1}{2}}, \quad (2.6.14)$$

which means the two vevs v_1 and v_2 combine into the SM vev v

$$v = \sqrt{v_1^2 + v_2^2} \approx 246 \text{ GeV}. \quad (2.6.15)$$

The parameter $\tan \beta$ is then introduced to parameterise the two vevs

$$\tan \beta \equiv \frac{v_2}{v_1}, \quad (2.6.16)$$

and the β is within the range $[0, \frac{\pi}{2}]$ if one requires the two vevs to be positive.

Setting the vevs from eq. (2.6.13) into eq. (2.6.12) and requiring the scalar potential to take minimum at this point, one can solve out the expressions for Higgs soft mass parameters

$$\begin{aligned} m_1^2 &= B_\mu \tan \beta - \frac{1}{8}(g_Y^2 + g_2^2)(v_1^2 - v_2^2) \\ m_2^2 &= B_\mu \tan \beta + \frac{1}{8}(g_Y^2 + g_2^2)(v_1^2 - v_2^2). \end{aligned} \quad (2.6.17)$$

Now consider the Higgs masses, they can be calculated using the equations

$$V_H^{(2)} = \frac{1}{2}m_{lm}^2 \phi_l \phi_m \quad m_m^2 = \left\langle \frac{\partial^2 V_H}{\partial \phi_l \partial \phi_m} \right\rangle. \quad (2.6.18)$$

The Higgs can be sort into *CP-odd (imaginary neutral)*, *CP-even (real neutral)* and *charged Higgs*. To calculate the masses, the general idea is to write all the mass terms in a combined form $\Phi \mathcal{M} \Phi$ and rotate the field Φ into mass basis by

diagonalize the mass matrix \mathcal{M} . The explicit steps are omitted here, only the results as given in the following:

CP-odd Higgs

Diagonalization results in one massless neutral Goldstone Boson G , which will be absorbed by the Z boson, and one neutral CP-odd Higgs boson A , also called *Pseudoscalar*. The masses are

$$m_{G^0}^2 = 0 \quad m_A^2 = \frac{2B_\mu}{\sin 2\beta}. \quad (2.6.19)$$

CP-even Higgs

Diagonalize the mass matrix one gets two neutral CP even Higgs bosons h and H with masses

$$m_{H,h}^2 = \frac{1}{2}[m_A^2 + M_Z^2 \pm \{(m_A^2 + M_Z^2)^2 - 4M_Z^2 m_A^2 \cos^2 2\beta\}^{\frac{1}{2}}], \quad (2.6.20)$$

the masses are taken to be $m_h < m_H$.

Charged Higgs

Diagonalization results in two massless Goldstone Bosons G^\pm that will be eaten by W^\pm and two massive charged Higgs H^\pm , the masses are

$$m_{G^\pm}^2 = 0 \quad m_{H^\pm}^2 = \left(\frac{B_\mu}{v_1 v_2} + \frac{1}{4}g_2^2\right)(v_1^2 + v_2^2). \quad (2.6.21)$$

Neutralino and Chargino

After spontaneous symmetry breaking, the electroweak gauginos λ_1 and λ_2 (or *winos* W_1 and W_2) mixed with the charged higgsinos and this allows one to rewrite the mass Lagrangian density into the form

$$-\mathcal{L}_{MASS}^c = (\psi^-)^T M \psi^+ + h.c., \quad (2.6.22)$$

where

$$\begin{aligned} \psi^+ &= \begin{pmatrix} \lambda^+ \\ \tilde{H}_u^+ \end{pmatrix}, & \psi^- &= \begin{pmatrix} \lambda^- \\ \tilde{H}_d^- \end{pmatrix}, \\ \lambda^\pm &= \frac{1}{\sqrt{2}}(\lambda_1 \mp i\lambda_2). \end{aligned} \quad (2.6.23)$$

The mass matrix M is diagonalized with unitary matrices U and V

$$U^* M V^{-1} = M_c^D, \quad (2.6.24)$$

these two matrices rotate the fields ψ^\pm into mass basis

$$\chi_k^+ = V_{km} \psi_m^+ \quad \chi_k^- = U_{km} \psi_m^-, \quad (2.6.25)$$

which are called charginos. The matrices U and V diagonalize the hermitian matrices $M M^\dagger$ and $M^\dagger M$ respectively. After diagonalization, the eigenvalues of the squared masses are

$$\begin{aligned} \tilde{M}_{2,1}^2 = \frac{1}{2} \left[|M_2^2| + |\mu^2| + 2M_W^2 \pm \{ (|M_2^2| - |\mu^2|)^2 \right. \\ \left. + 4M_W^4 \cos^2 2\beta + 4M_W^2 (|M_2^2| + |\mu^2| + 2 \operatorname{Re}(M_2 \mu) \sin 2\beta) \}^{\frac{1}{2}} \right]. \end{aligned} \quad (2.6.26)$$

Similarly, the neutral gauginos λ_0 and λ_3 (or *Bino* and *Wino*) and higgsinos can be defined in a vector

$$(\psi^0)^T \equiv (\lambda_0, \lambda_3, \tilde{H}_d^1, \tilde{H}_u^2), \quad (2.6.27)$$

this allows us to write the mass term Lagrangian density as

$$\mathcal{L}_{MASS}^n = -\frac{1}{2} (\psi^0)^T M^n \psi^0 + h.c., \quad (2.6.28)$$

the mass matrix M^n is

$$M^n = \begin{pmatrix} M_1 & 0 & -M_Z c_\beta s_W & M_Z s_\beta s_W \\ 0 & M_2 & M_Z c_\beta c_w & -M_Z s_\beta c_w \\ -M_Z c_\beta s_W & M_Z c_\beta c_w & 0 & -\mu \\ M_Z s_\beta s_W & -M_Z s_\beta c_w & -\mu & 0 \end{pmatrix}, \quad (2.6.29)$$

where c, s represent \cos and \sin , β is defined by eq. (2.6.16) and $c_w = \cos \theta_w$ with θ_w the Weinberg angle. As usual, rotate the fields into mass basis using the unitary matrix Z diagonalizes the mass matrix M^n :

$$\begin{aligned} \chi_l^0 &= Z_{ln} \psi_n^0 \\ M_D &= Z^* M^n Z^{-1}. \end{aligned} \quad (2.6.30)$$

The detailed expressions of matrix Z and mass eigenstates are omitted here and note that they are at best to be solved numerically. But one can still get some general ideas about the masses purely using the matrix eq. (2.6.29). If the parameters take the values $|\mu| \gg |M_{1,2}| \gg |M_z|$, then the light neutralinos will be mainly bino and wino like while the heavy two will be higgsino like neutralinos. If the hierarchy is reversed, the light neutralinos will be mainly higgsino like and the heavy ones will be wino like.

Sfermions

For the sfermion sector¹ one can also define a 6 component vector just as in the chargino and neutralino case, where

$$\tilde{f} = \begin{pmatrix} \tilde{f}_L \\ \tilde{f}_R \end{pmatrix} \quad (2.6.31)$$

for each fermion family. The Lagrangian density is then

$$- \mathcal{L}_{\tilde{f}} = \sum_{\tilde{f}} \tilde{f}^\dagger M_{\tilde{f}}^2 \tilde{f}, \quad (2.6.32)$$

where the squared mass matrix

$$M_{\tilde{f}}^2 = \begin{pmatrix} M_{LL}^2 & M_{LR}^2 \\ M_{RL}^2 & M_{RR}^2 \end{pmatrix} \quad (2.6.33)$$

contains the left-right mixing parts. Diagonalizing this matrix employs the unitary matrix W

$$\tilde{f}_M = W^{\tilde{f}} \tilde{f}, \quad M_D^{\tilde{f}} = W^{\tilde{f}} M_{\tilde{f}}^2 W^{\tilde{f}\dagger}, \quad (2.6.34)$$

this is equivalent to say

$$\tilde{f}_{iL} = W_{is}^{\tilde{f}} \tilde{f}_{M,s} \quad \tilde{f}_{iR} = W_{i+3,s}^{\tilde{f}} \tilde{f}_{M,s}. \quad (2.6.35)$$

In the end, there is still one important parity of MSSM need to be mentioned, the so called *R-Parity* or *matter parity*

$$P_R = (-1)^{3(B-L)+2s} \quad P_M = (-1)^{3(B-L)}, \quad (2.6.36)$$

where B and L are the baryon and lepton number and s is the spin of the particle. MSSM postulated that R-parity is conserved and assigned $P_R = -1$ for all the sparticles and $P_R = +1$ for the rests. Since R-parity is conserved, it means that there exists a *lightest supersymmetric particle*, *LSP*. All the sparticles will finally decay into the LSP and it is the most stable sparticle in MSSM. This property makes neutral LSP a natural good candidate for dark matter. The details of dark matter will be reviewed in chapter 5.

¹The scalar potential and Lagrangian density of the sfermion sector is omitted here, one can easily find thorough discussions in many textbooks, for example[11]

3 Neutrino Physics

Neutrino was first postulated by Wolfgang Pauli in 1930 when he tried to explain the energy conservation problem of the β decay. Enrico Fermi was then the first one that wrote down the interaction for β decay using the neutrinos. This happens to open a new area of particle physics called weak interaction, especially after the 70s where more and more particles are found which confirmed the theories that predicted them. We now know the fundamental particles are well described by the standard model of particle physics. Even though addressed to be "standard", it still fails to explain many problems properly, for example those related to the neutrinos.

One problem comes from the astronomical observations. Neutrinos are emitted from the Sun when Hydrogen fuse to Helium, mainly through a process called pp-chain[30]. The neutrino flux from the Sun was first measured by the experiment "Homestake" and it was found out that the measured flux is about only one third of the predicted value. A successful explanation states that neutrinos are massive particles, the flavor eigenstates are mixtures of mass eigenstates.

The main purpose of this chapter is to review basic ideas of neutrino mixing and neutrino mass. The neutrino mixing mechanism and neutrino oscillation for three flavor left-handed neutrinos are reviewed in section 3.1, and the seesaw mechanism is introduced in section 3.2. The references used in this review are [30, 34, 25, 16].

Neutrino Mixing and Oscillation

The mixing matrix of 3 flavor neutrinos, also called PMNS-matrix (Pontecorvo-Maki-Nakagawa-Sakata), takes the same form as the CKM matrix except with additional Majorana phase terms. The PMNS matrix is:

$$PMNS = \begin{pmatrix} 1 & 0 & 0 \\ 0 & c_{23} & s_{23} \\ 0 & -s_{23} & c_{23} \end{pmatrix} \begin{pmatrix} c_{13} & 0 & s_{13}e^{-i\delta} \\ 0 & 1 & 0 \\ -s_{13}e^{i\delta} & 0 & c_{13} \end{pmatrix} \begin{pmatrix} c_{12} & s_{12} & 0 \\ -s_{12} & c_{12} & 0 \\ 0 & 0 & 1 \end{pmatrix} \begin{pmatrix} e^{i\beta_1} & 0 & 0 \\ 0 & e^{i\beta_2} & 0 \\ 0 & 0 & 1 \end{pmatrix}, \tag{3.1.1}$$

where c_{23} and s_{23} represent $\cos\theta_{23}$ and $\sin\theta_{23}$, θ_{ij} is the mixing angle between neutrino flavors i and j . δ is the Dirac phase, when $\delta \neq n\pi$, $n = 0, \pm 1, \pm 2, \dots$

CP is violated. $\beta_{1,2}$ are the Majorana phases, they can be determined through neutrinoless double beta decay once the process is observed.

Since the flavor basis is a mixture of mass basis, an electron neutrino can constantly evolve into other flavors like muon and taon neutrinos. Quantum mechanically, we can write the neutrino of flavor j at the time t as:

$$|\nu_j(t)\rangle = \sum_a e^{-iE_a t} U_{ja} |\nu_a\rangle, \quad (3.1.2)$$

with the index a marking the mass eigenstates. The probability of finding neutrino of flavor j at the time t is then:

$$\begin{aligned} P_{\nu_{j'} \rightarrow \nu_j} &= |\langle \nu_{j'} | \nu_j(t) \rangle|^2 \\ &= \sum_{ab} \left| U_{j'a}^* U_{ja} U_{j'b} U_{jb}^* e^{-i(E_b - E_a)t} \right|. \end{aligned} \quad (3.1.3)$$

For relativistic neutrinos, the energy can be approximated by

$$E_j \approx |\vec{p}| + \frac{m_j^2}{2|\vec{p}|}, \quad (3.1.4)$$

the probability thus has the form

$$P \sim \sum_{ab} \left| U_{j'a}^* U_{ja} U_{j'b} U_{jb}^* \exp \left\{ -i \frac{\Delta m_{ab}^2}{2|\vec{p}|} L \right\} \right|, \quad (3.1.5)$$

where

$$\Delta m_{ab}^2 = m_a^2 - m_b^2, \quad (3.1.6)$$

and the time t is substituted with the Length L/c in natural unit because the probability is hard to track with time, the travelled length of neutrino is clearly more easy to control. Many experiments, for example solar and atmospheric neutrino oscillation, only measure mixing between two neutrinos. In this case, the mixing matrix components in eq. (3.1.5) is equal to $\sin^2 \theta_{ab}$.

The mixing angles and mass differences are determined through different processes. The 23 part is measured by atmospheric experiments (KamLand, (Super)KamioKande) and long baseline reactor experiments, 12 is measured by solar neutrinos and 13 is measured by the short baseline reactor experiments. Note that only the mass differences instead of the masses are measured, which leads to two mass hierarchies, i.e. normal ($m_1 < m_2 \ll m_3$) and inverted hierarchy ($m_3 \ll m_2 < m_1$). This hierarchy is until now not settled, but there has been an

indication showing the preference on normal hierarchy[14]. The probability can be measured by disappearance or appearance experiments. The exponential part of eq. (3.1.5) donates the oscillation. Current values are listed in table 3.1.

Parameter	Value	Comment
$\sin^2 \theta_{12}$	$0.307^{+0.013}_{-0.012}$	KamLAND+global solar; 3ν
$\sin^2 \theta_{23}$	$0.421^{+0.033}_{-0.025}$	Inverted ordering, quadrant I
	$0.592^{+0.023}_{-0.030}$	Inverted ordering, quadrant II
	$0.417^{+0.025}_{-0.028}$	Normal ordering, quadrant I
	$0.597^{+0.024}_{-0.030}$	Normal ordering, quadrant I
$\sin^2 \theta_{13}$	$(2.12 \pm 0.08) \cdot 10^{-2}$	
$\Delta m_{21}^2 (10^{-5} eV^2)$	7.53 ± 0.18	KamLAND+global+SBL+accelerator; 3ν
$\Delta m_{32}^2 (10^{-3} eV^2)$	-2.56 ± 0.04	Inverted mass hierarchy
	2.51 ± 0.05	Normal mass hierarchy

Table 3.1: The current PDG results on neutrino parameters[21]. In the comment column lists the relevent data sources, SBL is the abbreviation of short baseline reactor. The data are averaged by the author of [21] if no resource is shown.

Note that the eq. (3.1.5) only works for stable neutrinos propagating in the vacuum. Neutrinos can also decay into light neutrinos and interact with matter. In these two scenarios the possibilities take different forms with respect to eq. (3.1.5).

Neutrino mixing solves most of the puzzles but it also has anomalies, like the large mass difference measured from the LSND experiment where $\Delta m^2 = m_3^2 - \frac{m_2^2 + m_1^2}{2} \sim 1eV^2$ [16]. Also the absent of right-chirality in neutrino sector motives the right-handed neutrinos (also called *Sterile Neutrinos*), which are considered to interact only through gravitation. Their masses, depend on the exact model, can be several orders heavier than the active neutrinos. This property contains rich phenomenological consequences, such as explaining the dark matter, the evolution of the Universe and also the lightness of active neutrino mass. The mass model that involves sterile neutrinos is called *seesaw mechanism* as will be elaborated in the next section.

Seesaw I Mechanism

In this model right-handed neutrinos ν_{RS} are added to the SM fermions and the related Majorana mass terms is (in 4-spinor form):

$$\frac{1}{2}\bar{\nu}_R^c M_R \nu_R \quad (3.2.1)$$

and the Dirac mass term:

$$m_D \bar{\nu}_L \nu_R. \quad (3.2.2)$$

The neutrino mass part of the Lagrangian is then:

$$\mathcal{L}_{\nu \text{ mass}} = \frac{1}{2}\bar{\nu}_R^c M_R \nu_R - m_D \bar{\nu}_L \nu_R + h.c.. \quad (3.2.3)$$

This Lagrangian can be written in a compact form with neutrino mass matrix M if we define a basis

$$\nu = (\nu_L, \nu_R^c)^T, \quad (3.2.4)$$

the Lagrangian is then:

$$\mathcal{L}_{\nu \text{ mass}} = \frac{1}{2}\bar{\nu} M \nu, \quad (3.2.5)$$

with M defined as:

$$M = \begin{pmatrix} 0 & m_D \\ m_D^T & M_R \end{pmatrix}. \quad (3.2.6)$$

This matrix can be diagonalized by an orthogonal 6×6 matrix U . Take one generation of neutrinos as an example, the matrices M_R and m_D reduce to numbers, this yields two mass eigenvalues:

$$|m_{1,2}| = \frac{1}{2}(\sqrt{M_R^2 + 4m_D^2} \mp M_R). \quad (3.2.7)$$

The Majorana mass is not bounded by any constraints. This allows one to choose the Majorana mass to be much larger than the Dirac mass. When applying the relation $M_R \gg m_D$ to the mass eigenvalues in eq. (3.2.7), one can show that the two masses reduce to:

$$m_1 = \frac{m_D^2}{M_R}, \quad m_2 = M_R + \frac{m_D^2}{M_R} \sim M_R. \quad (3.2.8)$$

Raising Majorana mass will reduce m_1 and raise m_2 and vice versa, this explains the name "seesaw".

Inverse-Seesaw Mechanism

By adding a $U(1)$ gauge non-singlet right-handed neutrino S ¹ to the SM/MSSM Seesaw I Lagrangian, after electroweak symmetry breaking the neutrinos have the mass matrix[29]

$$M_\nu = \begin{pmatrix} 0 & m_D & 0 \\ m_D & 0 & M_R \\ 0 & M_R & M_S \end{pmatrix} \quad (3.3.1)$$

in the basis (ν_L, ν_R^c, S) , where m_D is the Dirac mass of $\nu_L \nu_R^c$, M_R is the Dirac mass of $\nu_R^c S$ and M_S is the Majorana mass of singlet S . This matrix has the eigenvalues

$$m_1 = \frac{m_D^2 M_S}{M_R^2}, \quad m_{2,3} = \frac{1}{2} [M_S \pm (M_S^2 + r M_R^2)^{1/2}], \quad (3.3.2)$$

where m_1 is the lightest neutrino mass. Since $m_D = Y_\nu \langle v \rangle$, $m_1 = \frac{(Y_\nu \langle V \rangle)^2 M_S}{M_R^2}$, while keeping M_R constant, one can get a relative big Yukawa coupling by setting the M_S to a small value without changing the neutrino mass m_1 . This fact can help achieving a large Yukawa for the measurements and maintain the small neutrino mass as indicated by the experiments.

¹This can also be realised by adding a vector-like gauge singlet fermion $N = N_R + N_L$ to the SM Lagrangian[26].

4 The Models

Minimal Inverse-Seesaw

The first studied model is the one reported in [9], which is MSSM with additional right-handed neutrino superfield that contains right-handed neutrinos and sneutrinos. The superpotential is

$$\mathcal{W} = \mathcal{W}_{MSSM} + \frac{1}{2}(M_R)_{ij}\hat{\nu}_{R,i}\hat{\nu}_{R,j} + (Y_\nu)_{ij}\hat{L}_i \cdot \hat{H}_u\hat{\nu}_{R,j}, \quad (4.1.1)$$

and the corresponding soft breaking terms are

$$\mathcal{V}^{soft} = \mathcal{V}_{MSSM}^{soft} + (m_{\tilde{\nu}_R}^2)_{ij}\tilde{\nu}_{R,i}^*\tilde{\nu}_{R,j} + \frac{1}{2}(B_{\tilde{\nu}})_{ij}\tilde{\nu}_{R,i}\tilde{\nu}_{R,j} + (T)_{ij}\tilde{L}_i \cdot H_u\tilde{\nu}_{R,j}. \quad (4.1.2)$$

The neutrino masses are explained by the seesaw I model, and the neutrino mixing matrix is parametrized by a *Casas-Ibarra* like parameterization:

$$U_{6 \times 6}^T = \begin{pmatrix} U_{al} & U_{ah} \\ U_{sl} & U_{sh} \end{pmatrix} \quad (4.1.3)$$

for $a = e, \mu, \tau$ and $s = s_1, s_2, s_3$, and the blocks are:

$$\begin{aligned} U_{al} &= U_{PMNS}H, & U_{ah} &= iU_{PMNS}Hm_l^{\frac{1}{2}}R^\dagger M_h^{-\frac{1}{2}}, \\ U_{sl} &= i\bar{H}M_h^{-\frac{1}{2}}Rm_l^{\frac{1}{2}}, & U_{sh} &= \bar{H}R^\dagger M_h^{-\frac{1}{2}}, \end{aligned} \quad (4.1.4)$$

with $m_l = \text{diag}(m_1, m_2, m_3)$ and $M_R = \text{diag}(M_4, M_5, M_6)$ for the light and heavy neutrino masses.

The U_{PMNS} matrix is defined in eq. (3.1.1), H and R are parametrized as:

$$\begin{aligned} H &= (I + m_l^{\frac{1}{2}}R^\dagger M_h^{-1}Rm_l^{\frac{1}{2}})^{-\frac{1}{2}}, \\ \bar{H} &= (I + M_h^{-\frac{1}{2}}Rm_lR^\dagger M_h^{-\frac{1}{2}})^{-\frac{1}{2}}, \end{aligned} \quad (4.1.5)$$

$$R = \begin{pmatrix} 1 & & \\ & c_{56} & s_{56} \\ & -s_{56} & c_{56} \end{pmatrix} \begin{pmatrix} c_{46} & s_{46} \\ & 1 \\ -s_{46} & c_{46} \end{pmatrix} \begin{pmatrix} c_{45} & s_{45} \\ -s_{45} & c_{45} \\ & & 1 \end{pmatrix}, \quad (4.1.6)$$

where $c_{ij} = \cos \theta'_{ij}$ and $\theta'_{ij} \rho_{ij} + i\gamma_{ij}$ are the mixing angles in this 6×6 mixing matrix. The sine and cosine of this angle are

$$\begin{aligned}\sin(\rho_{ij} + i\gamma_{ij}) &= \sin \rho_{ij} \cosh \gamma_{ij} + i(\cos \rho_{ij} \sinh \gamma_{ij}) \\ \cos(\rho_{ij} + i\gamma_{ij}) &= \cos \rho_{ij} \cosh \gamma_{ij} - i(\sin \rho_{ij} \sinh \gamma_{ij}).\end{aligned}\quad (4.1.7)$$

With these parametrizations, the Yukawa coupling and the mass matrix for right-handed neutrinos are:

$$\begin{aligned}Y_\nu &= -i \frac{\sqrt{2}}{v_u} U_{PMNS}^* H^* m_l^{\frac{1}{2}} (m_l R^\dagger + R^T M_h) M_h^{-\frac{1}{2}} \bar{H} \\ M_R &= \bar{H}^* M_h^{\frac{1}{2}} (I - M_h^{-1} R^* m_l^2 R^\dagger M_h^{-1}) M_h^{\frac{1}{2}} \bar{H}.\end{aligned}\quad (4.1.8)$$

From the above equation one can see that the Yukawa coupling can be enhanced exponentially by changing γ , i.e. the matrix R , without varying the neutrino masses, which is similar to the inverse-seesaw scenario. This model is in this sense "minimal inverse-seesaw".

For the use in numerical test the neutrino mass matrix is given here[9]:

$$M_{\bar{\nu}}^2 = \begin{pmatrix} M_{RR}^2 & M_{RI}^2 \\ M_{IR}^2 & M_{II}^2 \end{pmatrix}, \quad (4.1.9)$$

where

$$\begin{aligned}M_{RR}^2 &= \begin{pmatrix} m_{\bar{L}}^2 + \frac{1}{2} m_Z^2 \cos 2\beta + \frac{1}{2} v_u^2 Y_\nu Y_\nu^\dagger & \text{Re} \left[\frac{v_u}{\sqrt{2}} (T_\nu + Y_\nu M_R^\dagger - \mu^* Y_\nu \cot \beta) \right] \\ \text{Re} \left[\frac{v_u}{\sqrt{2}} (T_\nu^T + M_R^\dagger Y_\nu^T - \mu^* Y_\nu^T \cot \beta) \right] & m_{\bar{\nu}_R}^2 + M_R^\dagger M_R + \frac{1}{2} v_u^2 Y_\nu^\dagger Y_\nu + \text{Re}(B_{\bar{\nu}}) \end{pmatrix} \\ M_{II}^2 &= \begin{pmatrix} m_{\bar{L}}^2 + \frac{1}{2} m_Z^2 \cos 2\beta + \frac{1}{2} v_u^2 Y_\nu Y_\nu^\dagger & \text{Re} \left[\frac{v_u}{\sqrt{2}} (T_\nu - Y_\nu M_R^\dagger - \mu^* Y_\nu \cot \beta) \right] \\ \text{Re} \left[\frac{v_u}{\sqrt{2}} (T_\nu^T - M_R^\dagger Y_\nu^T - \mu^* Y_\nu^T \cot \beta) \right] & m_{\bar{\nu}_R}^2 + M_R^\dagger M_R + \frac{1}{2} v_u^2 Y_\nu^\dagger Y_\nu - \text{Re}(B_{\bar{\nu}}) \end{pmatrix} \\ M_{RI}^2 &= \begin{pmatrix} 0 & \text{Im} \left[\frac{v_u}{\sqrt{2}} (T_\nu + Y_\nu M_R^\dagger + \mu^* Y_\nu \cot \beta) \right] \\ -\text{Im} \left[\frac{v_u}{\sqrt{2}} (T_\nu^T + M_R^\dagger Y_\nu^T - \mu^* Y_\nu^T \cot \beta) \right] & -\text{Im}(B_{\bar{\nu}}) \end{pmatrix} \\ &= (M_{IR}^2)^T\end{aligned}\quad (4.1.10)$$

Neutrino Interactions

Notations

The neutrinos are Majorana particles, the spinors are written as:

$$\nu = \begin{pmatrix} \nu_{2,L\alpha} \\ \bar{\nu}_{2,R}^{\dot{\alpha}} \end{pmatrix} \quad \bar{\nu}_{2,R}^{\dot{\alpha}} = (i\sigma_2 \nu_{2,R}^*)^{\dot{\alpha}} \quad \nu_{2,L\alpha}^\dagger = \bar{\nu}_{2,L\dot{\alpha}}, \quad (4.2.1)$$

indices α and $\dot{\alpha}$ are raised and lowered by the matrices $\epsilon^{\alpha\beta} = -i\sigma_2$ and $\epsilon_{\dot{\alpha}\dot{\beta}} = i\sigma_2$. The neutrino mixing matrix is defined as:

$$\nu_{2,L\alpha} = \sum_j U_{ja}^* \nu_{2,Mj} \quad \bar{\nu}_{2,R\alpha} = \sum_j U_{j,a+3} \bar{\nu}_{2,Mj}, \quad (4.2.2)$$

here "M" marks the mass basis. The other mixing matrices are:

$$\begin{aligned} \tilde{l} : \quad \tilde{l}_{L,i} &= \sum_j R_{ji}^* \tilde{l}_j, \quad \bar{\tilde{l}}_{R,i} = \sum_j R_{j,i+3} \bar{\tilde{l}}_j \\ H^\pm : \quad H_d^- &= \sum_j Z_{j1}^+ H_j^-, \quad H_u^+ = \sum_j Z_{j2}^+ H_j^+. \end{aligned} \quad (4.2.3)$$

Via Z Boson

The lagrangian is:

$$\mathcal{L} = \frac{-g}{2 \cos \theta_w} Z_\mu \sum_{a=1}^3 \bar{\nu}_a \gamma^\mu P_L \nu_a, \quad (4.2.4)$$

to derive the Feynman rule of this interaction, we first write the 4-spinor Lagrangian

$$\mathcal{L} \sim \bar{\nu}_a \gamma^\mu P_L \nu_a \quad (4.2.5)$$

into 2-spinor form, this part of Lagrangian is then:

$$\begin{aligned} & \bar{\nu}_a \gamma^\mu P_L \nu_a \\ &= (\nu_{2,L\alpha}^\dagger, 0) \begin{pmatrix} \bar{\sigma}^\mu & 0 \\ 0 & \sigma^\mu \end{pmatrix} \begin{pmatrix} \nu_{2,L\alpha} \\ 0 \end{pmatrix} \\ &= \bar{\nu}_{2,L\dot{\alpha}} (\bar{\sigma}^\mu)^{\dot{\alpha}\alpha} \nu_{2,L\alpha}. \end{aligned} \quad (4.2.6)$$

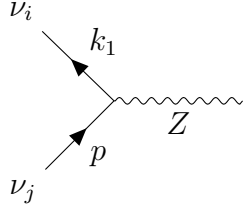
Rotate the neutrinos from flavor basis to mass basis and notice that[4]:

$$\bar{\nu}_{2,j\dot{\alpha}} (\bar{\sigma}^\mu)^{\dot{\alpha}\alpha} \nu_{2,i\alpha} = -\nu_{2,i}^\alpha (\sigma^\mu)_{\alpha\dot{\alpha}} \bar{\nu}_{2,j}^{\dot{\alpha}}, \quad (4.2.7)$$

we get:

$$\begin{aligned}
 \mathcal{L} &= \frac{-g}{2 \cos \theta_w} Z_\mu \sum_{a=1}^3 \sum_{i=1}^6 \sum_{j=1}^6 U_{ja} U_{ia}^* \bar{\nu}_{2,j} \bar{\sigma}^\mu \nu_{2,i} \\
 &= \frac{-g}{2 \cos \theta_w} Z_\mu \sum_{a=1}^3 \sum_{i=1}^6 \sum_{j=1}^6 \frac{1}{2} [U_{ja} U_{ia}^* \underbrace{\bar{\nu}_{2,j} \bar{\sigma}^\mu \nu_{2,i}}_{\bar{\nu}_j \gamma^\mu P_L \nu_i} - U_{ia} U_{ja}^* \underbrace{\bar{\nu}_{2,j} \bar{\sigma}^\mu \nu_{2,i}}_{\bar{\nu}_j \gamma^\mu P_R \nu_i}],
 \end{aligned} \tag{4.2.8}$$

therefore the vertex of the Feynman diagram is¹:



$$\begin{aligned}
 &= -\frac{i}{2 \cos \theta_w} g \sum_{a=1}^3 U_{ja} U_{ia}^* (\gamma_\mu P_L) + \frac{i}{2 \cos \theta_w} g \sum_{a=1}^3 U_{ia} U_{ja}^* (\gamma_\mu P_R) \\
 &= -\frac{i}{2 \cos \theta_w} g \gamma_\mu \left[\underbrace{\sum_{a=1}^3 U_{ja} U_{ia}^* P_L}_{o_{ji}} - \underbrace{\sum_{a=1}^3 U_{ia} U_{ja}^* P_R}_{o_{ji}^*} \right] \\
 &= -\frac{i}{2 \cos \theta_w} g \gamma_\mu [o_{ji} P_L - o_{ji}^* P_R].
 \end{aligned} \tag{4.2.9}$$

Via Higgs Boson

Write the spinors in 2-component form and rotate to the mass basis, the Lagrangian is then:

¹Here the whole vertex is multiplied by 2, because the neutrinos are Majorana particles, see [24], Appendix C and D.

$$\begin{aligned}
 -\mathcal{L} &= \sum_{m,n=1}^3 (Y_\nu)_{mn}^* \bar{\nu}_{4,Lm} H_u^0 \nu_{4,Rn} + h.c \\
 &= \sum_{m,n=1}^3 (Y_\nu)_{mn}^* \bar{\nu}_{2,Lm} H_u^0 \bar{\nu}_{2,Rn} + h.c \\
 &= \sum_{m,n=1}^3 \sum_{i=1}^6 \sum_{j=1}^6 (Y_\nu)_{mn}^* U_{im} \bar{\nu}_i H_u^0 U_{j(n+3)} \bar{\nu}_j + h.c \\
 &= \sum_{m,n=1}^3 \sum_{i=1}^6 \sum_{j=1}^6 \frac{1}{2} (Y_\nu)_{mn}^* [U_{im} U_{j(n+3)} \bar{\nu}_i \bar{\nu}_j H_u^0 + U_{jm} U_{i(n+3)} \underbrace{\bar{\nu}_j \bar{\nu}_i}_{=\bar{\nu}_i \bar{\nu}_j} H_u^0] + h.c.
 \end{aligned} \tag{4.2.10}$$

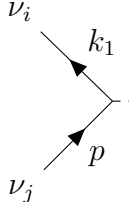
Noticing that $\bar{\nu}_i \bar{\nu}_j = \bar{\nu}_{4,i} P_R \nu_{4,j}$, write out the hermitian conjugate term explicitly, the final Lagrangian is then:

$$\begin{aligned}
 -\mathcal{L} &= \sum_{m,n=1}^3 \sum_{i=1}^6 \sum_{j=1}^6 \frac{1}{2} [(Y_\nu)_{mn}^* (U_{im} U_{j(n+3)} + U_{jm} U_{i(n+3)}) \bar{\nu}_{4,i} P_R \nu_{4,j} H_u^0 \\
 &\quad + (Y_\nu)_{mn} (U_{im}^* U_{j(n+3)}^* + U_{jm}^* U_{i(n+3)}^*) \bar{\nu}_{4,i} P_L \nu_{4,j} H_u^{0*}].
 \end{aligned} \tag{4.2.11}$$

H_u^0 is equal to[28]

$$H_u^0 = v_u + \frac{1}{\sqrt{2}} [\cos \alpha h^0 + \sin \alpha H^0 + i(\sin \beta G^0 + \cos \beta A^0)], \tag{4.2.12}$$

one can show that when the produced masses are much smaller than the initial mass, the G^0 part disappears. The vertex of the Feynman diagram is:



$$\begin{aligned}
 &= -\frac{i}{\sqrt{2}} \sum_{m,n=1}^3 [(Y_\nu)_{mn}^* (U_{im} U_{j(n+3)} + U_{jm} U_{i(n+3)}) P_R \eta_f \\
 &\quad + (Y_\nu)_{mn} (U_{im}^* U_{j(n+3)}^* + U_{jm}^* U_{i(n+3)}^*) P_L \eta_f^*] \\
 &= -\frac{i}{\sqrt{2}} (X_{ij} P_R + X_{ij}^* P_L),
 \end{aligned} \tag{4.2.13}$$

with X_{ij} defined as:

$$X_{ij} = \sum_{m,n=1}^3 (Y_\nu)_{mn}^* \eta_f (U_{im} U_{j(n+3)} + U_{jm} U_{i(n+3)}). \tag{4.2.14}$$

For simplicity, the different factors in front of the higgs parts are substituted with a combined notation η_f :

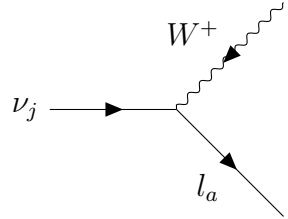
$$\eta_f = \begin{cases} \sin \alpha & f = h^0 \\ \cos \alpha & f = H^0 \\ i \cos \beta & f = A^0. \end{cases} \quad (4.2.15)$$

$W+l$

The Lagrangian is:

$$\begin{aligned} \mathcal{L} &= \sum_{a=1}^3 \frac{g}{\sqrt{2}} \bar{\nu}_a \gamma^\mu P_L W_\mu^+ l_a \\ &= \sum_{a=1}^3 \sum_{m=1}^3 \sum_{j=1}^6 \frac{g}{\sqrt{2}} \bar{\nu}_j U_{ja} U_{L,ma}^{e*} \gamma^\mu P_L W_\mu^+ l_m, \end{aligned} \quad (4.2.16)$$

and the corresponding vertex of the Feynman diagram is:



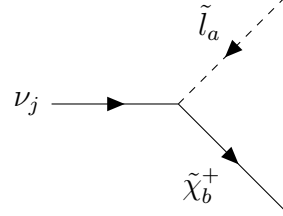
$$= -i \frac{2g}{\sqrt{2}} \bar{\nu}_j U_{ja} U_{L,ma}^{e*} \gamma^\mu P_L. \quad (4.2.17)$$

$\tilde{\chi}^+ \tilde{l}$

In mass basis the lagrangian is:

$$\begin{aligned} \mathcal{L} &= \sum_{j=1}^6 \sum_{a=1}^6 \sum_{b=1}^2 \bar{\nu}_j (d_{jab}^L P_L + d_{jab}^R P_R) \tilde{l}_a \tilde{\chi}_b \\ d_{jab}^L &= V_{b2}^* \sum_{m,n=1}^3 U_{j,3+m}^{\nu*} Y_{mn}^\nu R_{an}^* \\ d_{jab}^R &= -g U_{b1} \sum_{m=1}^3 U_{jm}^\nu R_{am}^* + U_{b2} \sum_{m,n=1}^3 U_{j,n}^\nu Y_{mn}^{e*} R_{a,3+m}^* \end{aligned} \quad (4.2.18)$$

where V , U are the mixing matrices of chargino and R is the mixing matrix of slepton. The corresponding vertex and Feynman diagram are:



The diagram shows a vertex where an incoming solid line labeled ν_j splits into two outgoing lines: a dashed line labeled \tilde{l}_a and a solid line labeled $\tilde{\chi}_b^+$.

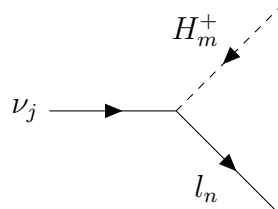
$$= -2i(d_{jab}^L P_L + d_{jab}^R P_R). \quad (4.2.19)$$

H^+l

The lagrangian is (take (ν_l, l) as an example):

$$\begin{aligned} \mathcal{L} &= \sum_{a,b=1}^3 (Y_\nu)_{ab} l_a H_u^+ \nu_{b+3}^c + (Y_e)_{ab} \nu_a H_d^- l_b^c + h.c. \\ &= \sum_{a,b=1}^3 \sum_{n=1}^3 \sum_{m=1}^2 \sum_{j=1}^6 [(Y_\nu)_{ab} U_{L,na}^{e*} l_n U_{j,b+3}^{\nu*} \nu_j Z_{m2}^+ H^+ + (Y_e)_{ab} U_{R,nb}^{e*} U_{ja}^* \nu_j l_n^c Z_{m1}^+ H^- \\ &\quad + (Y_\nu)_{ab}^* U_{L,na}^e \bar{l}_n U_{j,b+3}^\nu \bar{\nu}_j Z_{m2}^+ H^- + (Y_e)_{ab}^* U_{R,nb}^e U_{ja}^\nu \bar{\nu}_j \bar{l}_n^c Z_{m1}^+ H^+], \end{aligned} \quad (4.2.20)$$

the vertex of the feynman diagram is therefore:



The diagram shows a vertex where an incoming solid line labeled ν_j splits into two outgoing lines: a dashed line labeled H_m^+ and a solid line labeled l_n .

$$\begin{aligned} &= -2i \sum_{a,b=1}^3 [(Y_\nu)_{ab} U_{L,na}^{e*} U_{j,b+3}^{\nu*} Z_{m2}^+ P_L + (Y_e)_{ab}^* U_{R,nb}^e U_{ja}^\nu Z_{m1}^+ P_R] \\ &= -2i(D_{jmn}^L P_L + D_{jmn}^R P_R). \end{aligned} \quad (4.2.21)$$

BLSSM

The model receives its name from the $U(1)_{B-L}$ gauge group added to the MSSM, i.e. the gauge group has a structure $U(1)_Y \times SU(3)_c \times SU(2)_L \times U(1)_{B-L}$. This introduces two higgs singlets in addition to the MSSM: η and $\bar{\eta}$, the *bileptons*.

The superpotential and the soft breaking terms are[12]

$$\begin{aligned}
 W &= Y_u^{ij} \hat{U}_i \hat{Q}_j \hat{H}_u - Y_d^{ij} \hat{D}_i \hat{Q}_j \hat{H}_d - Y_e^{ij} \hat{E}_i \hat{L}_j \hat{H}_d + \mu \hat{H}_u \hat{H}_d \\
 &\quad + Y_\nu^{ij} \hat{L}_i \hat{H}_u \hat{\nu}_j - \mu' \hat{\eta} \hat{\bar{\eta}} + Y_x^{ij} \hat{\nu}_i \hat{\eta} \hat{\nu}_j, \\
 \mathcal{L}_{SB} &= \mathcal{L}_{MSSM} - m_\eta^2 |\eta|^2 - m_{\bar{\eta}}^2 |\bar{\eta}|^2 - m_{\nu,ij}^2 (\tilde{\nu}_i^c)^* \tilde{\nu}_j^c \\
 &\quad + (-\lambda_{\tilde{B}} \lambda_{\tilde{B}'} M_{BB'} - \frac{1}{2} \lambda_{\tilde{B}} \lambda_{\tilde{B}'} M_{B'} - \eta \bar{\eta} B'_\mu + T_\nu^{ij} H_u \tilde{\nu}_i^c \tilde{L}_j + T_x^{ij} \eta \tilde{\nu}_i^c \tilde{\nu}_j^c + h.c.),
 \end{aligned} \tag{4.3.1}$$

the chiral superfield contents are listed in table 4.1.

Superfield	Spin 0	Spin $\frac{1}{2}$	Generations	$(U(1)_Y \times SU(2)_L \times SU(3)_c \times U(1)_{B-L})$
\hat{Q}	\tilde{Q}	Q	3	$(\frac{1}{6}, 2, 3, \frac{1}{6})$
\hat{D}	\tilde{d}^c	d^c	3	$(\frac{1}{3}, 1, \bar{3}, -\frac{1}{6})$
\hat{U}	\tilde{u}^c	u^c	3	$(-\frac{2}{3}, 1, \bar{3}, -\frac{1}{6})$
\hat{L}	\tilde{L}	L	3	$(-\frac{1}{2}, 2, 1, -\frac{1}{2})$
\hat{E}	\tilde{e}^c	e^c	3	$(1, 1, 1, \frac{1}{2})$
$\hat{\nu}$	$\tilde{\nu}^c$	ν^c	3	$(0, 1, 1, \frac{1}{2})$
\hat{H}_d	H_d	\tilde{H}_d	1	$(-\frac{1}{2}, 2, 1, 0)$
\hat{H}_u	H_u	\tilde{H}_u	1	$(\frac{1}{2}, 2, 1, 0)$
$\hat{\eta}$	η	$\tilde{\eta}$	1	$(0, 1, 1, -1)$
$\hat{\bar{\eta}}$	$\bar{\eta}$	$\tilde{\bar{\eta}}$	1	$(0, 1, 1, 1)$

Table 4.1: The chiral superfields in the BLSSM. The table is taken from [12].

When the doublet and singlet Higgs acquire vevs, the new gauge group is spontaneously broken into $SU(3)_c \times U(1)_{em}$ [12]:

$$\begin{aligned}
 H_d^0 &= \frac{1}{\sqrt{2}}(\sigma_d + v_d + i\phi_d), & H_u^0 &= \frac{1}{\sqrt{2}}(\sigma_u + v_u + i\phi_u) \\
 \eta &= \frac{1}{\sqrt{2}}(\sigma_\eta + v_\eta + i\phi_\eta), & \bar{\eta} &= \frac{1}{\sqrt{2}}(\sigma_{\bar{\eta}} + v_{\bar{\eta}} + i\phi_{\bar{\eta}}),
 \end{aligned} \tag{4.3.2}$$

which generates a Z' boson, one additional pseudoscalar A_η , four scalar Higgs bosons and twelve physical sneutrinos (real and imaginary, six of each kind). The vevs of the singlets define the parameter $\tan \beta' = \frac{v_u}{v_{\bar{\eta}}}$. One important consequence of implementing a second abelian gauge group results in general in the *gauge kinetic mixing*. The non-canonical covariant derivative takes the form

$$D_\mu = \partial_\mu - iQ_\phi^T G A, \tag{4.3.3}$$

where Q_ϕ is the charge vector of the field ϕ with respect to the two Abelian fields, A is the gauge bosons and

$$G = \begin{pmatrix} g_{YY} & g_{YB} \\ g_{BY} & g_{BB} \end{pmatrix} \tag{4.3.4}$$

is the gauge coupling matrix.

For the later use in numerical calculations, it is worth writing down the squared mass matrices and the relevant approximations of the Higgs bosons and the right-handed sneutrinos. The squared mass matrix of Higgs bosons in the basis $(\sigma_d, \sigma_u, \sigma_\eta, \sigma_{\bar{\eta}})$ is[5]

$$m_{h,T}^2 = \begin{pmatrix} m_{A^0}^2 s_\beta^2 + g_\Sigma^2 v_u^2 & -m_{A^0}^2 c_\beta s_\beta - g_\Sigma^2 v_u v_d & \frac{\bar{g}_{BL}}{2} v_d v_\eta & -\frac{\bar{g}_{BL}}{2} v_d v_{\bar{\eta}} \\ -m_{A^0}^2 c_\beta s_\beta - g_\Sigma^2 v_u v_d & m_{A^0}^2 c_\beta^2 + g_\Sigma^2 v_d^2 & -\frac{\bar{g}_{BL}}{2} v_u v_\eta & \frac{\bar{g}_{BL}}{2} v_u v_{\bar{\eta}} \\ \frac{\bar{g}_{BL}}{2} v_d v_\eta & -\frac{\bar{g}_{BL}}{2} v_u v_\eta & m_{A_\eta}^2 c_{\beta'}^2 + g_{BL}^2 v_\eta^2 & -m_{A_\eta}^2 c_{\beta'} s_{\beta'} - g_{BL}^2 v_\eta v_{\bar{\eta}} \\ -\frac{\bar{g}_{BL}}{2} v_d v_{\bar{\eta}} & \frac{\bar{g}_{BL}}{2} v_u v_{\bar{\eta}} & -m_{A_\eta}^2 c_{\beta'} s_{\beta'} - g_{BL}^2 v_\eta v_{\bar{\eta}} & m_{A_\eta}^2 s_{\beta'}^2 + g_{BL}^2 v_{\bar{\eta}}^2 \end{pmatrix}, \quad (4.3.5)$$

where $g_\Sigma^2 = \frac{1}{4}(g_1^2 + g_2^2 + \bar{g}^2)$,

$$\bar{g} = \frac{g_{YB} g_{BB} + g_{BY} g_{YY}}{\sqrt{g_{BB}^2 + g_{BY}^2}}, \quad (4.3.6)$$

g_1 , g_2 and g_{BL} are the couplings of $U(1)_Y$, $SU(2)_L$ and $U(1)_{B-L}$ gauge groups respectively. The mass of the new pseudoscalar is given by[5]

$$m_{A_\eta}^2 = \frac{2B_{\mu'}}{\sin 2\beta'}, \quad (4.3.7)$$

and the Z' mass is approximated by[5]

$$M_{Z'} \approx g_{BL} x, \quad x = \sqrt{v_\eta^2 + v_{\bar{\eta}}^2}. \quad (4.3.8)$$

The sneutrino has the form

$$\tilde{\nu} = \frac{1}{\sqrt{2}}(\tilde{\nu}_S + i \tilde{\nu}_P), \quad (4.3.9)$$

where $\tilde{\nu}_S$ denotes scalar- and $\tilde{\nu}_P$ denotes pseudoscalar sneutrino. Their masses can be approximated by[5]

$$\begin{aligned} m_{\tilde{\nu}_S}^2 &\approx m_{\nu^c}^2 + M_{Z'}^2 \left(\frac{1}{4} \cos(2\beta') + \frac{2Y_x^2}{g_{BL}^2} \sin^2 \beta' \right) + M_{Z'} \frac{\sqrt{2}Y_x}{g_{BL}} (A_x \sin \beta' - \mu' \cos \beta') \\ m_{\tilde{\nu}_P}^2 &\approx m_{\nu^c}^2 + M_{Z'}^2 \left(\frac{1}{4} \cos(2\beta') + \frac{2Y_x^2}{g_{BL}^2} \sin^2 \beta' \right) - M_{Z'} \frac{\sqrt{2}Y_x}{g_{BL}} (A_x \sin \beta' - \mu' \cos \beta') \end{aligned} \quad (4.3.10)$$

for the scalars (S) and pseudoscalars (P) when the gauge kinetic mixing and the left-right mixing neglected.

5 Dark Matter

In this chapter, the ideas and formulas that will be useful to understand the numerical calculations are introduced. For further enlightening readings please consult [7, 22, 8]. In this thesis only the right-handed sneutrinos and sterile neutrinos are good DM candidates, thus the following discussions will be mainly focus on ν_R and $\tilde{\nu}_R$ DM.

As pointed out by F. Zwicky in 1937, the total mass of the Coma cluster estimated using Virial theorem is much larger than the luminous mass[35]. The non-luminous contribution to the mass is then denoted as *Dark Matter, DM* by Zwicky, which now is assumed to be objects or particles that do not or only weakly interact with the electromagnetic radiations. In 1970 V. Rubin and W. Ford pointed out that the rotational curves observed from M31 indicates that only 57% of the mass is contained within 24 kpc of the radius. The rest mass lies in the outside part of this range forming the *dark matter halo*, where no optical emission had been detected[32].

To explain what DM consists of, many models are invented, different candidates are brought up from both cosmology and particle physics point of view, such as *Massive Compact Halo Object, MACHO*, extra dimension, axion, neutrinos, sterile neutrinos and so on. Being able to explain the neutrino mass and being the only extension of space-time symmetry beyond SM, sterile neutrino and SUSY particles are the frequently studied DM candidates. In the following, the production mechanism that is related to these two kinds of candidates will be first introduced, it is then followed by a brief discussion of the detection method.

Production Mechanism and Relic Density

For particle DM candidates, they can be generated thermally or non-thermally. For most WIMP particles, like the SUSY LSPs, they are produced thermally while sterile neutrinos, especially the keV range ones, are produced through non-thermal processes.

Thermal Production

In general, when the temperature of the Universe is larger than the DM particle mass m_χ , the dark matter particles are relativistic. At this stage, the dark matter particles are on the one hand produced by the collisions of other particles and on the other hand they are also consumed by the annihilation and coannihilation processes. The total effect is, the DM density within a comoving volume a^3 maintains equilibrium. Define the reaction rate for one species of DM particle as

$$\Gamma = n\sigma v, \quad (5.1.1)$$

where n is the number density within the comoving volume, σ is the cross-section, v is the velocity of the particle, then at this stage

$$\Gamma \gg H, \quad (5.1.2)$$

the DM particles are in thermal equilibrium.

As the Universe expands the temperature drops down. The number density of DM particle is diluted by the expansion where in the meanwhile the other particles do not have enough kinetic energy to produce DM particles anymore[22]. The reaction rate Γ decreases and finally drops below the Hubble constant H . The DM particles are neither produced nor consumed efficiently, the number density within a comoving volume remains constant thereafter. The DM particles are said to *freeze-out* or decouple from the thermal equilibrium, and temperature at the time when $\Gamma = H$ is called freeze-out temperature T_{FO} . Depending on the mass to temperature ratio at freeze-out, the dark matter can be categorised into mainly three species[7, 8]:

1. $m_\chi \ll T_{FO}$ is called *hot dark matter* since when decoupled, the particles are relativistic. This scenario is already excluded because when assumed, the Universe cannot form the fine structures that are observed today;
2. $m_\chi \gg T_{FO}$ is called *cold dark matter*, this case is more frequently studied and is one of the assumptions of the standard cosmological model Λ CDM. The most representative candidate is the *Weakly Interacting Massive Particles*, *WIMPs*;
3. if the particles are relativistic when decoupled but are cooled down to be non-relativistic, they are called *warm dark matter*, the sterile neutrinos, depending on the masses that are given in different models, can be categorised into this type.

The whole evolution process for SUSY particles can be described by[6]

$$\frac{dN}{dt} = -3HN - \langle \sigma_{eff} v \rangle_T (N^2 - N_{eq}^2), \quad (5.1.3)$$

where N is the number density of all the odd particles within a comoving volume, σ_{eff} is the effective annihilation cross-section contains production, annihilation and coannihilation processes¹. Since the particles follow the Boltzmann distribution, the reaction rate is averaged over the temperature. The particle density in equilibrium is[6]

$$N_{eq} = \sum_{\text{odd particles}} n^i \int \frac{dp^3}{(2\pi)^3} \left(e^{\frac{\sqrt{p^2 + M_i^2}}{T}} \pm 1 \right)^{-1} \approx \sum_{\text{odd particles}} n^i \int \frac{dp^3}{(2\pi)^3} e^{-\frac{\sqrt{p^2 + M_i^2}}{T}}. \quad (5.1.4)$$

Define two parameters

$$Y = \frac{N}{s} \quad x = \frac{m_\chi}{T}, \quad (5.1.5)$$

where s is the entropy density per comoving volume. Convert eq. (5.1.4) with Y and x and notice that in standard cosmology model the entropy density is conserved during the expansion:

$$\frac{ds}{dt} = -3Hs, \quad (5.1.6)$$

the evolution equation eq. (5.1.4) can be written as[6]

$$\frac{dY}{dx} = \frac{1}{3H} \langle \sigma_{eff} v \rangle_T (Y^2 - Y_{eff}^2). \quad (5.1.7)$$

The Hubble constant is given by the Friedman equation as[8]

$$H^2 = \frac{8\pi}{3M_p^2} \rho. \quad (5.1.8)$$

For the relativistic particles the energy density and the entropy density are[8]

$$\rho(T) = \frac{\pi^2}{30} g_{eff}(T) T^4 \quad s = \frac{2\pi^2}{45} h_{eff}(T) T^3, \quad (5.1.9)$$

where g_{eff} and h_{eff} are the effective degree of freedom and they are related by the parameter[8]

$$g_*^{1/2} = \frac{h_{eff}}{g_{eff}^{1/2}} \left(1 + \frac{T}{3h_{eff}} \frac{dh_{eff}}{dT} \right). \quad (5.1.10)$$

¹The complete form of reaction rate taking into account of coannihilation contributions can not be easily implemented. For a thorough discussion please consult [8] chapter 7.2.2.

Adopting $g_*^{1/2}$ and H to rewrite the evolution equation eq. (5.1.7)[8, 22]

$$\frac{dY}{dx} = -\sqrt{\frac{\pi M_p^2}{45}} \frac{g_*^{1/2} m}{x^2} \langle \sigma_{eff} v \rangle_T (Y^2 - Y_{eq}^2), \quad (5.1.11)$$

this equation can be solved numerically by integrating from $x = 0$ to $x_0 = m_\chi T_0$ [22] to find the present Y_0^2 . The relic density is therefore[8]

$$\Omega_\chi h^2 = \frac{\rho_\chi^0 h^2}{\rho_c^0} = \frac{m_\chi s_0 Y_0 h^2}{\rho_c^0} = 2.755 \times 10^8 Y_0 m_\chi / GeV, \quad (5.1.12)$$

where $\rho_c^0 = \frac{3H_0^2}{8\pi G} = 1.9 \cdot 10^{-29} h^2 g cm^{-3}$ is the present critical density[7], and s_0 is the present day entropy density. As a comparison for the future calculations on relic density, the currently reported cold non-baryonic matter density is [21]

$$\Omega_{nbm} h^2 = 0.1186 \pm 0.0020. \quad (5.1.13)$$

As illustrated in fig. 5.1, the Y_0 value decreases with the increasing reaction rate. This is ususally called *the weakest wins*. This is due to the fact that for particles with higher annihilation cross-section, they are more likely to get exhausted before decoupling from the equilibrium. This observation can be used in fine-tuning the parameters to match with the current dark matter density.

Nonthermal Generation

As mentioned in section 3.1, when neutrinos are produced initially in the plasma, the neutrino oscillations get modified by the matter inside the plasma. Assume only one species each for active neutrino and sterile neutrino, then the effective mixing angle in the plasma is[20]

$$\sin^2 2\theta_m = \frac{\Delta^2(p) \sin^2 2\theta}{\Delta^2(p) \sin^2 2\theta + [\Delta(p) \cos(2\theta) - V_D - V_T]^2}, \quad (5.1.14)$$

where θ_m is the mixing angle in the plasma, θ is the mixing angle in the vacuum, $\Delta(p) = \Delta m^2 / (2p)$, Δm^2 is the mass-squared splitting in the vacuum. V_D is the density potential, which only takes values when the lepton asymmetry is present. V_T is the temperature potential that comes from higher order corrections and scattering with the background particles. If the parameters are set properly, a resonance can be induced. Based on this consideration, two models are proposed:

²Theoretically the equation eq. (5.1.11) can be solved this way, but in micrOMEGAS a Runge-Kutta method is employed to find the initial point and approximations are also adopted during the numerical calculation. For details see [6] chapter 6.3.

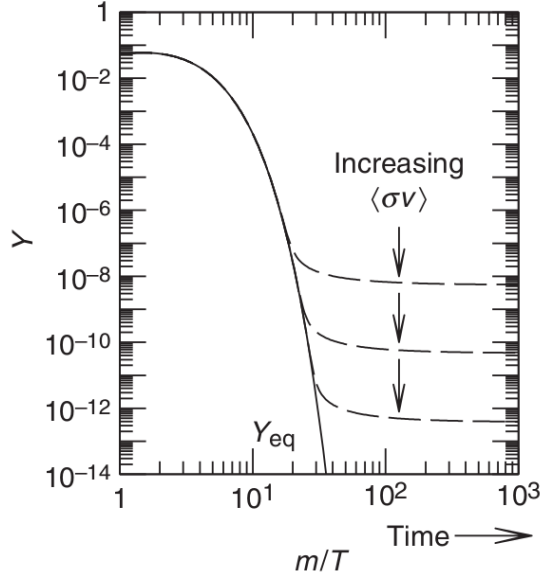


Figure 5.1: The evolution of the DM number density. As pointed by the arrow, the higher reaction rate will result in lower Y_0 value and thus a smaller amount of the DM will contribute to the relic density. This relation is called "the weakest wins". Figure taken from G. Bertone, "Particle Dark Matter"[8].

Dodelson-Widrow Mechanism (Non-Resonant Production)[10] The sterile neutrinos are produced non-resonantly through the oscillation from active neutrinos to sterile neutrinos, by letting the production time longer than the oscillation time. The proposed DM has a mass about 100 eV. This mechanism, even though being simple and nice, is ruled out by the X-Ray observations[18].

Shi-Fuller Mechanism (Resonant Production)[33] The level-crossing is enhanced by the lepton asymmetry \mathcal{L}_α which impacts on the density potential V_D . This mechanism restricts the DM to be produced at a temperature below 150 MeV, which acquires a lepton asymmetry for at least one flavor to be about $10^{-3} \sim 10^{-1}$, this results in a 100 eV to 10 keV sterile neutrino DM.

Except the two mechanism mentioned above, the sterile neutrino DM can also be generate through the decay of a singlet scalar boson.

Decay of a Singlet Scalar[20] The Lagrangian is

$$\mathcal{L}_{int} = \frac{y}{2} \overline{(\nu_R)^c} \nu_R S + h.c., \quad (5.1.15)$$

where the field S is the singlet scalar boson. The DM density depends no more on the mixing angle but to depend totally on the coupling constant y . Whether the DM will be cold or warm depends on the explicit models.

Detection

DM particles, if exist, can be detected directly or indirectly. The idea of direct detection is to measure the recoil energy when the DM is scattered by the nucleus. This idea can be realised in three ways, i.e. through scintillation (DAMA/LIBRA), ionization (XENON, LUX, XMASS) and photon detection (CDMS, CRESST, EDELWEISS) [8]. The disadvantage of this detection scheme is, it only applies to WIMP like particles and the signal is also not strong. For example, a 100 GeV neutralino travels at a speed of 220 km/s can maximally pass 26.9 keV to the nucleus, where the real energy emitted is certainly fewer, a naturally radioactive event will easily make this signal undetectable [22]. Until now, only the DAMA/LIBRA has claimed the detection of this signal which is unfortunately not observed by any other experiments of the same kind.

The other detection scheme is to detect the byproducts of the decay or annihilation of DM particles, such as photons. By observing the X-Ray signals in the outer space, certain constrains are set to the mass of DM particles. For sterile neutrino DM, the upper limit is set by the non-detection of the X-Ray produced by the neutrino decays. If the DM obeys Fermi-Dirac statistics, then the so called *Tremaine-Gunn bound* is set with the *dwarf spherical satellites*, $dSph$, which requires the sterile neutrino mass to be at least 0.5 keV. Another lower bound is set by the observation of Lyman- α forest, which takes different bounds depending on the analysis [8]. A summary of the astronomical constraints on keV range sterile neutrino dark matter is given in fig. 5.2 [17], where the bounds are production model independent.

Take *NuSTAR* bound as an example, this bound is set by the observed flux as [17]

$$\begin{aligned}
 F &= \frac{\Gamma}{4\pi m_\chi} \Delta\Omega \mathcal{J} \\
 &\approx 2.6 \times 10^{-6} \text{cm}^{-2} \text{s}^{-1} \left(\frac{m_\chi}{20 \text{keV}} \right)^4 \left(\frac{\sin^2 2\theta}{10^{-14}} \right) \\
 &\quad \times \left(\frac{\Delta\Omega}{4 \text{deg}^2} \right) \left(\frac{\mathcal{J}}{40 \text{GeV cm}^{-3} \text{kpc sr}^{-1}} \right),
 \end{aligned} \tag{5.2.1}$$

where [17]

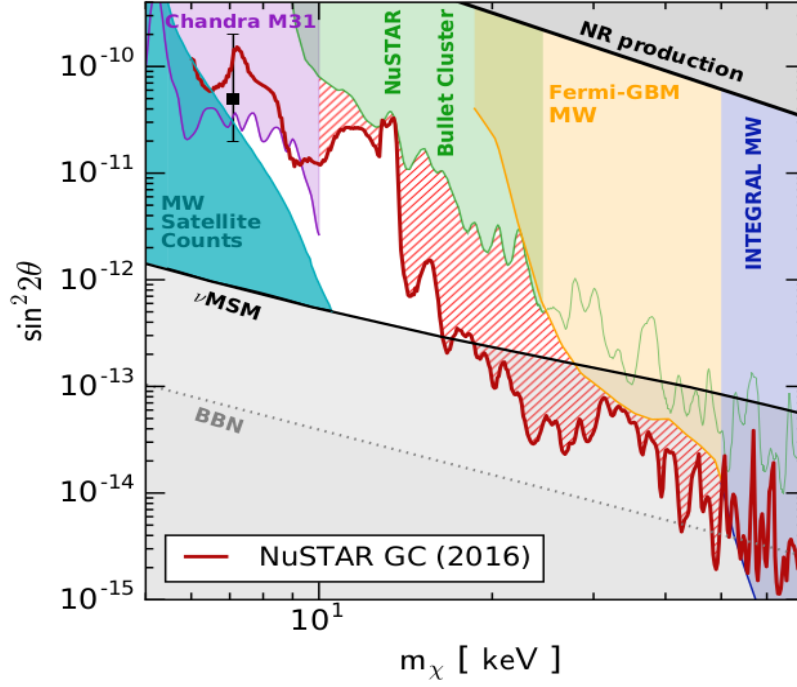


Figure 5.2: The summary of constraints on keV range sterile neutrino dark matter shown in the *nuSTAR* paper [17]. All the constraints except the ν MSM are model independent. The allowed region is the white area and the area between ν MSM and BBN line if no ν MSM model is considered. The point marked with a square is the 3.5 keV X-Ray, which was suspected to be a signal of sterile neutrino dark matter with mass 7 keV.

$$\Gamma = 1.38 \cdot 10^{-32} \text{s}^{-1} \left(\frac{\sin^2 2\theta}{10^{-10}} \right) \left(\frac{m_\chi}{\text{keV}} \right)^5 \quad (5.2.2)$$

is the decay width of the DM particle χ , m_χ is its mass, $\Delta\Omega$ is the average solid angle and \mathcal{J} is the J-factor that parameterizes the DM distribution in the FOV. The $\Delta\Omega$ and \mathcal{J} depends on the instrument and the galaxy profile, which is independent factors of the DM production model. Thus the DM mixing angle is bounded by eq. (5.2.1) for different masses. Since the mixing angle takes small values which makes $\sin \theta \approx \theta$ possible, the mixing angle in our model is then

$$\sin^2 2\theta = \sum_{a=1}^3 |U_{i,4}|^2. \quad (5.2.3)$$

This equation is used later in the comparison with the *NuSTAR* bounds.

6 Analytical Calculations of the Decay Widths

The calculations of the three-body decay take the Feynman-'t Hooft gauge, and the loop calculations take non-linear gauge as discussed in [23].

Three-body-decay

Via Z Boson

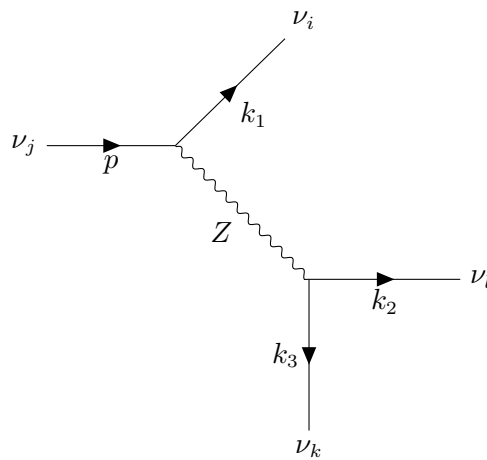


Figure 6.1: The Feynman diagram of the three-body decay mediated by a Z boson.

The corresponding Feynman diagram is shown in fig. 6.1. It is worth noting that the contribution of s-channel dominates. Since the neutrino mixing matrix U is quasi-unitary, similar to the *GIM Mechanism (Glashow-Iliopoulos-Maiani Mechanism)*, the combination $U_{ja}U_{ia}^*$ can be approximated to be 0 when $j \neq i$. Feynman diagrams of other decay channels by exchanging the indices are thus

suppressed. The matrix elements are:

$$\begin{aligned}
 \mathcal{M} &= \bar{u}_{2,l} \frac{-i}{2} \frac{g}{\cos \theta_W} \gamma_\mu (o_{lk} P_L - o_{lk}^* P_R) v_{3,k} \frac{-i g^{\mu\nu}}{q^2 - m_Z^2} \bar{v}_{1,i} \frac{-i}{2} \frac{g}{\cos \theta_W} \gamma_\nu (o_{ij} P_L - o_{ij}^* P_R) u_{p,j} \\
 &= \frac{-i g^2}{4 \cos^2 \theta_W m_Z^2} \bar{u}_2 \gamma_\mu (o_{lk} P_L - o_{lk}^* P_R) v_3 \bar{v}_1 \gamma^\mu (o_{ij} P_L - o_{ij}^* P_R) u_p \\
 \mathcal{M}^\dagger &= \frac{i g^2}{4 \cos^2 \theta_W m_Z^2} \bar{u}_p (o_{ij}^* P_R - o_{ij} P_L) \gamma^\nu v_1 \bar{v}_3 (o_{lk}^* P_R - o_{lk} P_L) \gamma_\nu u_2.
 \end{aligned} \tag{6.1.1}$$

Once the indices are given to the respective particles, they are omitted in the spinors in the following calculations.

Using eq. (6.1.1) and notice that $q^2 \ll m_Z^2$, one get:

$$\begin{aligned}
 \frac{1}{2} \sum_{\text{Spins}} |\mathcal{M}|^2 &= \frac{g^4}{2 \times 16 \cos^4 \theta_W m_Z^4} \underbrace{\bar{u}_2 \gamma_\mu (o_{lk} P_L - o_{lk}^* P_R) v_3 \bar{v}_1 \gamma^\mu (o_{ij} P_L - o_{ij}^* P_R) u_p}_{A := G_F^2} \\
 &\quad \times \bar{u}_p (o_{ij}^* P_R - o_{ij} P_L) \gamma^\nu v_1 \bar{v}_3 (o_{lk}^* P_R - o_{lk} P_L) \gamma_\nu u_2 \\
 &= A \text{Tr} [k_2 \gamma_\nu (o_{lk} P_L - o_{lk}^* P_R) k_3 (o_{lk}^* P_R - o_{lk} P_L) \gamma_\mu] \\
 &\quad \times \text{Tr} [k_1 \gamma^\mu (o_{ij} P_L - o_{ij}^* P_R) (\not{p} + m_j) (o_{ij}^* P_R - o_{ij} P_L) \gamma^\nu] \\
 &= 64 A (k_2 k_1) (k_3 p) |o_{lk}|^2 |o_{ij}|^2.
 \end{aligned} \tag{6.1.2}$$

Notice that, when integrating the expression in momentum space, $(k_2 p)(k_3 k_1)$ and $(k_2 k_1)(k_3 p)$ give the same result. This is employed in all the calculations of decay width when necessary for simplicity.

The total decay width of ν_j decay via Z boson into different final states is ¹:

$$\begin{aligned}
 \Gamma &= \sum_{i,k,l=1}^3 \int \frac{1}{2E} (2\pi)^4 Dk_1 Dk_2 Dk_3 \delta^{(4)}(p - k_1 - k_2 - k_3) |\mathcal{M}|^2 \\
 &= \sum_{i,k,l=1}^3 \int (2\pi)^4 \frac{1}{2E} \frac{1}{2E_1} \frac{1}{2E_2} \frac{1}{2E_3} \frac{d^3\mathbf{k}_1}{(2\pi)^3} \frac{d^3\mathbf{k}_2}{(2\pi)^3} \frac{d^3\mathbf{k}_3}{(2\pi)^3} \delta(p - k_1 - k_2 - k_3) \\
 &\quad \times 64A(k_1 k_2)(pk_3)(|o_{lk}|^2 |o_{ij}|^2) \\
 &= 4A \sum_{i,k,l=1}^3 \int \frac{1}{(2\pi)^5} \frac{1}{E} \frac{d^3\mathbf{k}_1}{E_1} \frac{1}{6} \pi (g^{\mu\nu} q^2 + 2q^\mu q^\nu) k_{1,\mu} p_\nu (|o_{lk}|^2 |o_{ij}|^2) \\
 &= 4A \sum_{i,k,l=1}^3 \int \frac{1}{(2\pi)^5} \frac{1}{E} \frac{d^3\mathbf{k}_1}{E_1} \frac{1}{6} \pi [(k_1 p) q^2 + 2(qk_1)(qp)] (|o_{lk}|^2 |o_{ij}|^2),
 \end{aligned} \tag{6.1.3}$$

where $q = p - k_1$ and $\int d\Omega$ integrates over all the directions of emitted neutrinos. In the rest frame of the heavy neutrino ν_j ,

$$p = (m_j, \mathbf{0}), \quad q = (m_j - E_1, -\mathbf{k}_1), \tag{6.1.4}$$

using these relations, the decay width is:

$$\begin{aligned}
 \Gamma &= 4A \sum_{i,k,l=1}^3 \int \frac{1}{(2\pi)^5} \frac{1}{E} \frac{d^3\mathbf{k}_1}{E_1} \frac{1}{6} \pi [(m_j E_1) \underbrace{[(m_j - E_1)^2 - |\mathbf{k}_1|^2]}_{m_j^2 - 2m_j E_1} \\
 &\quad + 2m_j \underbrace{[(m_j - E_1)E_1 + |\mathbf{k}_1|^2]}_{m_j E_1} (m_j - E_1)] (|o_{lk}|^2 |o_{ij}|^2).
 \end{aligned} \tag{6.1.5}$$

Since

$$d^3\mathbf{k}_1 = |\mathbf{k}_1| E_1 dE_1 d\Omega, \tag{6.1.6}$$

¹Followed the calculations in QFT of F.Mandl, G.Shaw [27].

the decay width is then:

$$\begin{aligned}
 \Gamma &= 4A \sum_{i,k,l=1}^3 \int \frac{1}{(2\pi)^5} \frac{1}{m_j} E_1 \frac{1}{6} \pi [(m_j E_1)(m_j^2 - 2m_j E_1) + 2m_j(m_j E_1)(m_j - E_1)] dE_1 d\Omega (|o_{lk}|^2 |o_{ij}|^2) \\
 &= \sum_{i,k,l=1}^3 (|o_{lk}|^2 |o_{ij}|^2) \int_0^{\frac{m_j}{2}} 4G_F^2 \frac{1}{(2\pi)^5} \frac{1}{6} \pi (3m_j^2 E_1^2 - 4m_j E_1^3) dE_1 d\Omega \\
 &= \sum_{i,k,l=1}^3 (|o_{lk}|^2 |o_{ij}|^2) 4G_F^2 \frac{1}{(2\pi)^5} \frac{1}{6} \pi \frac{m_j^5}{16} \times 4\pi \\
 &= \sum_{i,k,l=1}^3 (|o_{lk}|^2 |o_{ij}|^2) \frac{G_F^2}{192\pi^3} m_j^5,
 \end{aligned} \tag{6.1.7}$$

with the complete form of coefficients:

$$|o_{lk}|^2 |o_{ij}|^2 = \left| \sum_{a=1}^3 U_{la} U_{ka}^* \right|^2 \left| \sum_{a=1}^3 U_{ia} U_{ja}^* \right|^2. \tag{6.1.8}$$

Via Higgs Boson

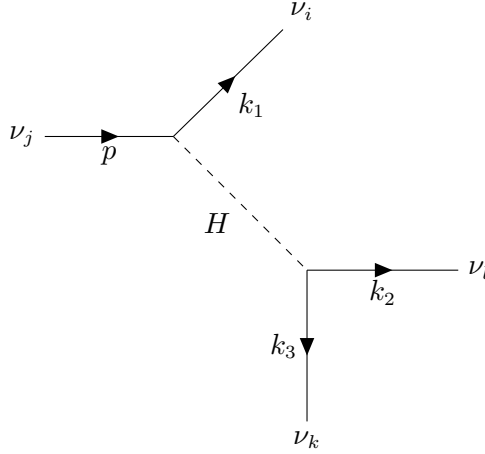


Figure 6.2: The Feynman diagram of the three-body decay mediated by a H boson.

The Feynman diagram is shown in fig. 6.2. With the vertex eq. (4.2.13), the matrix

elements for the s channel are:

$$\begin{aligned}\mathcal{M}_{H,s} &= \sum_f \frac{-i}{2m_f^2} \bar{u}_2(X_{lk}P_R + X_{lk}^*P_L)v_3\bar{v}_1(X_{ij}P_R + X_{ij}^*P_L)u_p \\ \mathcal{M}_{H,s}^\dagger &= \sum_f \frac{i}{2m_f^2} \bar{u}_p(X_{ij}P_R + X_{ij}^*P_L)v_1\bar{v}_3(X_{lk}P_R + X_{lk}^*P_L)u_2,\end{aligned}\tag{6.1.9}$$

and for the t-channel are:

$$\begin{aligned}\mathcal{M}_{H,t} &= \sum_f \frac{-i}{2m_f^2} \bar{u}_2(X_{lj}P_R + X_{lj}^*P_L)u_p\bar{v}_1(X_{ik}P_R + X_{ik}^*P_L)v_3 \\ \mathcal{M}_{H,t}^\dagger &= \sum_f \frac{i}{2m_f^2} \bar{v}_3(X_{ik}P_R + X_{ik}^*P_L)v_1\bar{u}_p(X_{lj}P_R + X_{lj}^*P_L)u_2.\end{aligned}\tag{6.1.10}$$

$|\mathcal{M}_{H,s}|^2$ and $|\mathcal{M}_{H,t}|^2$

The amplitude is:

$$\begin{aligned}\frac{1}{2} \sum_{spins} |\mathcal{M}_{H,s}|^2 &= \sum_{f,f'} \frac{1}{8m_f^2 m_{f'}^2} \bar{u}_2(X_{lk}P_R + X_{lk}^*P_L)v_3\bar{v}_1(X_{ij}P_R + X_{ij}^*P_L)u_p \\ &\quad \times \bar{u}_p(X'_{ij}P_R + X'^*_{ij}P_L)v_1\bar{v}_3(X'_{lk}P_R + X'^*_{lk}P_L)u_2 \\ &= \sum_{f,f'} \frac{1}{8m_f^2 m_{f'}^2} \text{Tr}[(\not{k}_2 + m_k)(X_{lk}P_R + X_{lk}^*P_L)(\not{k}_3 - m_l)(X'_{lk}P_R + X'^*_{lk}P_L)] \\ &\quad \times \text{Tr}[(\not{k}_1 - m_i)(X_{ij}P_R + X_{ij}^*P_L)(\not{p} + m_j)(X'_{ij}P_R + X'^*_{ij}P_L)] \\ &= \sum_{f,f'} \frac{1}{2m_f^2 m_{f'}^2} (k_2 k_3)(pk_1)(X'^*_{ij}X_{ij} + X'_{ij}X^*_{ij})(X'^*_{lk}X_{lk} + X^*_{lk}X'_{lk}) \\ &= \sum_{f,f'} \frac{2}{m_f^2 m_{f'}^2} \text{Re}(X_{lk}X'^*_{lk}) \text{Re}(X_{ij}X'^*_{ij})(k_2 k_3)(pk_1).\end{aligned}\tag{6.1.11}$$

Similarly,

$$\begin{aligned}\frac{1}{2} \sum_{spins} |\mathcal{M}_{H,t}|^2 &= \sum_{spins} \sum_{f,f'} \frac{1}{8m_f^2 m_{f'}^2} \bar{u}_2(X_{lj}P_R + X_{lj}^*P_L)u_p\bar{v}_1(X_{ik}P_R + X_{ik}^*P_L)v_3 \\ &\quad \times \bar{v}_3(X'_{ik}P_R + X'^*_{ik}P_L)v_1\bar{u}_p(X'_{lj}P_R + X'^*_{lj}P_L)u_2 \\ &= \sum_{f,f'} \frac{2}{m_f^2 m_{f'}^2} \text{Re}(X_{ik}X'^*_{ik}) \text{Re}(X_{lj}X'^*_{lj})(k_1 k_3)(pk_2).\end{aligned}\tag{6.1.12}$$

The prime ' here is employed to distinguish between the matrix element and its hermitian conjugate, since there can be three contributions of neutral higgs from every part, i.e, $\mathcal{M}_{H,s} = \sum_f \mathcal{M}_{H,s}(\eta_f) = \mathcal{M}_{H^0,s} + \mathcal{M}_{h^0,s} + \mathcal{M}_{A^0,s}$. Notice that, the indices f is also contained in the vertices, a summation must be applied both to the higgs mass and the matrices X and X' .

The mixed terms between higgs-channels

Using equation eq. (6.1.9) and eq. (6.1.10), the mixed terms are:

$$\begin{aligned}
 \frac{1}{2} \sum_{spins} \mathcal{M}_{H,s} \mathcal{M}_{H,t}^\dagger &= \sum_{spins} \sum_{f,f'} \frac{1}{8m_f^2 m_{f'}^2} \bar{u}_2 (X_{lk} P_R + X_{lk}^* P_L) v_3 \bar{v}_1 (X_{ij} P_R + X_{ij}^* P_L) u_p \\
 &\quad \times \bar{v}_3 (X'_{ik} P_R + X'_{ik} P_L) v_1 \bar{u}_p (X'_{lj} P_R + X'_{lj} P_L) u_2 \\
 &= \sum_{f,f'} \frac{1}{8m_f^2 m_{f'}^2} \text{Tr}[\not{k}_2 (X_{lk} P_R + X_{lk}^* P_L) \not{k}_3 (X'_{ik} P_R + X'_{ik} P_L) \\
 &\quad \not{k}_1 (X_{ij} P_R + X_{ij}^* P_L) (\not{p} + m_j) (X'_{lj} P_R + X'_{lj} P_L)] \\
 &= \sum_{f,f'} \frac{1}{4m_f^2 m_{f'}^2} \left[X_{lk} X_{ik}^* X_{ij} X'_{lj} (i\epsilon^{\mu\nu\alpha\beta} k_{1\mu} k_{2\nu} k_{3\alpha} p_\beta + (k_1 p)(k_2 k_3)) \right. \\
 &\quad \left. + X_{lk}^* X'_{ik} X_{ij}^* X'_{lj} (-i\epsilon^{\mu\nu\alpha\beta} k_{1\mu} k_{2\nu} k_{3\alpha} p_\beta + (k_1 p)(k_2 k_3)) \right] \\
 &= \sum_{f,f'} \frac{1}{2m_f^2 m_{f'}^2} (k_2 k_3)(k_1 p) \text{Re}(X_{lk} X_{ik}^* X_{ij} X'_{lj}),
 \end{aligned} \tag{6.1.13}$$

where the last step in eq. (6.1.13) the ϵ tensor term vanished because:

$$\epsilon^{\mu\nu\alpha\beta} k_{1\mu} k_{2\nu} k_{3\alpha} p_\beta = \underbrace{\epsilon^{\mu\nu\alpha\beta}}_{\text{antisym.}} \underbrace{k_{1\mu} k_{2\nu} k_{3\alpha} (k_1 + k_2 + k_3)_\beta}_{\text{sym.}} = 0. \tag{6.1.14}$$

Also for the other mixed term:

$$\begin{aligned}
 \frac{1}{2} \sum_{spins} \mathcal{M}_{H,t} \mathcal{M}_{H,s}^\dagger &= \sum_{spins} \sum_{f,f'} \frac{1}{8m_f^2 m_{f'}^2} \bar{u}_2 (X'_{lj} P_R + X'^*_{lj} P_L) u_p \bar{v}_1 (X'_{ik} P_R + X'^*_{ik} P_L) v_3 \\
 &\quad \times \bar{u}_p (X_{ij} P_R + X^*_{ij} P_L) v_1 \bar{v}_3 (X_{lk} P_R + X^*_{lk} P_L) u_2 \\
 &= \sum_{f,f'} \frac{1}{8m_f^2 m_{f'}^2} \text{Tr}[\not{k}_2 (X'_{lj} P_R + X'^*_{lj} P_L) (\not{p} + m_j) (X_{ij} P_R + X^*_{ij} P_L) \\
 &\quad \not{k}_1 (X'_{ik} P_R + X'^*_{ik} P_L) \not{k}_3 (X_{lk} P_R + X^*_{lk} P_L)] \\
 &= \sum_{f,f'} \frac{1}{2m_f^2 m_{f'}^2} (k_2 k_3) (k_1 p) \text{Re}(X_{lk} X'^*_{ik} X_{ij} X'^*_{lj}).
 \end{aligned} \tag{6.1.15}$$

So one get

$$\frac{1}{2} \sum_{spins} \mathcal{M}_{H,t} \mathcal{M}_{H,s}^\dagger + h.c. = \sum_{f,f'} \frac{1}{m_f^2 m_{f'}^2} (k_2 k_3) (k_1 p) \text{Re}(X_{lk} X'^*_{ik} X_{ij} X'^*_{lj}). \tag{6.1.16}$$

The mixed terms involving Z-channel

$$\begin{aligned}
 \frac{1}{2} \sum_{spins} \mathcal{M}_Z \mathcal{M}_{H,s}^\dagger &= \frac{1}{2} \sum_{spins} \frac{-ig^2}{4 \cos^2 \theta_w m_z^2} \sum_f \frac{i}{2m_f^2} \bar{u}_2 \gamma_\mu (o_{lk} P_L - o_{lk}^* P_R) v_3 \bar{v}_1 \gamma^\mu (o_{ij} P_L - o_{ij}^* P_R) u_p \\
 &\quad \times \bar{u}_p (X_{ij} P_R + X^*_{ij} P_L) v_1 \bar{v}_3 (X_{lk} P_R + X^*_{lk} P_L) u_2 \\
 &= \sum_f \frac{g^2}{16m_W^2 m_f^2} \text{Tr}[\not{k}_2 \gamma^\mu (o_{lk} P_L - o_{lk}^* P_R) \not{k}_3 (X_{lk} P_R + X^*_{lk} P_L)] \\
 &\quad \times \text{Tr}[\not{k}_1 \gamma_\mu (o_{ij} P_L - o_{ij}^* P_R) (\not{p} + m_j) (X_{ij} P_R + X^*_{ij} P_L)] \\
 &= 0 \quad (\text{because } m_i = m_l = m_k = 0),
 \end{aligned} \tag{6.1.17}$$

therefore

$$\mathcal{M}_{H,s} \mathcal{M}_Z^\dagger = 0 \quad (m_i = m_l = m_k = 0) \tag{6.1.18}$$

for the s-channel, and

$$\begin{aligned}
 \frac{1}{2} \sum_{spins} \mathcal{M}_z \mathcal{M}_{H,t}^\dagger &= \frac{1}{2} \sum_{spins} \frac{-ig^2}{4 \cos^2 \theta_w m_z^2} \sum_f \frac{i}{2m_f^2} \bar{u}_2 \gamma_\mu (o_{lk} P_L - o_{lk}^* P_R) v_3 \bar{v}_1 \gamma^\mu (o_{ij} P_L - o_{ij}^* P_R) u_p \\
 &\quad \times \bar{v}_3 (X_{ik} P_R + X_{ik}^* P_L) v_1 \bar{u}_p (X_{lj} P_R + X_{lj}^* P_L) u_2 \\
 &= \sum_f \frac{g^2}{16m_w^2 m_f^2} \times \text{Tr}[\not{k}_2 \gamma^\mu (o_{lk} P_L - o_{lk}^* P_R) \not{k}_3 (X_{ik} P_R + X_{ik}^* P_L) \\
 &\quad \not{k}_1 \gamma_\mu (o_{ij} P_L - o_{ij}^* P_R) (\not{p} + m_j) (X_{lj} P_R + X_{lj}^* P_L)] \\
 &= \sum_f \frac{g^2}{m_w^2 m_f^2} \text{Re}(o_{lk} X_{ik} o_{ij}^* X_{lj}^*) (k_1 k_3) (k_2 p),
 \end{aligned} \tag{6.1.19}$$

$$\begin{aligned}
 \frac{1}{2} \sum_{spins} \mathcal{M}_{H,t} \mathcal{M}_z^\dagger &= \frac{1}{2} \sum_{spins} \sum_f \frac{-i}{2m_f^2} \frac{ig^2}{4 \cos^2 \theta_w m_z^2} \bar{u}_2 (X_{lj} P_R + X_{lj}^* P_L) u_p \bar{v}_1 (X_{ik} P_R + X_{ik}^* P_L) v_3 \\
 &\quad \times \bar{u}_p (o_{ij}^* P_R - o_{ij} P_L) \gamma^\nu v_1 \bar{v}_3 (o_{lk}^* P_R - o_{lk} P_L) \gamma_\nu u_2 \\
 &= \sum_f \frac{g^2}{16m_w^2 m_f^2} \text{Tr}[\not{k}_2 (X_{lj} P_R + X_{lj}^* P_L) (\not{p} + m_j) (o_{ij}^* P_R - o_{ij} P_L) \gamma_\nu \\
 &\quad \not{k}_1 (X_{ik} P_R + X_{ik}^* P_L) \not{k}_3 (o_{lk}^* P_R - o_{lk} P_L) \gamma^\nu] \\
 &= \sum_f \frac{g^2}{m_w^2 m_f^2} \text{Re}(o_{lk} X_{ik} o_{ij}^* X_{lj}^*) (k_1 k_3) (k_2 p),
 \end{aligned} \tag{6.1.20}$$

for t-channel.

Combining the results of $\mathcal{M}_Z \mathcal{M}_{H,t}^\dagger$ and $\mathcal{M}_{H,t} \mathcal{M}_z^\dagger$, one get

$$\frac{1}{2} \sum_{spins} \mathcal{M}_Z \mathcal{M}_{H,t}^\dagger + h.c. = \sum_f \frac{2g^2}{m_w^2 m_f^2} \text{Re}(X_{lj}^* X_{ik} o_{ij}^* o_{lk}) (k_1 k_3) (k_2 p). \tag{6.1.21}$$

Total decay width of three-body decay

From the calculations of the process via Z boson, since we set the light neutrinos to be massless, we see that the overall effect of the integration of $(pk_2)(k_1 k_3)$ in the momentum space is to multiply the factor of $|\mathcal{M}|^2$ with $\frac{m_j^5}{64 \times 192 \pi^3}$, so the total decay width of the three-body decay is:

$$\Gamma_{3\nu} = \frac{m_j^5}{64 \times 192 \pi^3} \sum_{i,k,l=1}^3 \left(64 G_F^2 |o_{lk}|^2 |o_{ij}|^2 + \sum_f \frac{2g^2}{m_W^2 m_f^2} \text{Re}(X_{lj}^* X_{ik} o_{ij}^* o_{lk}) \right)$$

$$\begin{aligned}
 & + \sum_{f,f'} \frac{1}{m_f^2 m_{f'}^2} \left[2 \operatorname{Re}(X_{lk} X_{lk}^*) \operatorname{Re}(X_{ij} X_{ij}^*) + 2 \operatorname{Re}(X_{ik} X_{ik}^*) \operatorname{Re}(X_{lj} X_{lj}^*) \right. \\
 & \left. + \operatorname{Re}(X_{lk} X_{ik}^* X_{ij} X_{lj}^*) \right], \tag{6.2.1}
 \end{aligned}$$

where

$$\begin{aligned}
 o_{ij} &= \sum_{a=1}^3 U_{ai} U_{aj}^* \\
 X_{ij} &= \sum_{m,n=1}^3 (Y_\nu)_{mn}^* \eta_f (U_{im} U_{j(n+3)} + U_{jm} U_{i(n+3)}). \tag{6.2.2}
 \end{aligned}$$

Loops

The calculations follow the paper of H.E Haber and Daniel Wyler[23]. The notations in the paper are:

$$\begin{aligned}
 G &= g_L P_L + g_R P_R & F &= f_L P_L + f_R P_R \\
 G^* &= g_L^* P_L + g_R^* P_R & F^* &= f_L^* P_L + f_R^* P_R \\
 \tilde{G} &= g_R P_L + g_L P_R & \tilde{F} &= f_R P_L + f_L P_R \\
 \tilde{G}^* &= g_R^* P_L + g_L^* P_R & \tilde{F}^* &= f_R^* P_L + f_L^* P_R, \tag{6.3.1}
 \end{aligned}$$

where the F and G are the couplings of incoming and outgoing neutrinos respectively. The indices j and i mark the incoming and outgoing neutrino. The I^2 , I , J and K are loop integrals defined as:

$$I = \frac{1}{m_j^2 - m_i^2} \int_0^1 \frac{dx}{1-x} \log \left(\frac{m^2 x + M^2(1-x) - m_j^2 x(1-x)}{m^2 x + M^2(1-x) - m_i^2 x(1-x)} \right) \tag{6.3.2}$$

$$J = \frac{1}{m_j^2 - m_i^2} \int_0^1 \frac{dx}{x} \log \left(\frac{m^2 x + M^2(1-x) - m_j^2 x(1-x)}{m^2 x + M^2(1-x) - m_i^2 x(1-x)} \right) \tag{6.3.3}$$

$$I^2 = \frac{1}{m_j^2 - m_i^2} \int_0^1 dx \log \left(\frac{m^2 x + M^2(1-x) - m_j^2 x(1-x)}{m^2 x + M^2(1-x) - m_i^2 x(1-x)} \right) \tag{6.3.4}$$

$$\begin{aligned}
 K &= \frac{-1}{m_j^2 - m_i^2} \int_0^1 dx \left[1 + \frac{m^2 x + M^2(1-x) - m_j^2 x(1-x)}{x(1-x)(m_j^2 - m_i^2)} \right. \\
 & \quad \left. \times \log \left(\frac{m^2 x + M^2(1-x) - m_j^2 x(1-x)}{m^2 x + M^2(1-x) - m_i^2 x(1-x)} \right) \right]. \tag{6.3.5}
 \end{aligned}$$

m is the mass of the loop fermions and M is the mass of loop bosons.

W^+l Loop

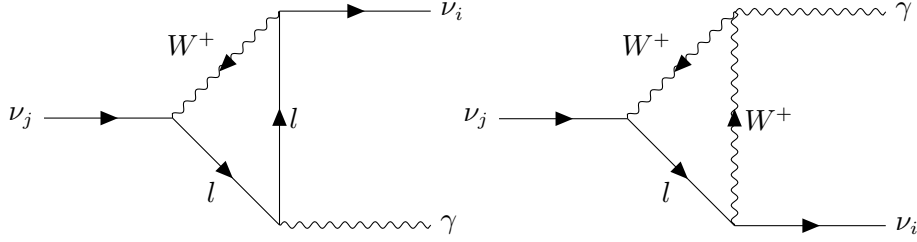


Figure 6.3: The Feynman diagrams of the W^+l loop.

The Feynman diagrams are shown in fig. 6.3. To calculate these loop diagrams, the equation (47) in Haber's paper was used.

$$\begin{aligned}
 \mathcal{M}_w &= eq(47) \\
 &= \frac{-eg^2}{8\pi^2} \sum_k \bar{u}(k_1) [m_j(\tilde{G}\tilde{F} - G^*F^*)(I^2 - J - K) \\
 &\quad - m_i(GF - \tilde{G}^*\tilde{F}^*)(J - K) + 2m_k(\tilde{G}F - G^*\tilde{F}^*)J] \not{k}_2 \not{\epsilon}^* u(p),
 \end{aligned} \tag{6.3.6}$$

where m_k is the loop fermion mass. For this loop, the vertices are (to be consistent with the paper, the coupling constant g and the four-momentum γ_μ are already removed.):

$$F = \underbrace{\sum_{a=1}^3 \frac{1}{\sqrt{2}} U_{ja} U_{L,ma}^{e*}}_{f_L} P_L, \quad G = \underbrace{\sum_{a'=1}^3 \frac{1}{\sqrt{2}} U_{ia'} U_{L,ma'}^{e*}}_{g_L} P_L. \tag{6.3.7}$$

Setting all the known expressions, the matrix element \mathcal{M}_w is therefore:

$$\begin{aligned}
 \mathcal{M}_w &= \sum_{m=1}^6 \frac{-eg^2}{16\pi^2} \bar{u}(k_1) \underbrace{[m_j(I^2 - J - K)]}_A \underbrace{\left(\sum_{a,a'=1}^3 U_{ia'} U_{ja} U_{L,ma}^{e*} U_{L,ma'}^{e*} P_R \right)}_r \\
 &\quad - \underbrace{\sum_{a,a'=1}^3 U_{ia'}^* U_{ja}^* U_{L,ma}^e U_{L,ma'}^e P_L}_{r^*} - \underbrace{m_i(J - K)}_B (rP_L - r^*P_R) \not{k}_2 \not{\epsilon}^* u(p) \\
 &= \sum_{m=1}^6 \frac{-eg^2}{16\pi^2} \bar{u}(k_1) [(Ar + Br^*)P_R - (Ar^* + Br)P_L] \not{k}_2 \not{\epsilon}^* u(p) \\
 &= \sum_{m=1}^6 \frac{-eg^2}{16\pi^2} \bar{u}(k_1) [(A - B)(r - r^*) + (A + B)(r + r^*)\gamma_5] \not{k}_2 \not{\epsilon}^* u(p) \\
 &= \sum_{m=1}^6 \frac{-eg^2}{16\pi^2} \bar{u}(k_1) [a_w + b_w \gamma_5] \not{k}_2 \not{\epsilon}^* u(p) \\
 \mathcal{M}_w^\dagger &= \sum_{m=1}^6 \frac{-eg^2}{16\pi^2} \bar{u}(p) \not{\epsilon} \not{k}_2 [a_w^* - b_w^* \gamma_5] u(k_1),
 \end{aligned} \tag{6.3.8}$$

where

$$A = m_j(I^2 - J - K), \quad B = m_i(J - K), \quad r = \sum_{a,a'=1}^3 U_{ia'} U_{ja} U_{L,ma}^{e*} U_{L,ma'}^{e*} \tag{6.3.9}$$

$$a_w = 2i(A - B) \text{Im}(r) \quad b_w = 2(A + B) \text{Re}(r).$$

$\tilde{\chi}^+ \tilde{l}$ Loop

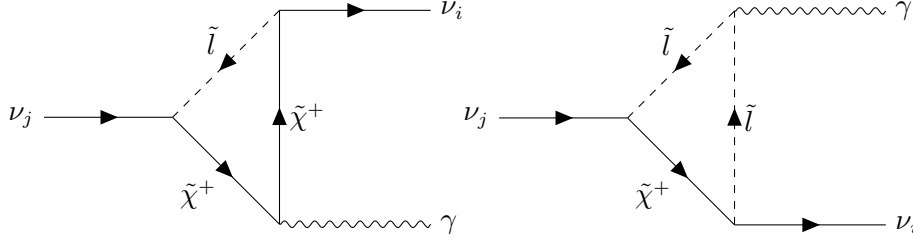
To calculate this loop, the equation (51) in Haber's paper is used:

$$\begin{aligned}
 \mathcal{M}_s &= \frac{-eg^2}{32\pi^2} \sum_c e_c \bar{u}(k_1) [m_j(G\tilde{F} - \tilde{G}^* F^*)(I^2 - K) \\
 &\quad + m_i(\tilde{G}F - G^* \tilde{F}^*)K + m_c(GF - \tilde{G}^* \tilde{F}^*)I] \not{k}_2 \not{\epsilon}^* u(p),
 \end{aligned} \tag{6.3.10}$$

m_c is the chargino mass.

The Feynman diagrams are shown in fig. 6.4. $f_{L/R}$, $G_{L/R}$ are defined as:

$$\begin{aligned}
 g_L &= d_{iab}^L, & g_R &= d_{iab}^R \\
 f_L &= d_{jab}^L, & f_R &= d_{jab}^R.
 \end{aligned} \tag{6.3.11}$$


Figure 6.4: The Feynman diagrams of the $\tilde{\chi}^+ \tilde{l}$ loop.

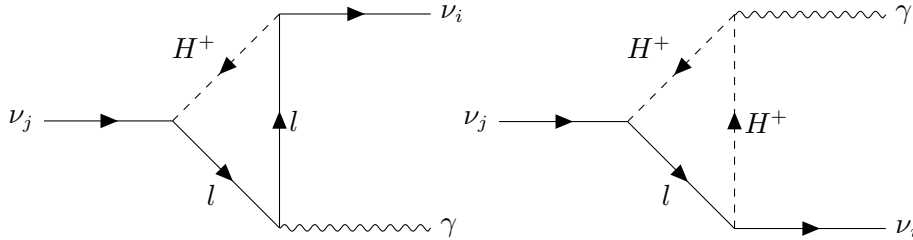
The matrix elements are:

$$\begin{aligned} \mathcal{M}_c &= \sum_c \frac{-eg^2}{32\pi^2} \bar{u}(k_1) [a_c + b_c \gamma^5] \not{k}_2 \not{\epsilon}^* u(p) \\ \mathcal{M}_c^\dagger &= \sum_c \frac{-eg^2}{32\pi^2} \bar{u}(p) \not{\epsilon} \not{k}_2 [a_c^* - b_c^* \gamma^5] u(k_1), \end{aligned} \quad (6.3.12)$$

where the abbreviations are:

$$\begin{aligned} A_c &= m_j(I^2 - K), \quad B_c = m_i K, \quad C_c = m_c I; \\ O_1 &= d_{iab}^R d_{jab}^L - d_{iab}^{L*} d_{jab}^{R*} \\ O_2 &= d_{iab}^R d_{jab}^R - d_{iab}^{L*} d_{jab}^{L*} \\ a_c &= 2i[(A + B) \text{Im}(O_1) + C \text{Im}(O_2)] \\ b_c &= 2[(A - B) \text{Re}(O_1) + C \text{Re}(O_2)]. \end{aligned} \quad (6.3.13)$$

$H^+ l$ Loop


Figure 6.5: The Feynman diagrams of the $H^+ l$ loop.

This loop also uses the equation (51) from Haber's paper:

$$\begin{aligned} \mathcal{M}_h &= \frac{-eg^2}{32\pi^2} \sum_l e_l \bar{u}(k_1) [m_j (G\tilde{F} - \tilde{G}^* F^*) (I^2 - K) \\ &\quad + m_i (\tilde{G}F - G^* \tilde{F}^*) K + m_l (GF - \tilde{G}^* \tilde{F}^*) I] \not{k}_2 \not{\epsilon}^* u(p), \end{aligned} \quad (6.3.14)$$

m_l is the loop lepton mass. The Feynman diagrams are shown in fig. 6.5. The matrix elements are:

$$\begin{aligned}\mathcal{M}_h &= \sum_l \frac{-eg^2}{32\pi^2} \bar{u}(k_1) [a_h + b_h \gamma^5] \not{k}_2 \not{\epsilon}^* u(p) \\ \mathcal{M}_h^\dagger &= \sum_l \frac{-eg^2}{32\pi^2} \bar{u}(p) \not{\epsilon} \not{k}_2 [a_h^* - b_h^* \gamma^5] u(k_1),\end{aligned}\tag{6.3.15}$$

where the abbreviations are:

$$\begin{aligned}A_h &= m_j(I^2 - K), \quad B_h = m_i K, \quad C_h = m_l I; \\ O_1 &= g_R f_L - g_L^* f_R^* = D_{imn}^R D_{jmn}^L - D_{imn}^{L*} D_{jmn}^{R*} \\ O_2 &= g_R f_R - g_L^* f_L^* = D_{imn}^R D_{jmn}^R - D_{imn}^{L*} D_{jmn}^{L*},\end{aligned}\tag{6.3.16}$$

$$\begin{aligned}a_h &= 2i[(A + B) \text{Im}(O_1) + C \text{Im}(O_2)] \\ b_h &= 2[(A - B) \text{Re}(O_1) + C \text{Re}(O_2)].\end{aligned}\tag{6.3.17}$$

Decay width

Take W^+l loop as an example, the $|\mathcal{M}_w|^2$ is:

$$\begin{aligned}\frac{1}{2} \sum_{spins} \sum_{pol} |\mathcal{M}|^2 &= \frac{1}{2} \sum_{spins} \sum_{pol} \sum_{i=1}^3 \frac{e^2 g^4}{16^2 \pi^4} \bar{u}(k_1) [a_w + b_w \gamma^5] \not{k}_2 \not{\epsilon}^* u(p) \bar{u}(p) \not{\epsilon} \not{k}_2 \\ &\quad \times [a_w'^* - b_w'^* \gamma^5] u(k_1) \\ &= \sum_{i=1}^3 \sum_{pol} \frac{e^2 g^4}{2 \times 16^2 \pi^4} \text{Tr}[(\not{k}_1 + m_i)(a_w + b_w \gamma^5) \not{k}_2 \not{\epsilon}^* (\not{p} + m_j) \not{\epsilon} \not{k}_2 (a_w'^* - b_w'^* \gamma^5)] \\ &= \sum_{i=1}^3 \frac{e^2 g^4}{2 \times 16^2 \pi^4} \times 16 \underbrace{(k_1 k_2)(k_2 p)}_{\frac{1}{4}(m_j^2 - m_i^2)^2} (a_w a_w'^* + b_w b_w'^*) \\ &= \sum_{i=1}^3 \frac{e^2 g^4}{128 \pi^4} (m_j^2 - m_i^2)^2 (a_w a_w'^* + b_w b_w'^*),\end{aligned}\tag{6.3.18}$$

where the summation over loop fermions are already contained in the matrix elements, the prime ' is used to make a difference when performing summations.

Combining all the results above, the total $|\mathcal{M}|^2$ is:

$$\frac{1}{2} \sum_{spins} \sum_{pol} |\mathcal{M}_{total}|^2 = \tag{6.3.19}$$

$$\begin{aligned}
 & \sum_{i=1}^3 \frac{e^2 g^4 (m_j^2 - m_i^2)^2}{4 \times 128 \pi^4} [4(a_w a_w'^* + b_w b_w'^*) + (a_h a_h'^* + b_h b_h'^*) + (a_c a_c'^* + b_c b_c'^*) \\
 & + 2(a_w a_h^* + b_w b_h^*) + 2(a_w a_c^* + b_w b_c^*) + 2(a_h a_w^* + b_h b_w^*) \\
 & + (a_h a_c^* + b_h b_c^*) + 2(a_c a_w^* + b_c b_w^*) + (a_c a_h^* + b_c b_h^*)].
 \end{aligned} \tag{6.3.20}$$

Define what's within the bracket as g_{coup} , the total decay width is then:

$$\begin{aligned}
 \Gamma &= \sum_{i=1}^3 \int \frac{1}{32\pi^2} \frac{p'}{E^2} |\mathcal{M}|^2 d\Omega \\
 &= \sum_{i=1}^3 \frac{e^2 g^4}{4 \times 128 \pi^4} \frac{1}{32\pi^2} \frac{(m_j^2 - m_i^2)^3}{2m_j^5} g_{coup} m_j^2 \times 4\pi \\
 &= \sum_{i=1}^3 \frac{\alpha^3}{256\pi^2 \sin^4 \theta_w} \frac{(m_j^2 - m_i^2)^3}{m_j^5} g_{coup} m_j^2 \\
 &= \sum_{i=1}^3 \frac{(m_j^2 - m_i^2)^3}{8\pi m_j^5} \underbrace{\frac{\alpha^3}{32\pi \sin^4 \theta_w} g_{coup} m_j^2}_{:=g_{\nu_j \nu_i \gamma}^2},
 \end{aligned} \tag{6.3.21}$$

where during the calculations the following relations are used:

$$\begin{aligned}
 p' &= \frac{1}{2\sqrt{s}} [s - (m'_1 + m'_2)^2][s - (m'_1 - m'_2)^2]^{\frac{1}{2}} \\
 &= \frac{m_j^2 - m_i^2}{2m_j} \quad (\text{with } s = m_j^2, \quad m'_1 = m_i, \quad m'_2 = 0), \\
 \alpha &= \frac{e^2}{4\pi}, \\
 g &= \frac{e}{\sin \theta_w}.
 \end{aligned} \tag{6.3.22}$$

Approximation

The loop integral can be rewritten using dilogarithm

$$\text{Li}_2(z) = - \int_0^z \frac{\log(1-u)}{u} du \tag{6.3.23}$$

as[23]²

$$\begin{aligned}
 I &= \frac{-1}{m_j^2 - m_i^2} \left[\text{Li}_2 \left(\frac{m_j^2 + m^2 - M^2 + \lambda_j^{1/2}}{2m^2} \right) + \text{Li}_2 \left(\frac{m_j^2 + m^2 - M^2 - \lambda_j^{1/2}}{2m^2} \right) \right. \\
 &\quad \left. - \text{Li}_2 \left(\frac{m_i^2 + m^2 - M^2 + \lambda_i^{1/2}}{2m^2} \right) - \text{Li}_2 \left(\frac{m_i^2 + m^2 - M^2 - \lambda_i^{1/2}}{2m^2} \right) \right] \\
 I + J &= \frac{1}{m_j^2 - m_i^2} \left[\log^2 \left(\frac{m^2 + M^2 - m_j^2 + \lambda_j^{1/2}}{2mM} \right) - \log^2 \left(\frac{m^2 + M^2 - m_i^2 + \lambda_i^{1/2}}{2mM} \right) \right] \\
 \lim_{m, M \rightarrow \infty} I^2 &= \frac{-1}{(M^2 - m^2)^2} \left[\frac{m^2 + M^2}{2} - \frac{m^2 M^2}{M^2 - m^2} \log \left(\frac{M^2}{m^2} \right) \right] \\
 K &= \frac{-1}{m_j^2 - m_i^2} \left[1 + m^2 I + M^2 J - m_j^2 I^2 \right].
 \end{aligned} \tag{6.3.24}$$

When considering keV range neutrinos, the loop integrals I , J and K can be simplified using the expansion around 0 to the second order with respect to

$$y = \left(\frac{m}{M} \right)^2 \quad x = \left(\frac{m_j}{M} \right)^2 \tag{6.3.25}$$

as

$$\begin{aligned}
 I &= \frac{1}{36M^2} \left\{ 2(93y^2 + 42y + 11)x^2 + 9(8y^2 + 6y + 1)x \right. \\
 &\quad \left. + 6 \left[2(18y^2 + 6y + 1)x^2 + 3(8y^2 + 4y + 1)x + 6(2y^2 + 2y + 1) \right] \log(y) + 36 \right\} \\
 J &= \frac{1}{36M^2} \left\{ (-78y^2 + 24y + 14)x^2 - 9(4y^2 - 2y - 3)x \right. \\
 &\quad \left. - 18y \left[2(5y + 1)x^2 + (7y + 2)x + 4y + 2 \right] \log(y) - 36 \right\} \\
 K &= \frac{1}{144M^2} \left\{ 3 \left[5(6y^2 - 11y - 5) + 36y(6y + 1) \log(y) \right] x^2 + 36y \left[2 \log(y) - 3 \right] \right. \\
 &\quad \left. + 8 \left[-3y^2 + 6(9y + 2) \log(y)y - 23y - 7 \right] x + 72y^2 \left[3 \log(y) - 1 \right] \right. \\
 &\quad \left. + \frac{36 \left(3m^6 - 7M^2 m^4 + 9M^4 m^2 + 4M^4 \log \left(\frac{M^2}{m^2} \right) m^2 - 5M^6 \right)}{(M^2 - m^2)^3} - \frac{144y}{x} \right\}.
 \end{aligned} \tag{6.3.26}$$

²A small remark should be given here, the sign of the third term of I in the original expression is wrong.

For I^2 both the approximation

$$\begin{aligned}
 I^2 = & x \left[y \left(-\frac{23 - 12 \log(y)}{18M^2} - \frac{1}{3M^2} \right) - \frac{1}{18M^2} \right] + y \left(-\frac{3 - 2 \log(y)}{4M^2} - \frac{2}{M^2} \right) \\
 & + \frac{1}{x^2} \left(\frac{\log(y)}{2M^2} - \frac{y \log(y)}{2M^2} \right) + \frac{1}{x} \left[-\frac{\log(y)}{2M^2} + y \left(-\frac{\log(y)}{M^2} - \frac{3}{2M^2} \right) + \frac{1}{M^2} \right] \\
 & - \frac{7}{4M^2}
 \end{aligned} \tag{6.3.27}$$

and the expression given in eq. (6.3.24) are used. Therefore mixed notations show up in the approximation of K . All the approximations are implemented in **SPheno-4.0.3** for the later use of numerical calculations.

7 Numerical Results Model I

The numerical results of the first model is shown and discussed in this section. The neutrino DM scenario was first probed to see how decay widths and branching ratios change with the variation of various parameters. Later it is shown that the sterile neutrino DM is excluded by *NuSTAR* data. The sneutrino DM scenario is tested with *micrOMEGAS* which is also ruled out due to the overproduced relic density.

Neutrino Decay

The inverse of the decay width is the life time of the particle, which should be significantly larger than the age of the Universe, i.e[21]

$$13.80 \pm 0.04 \text{ Gyr} \sim 4.35 \cdot 10^{17} s = 6.61 \times 10^{41} \text{ GeV}^{-1}. \quad (7.1.1)$$

For later comparison with the astronomical data, the decay widths are calculated with varied variables. The calculations are done with *SPheno-4.0.3* using Model *SeesawIe*. *SPheno* is generated by the *SARAH-4.9.0* which calculates all the desired decay widths. The parameterization in chapter 4 is written additionally in the *Mathematica* notebook `calDiagonal.nb`¹ which changes the *SPheno* input file `LesHouches.in.SeesawIe`.

The constant parameters and the variables are listed in the table 7.1. The variation intervals are set according to the former work published in [9]. Only one variable are varied at one time, the results are read from the *SPheno.spc.SeesawIe* files.

The branching ratio of three-body decay is about 88% and of radiative decay is about 11%, as shown in figs. 7.1a and 7.1c. They remain almost constant for different variables except for neutrino mass $M_{\nu 4}$. Thus in the following only the branching ratio plotted against $M_{\nu 4}$ is discussed. Equation eq. (4.1.7) indicates that the γ adjusts the amplitude of the trigonometric function \sin and \cos and thus the amplitude of the neutrino mixing matrix U , where ρ adjusts the phase.

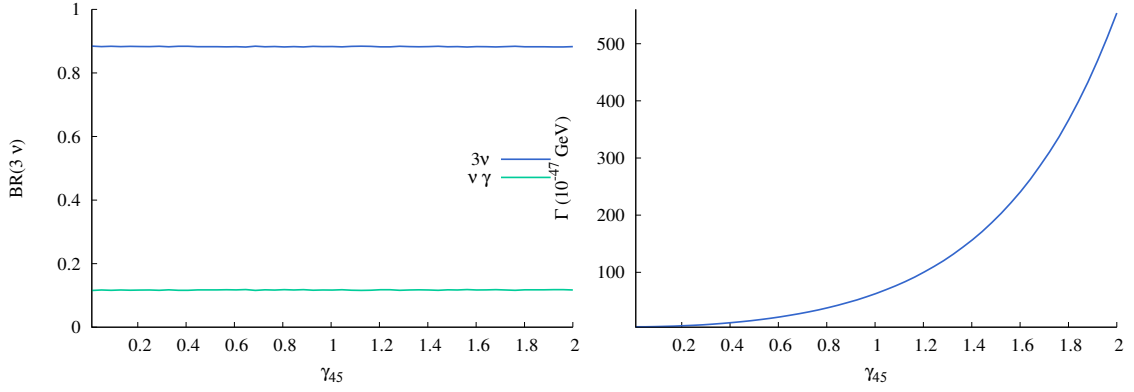
¹This `.nb` file is written by J. Jones-Pérez.

Constants		Varied Parameters		
Parameter	Value	Parameter	Value	Variation Interval
$\sin \theta_{12}$	$\sqrt{0.304}$	$m_{\nu,4}$	$7 \cdot 10^{-6} \text{ GeV}$	$[1 \text{ keV}, 1 \text{ GeV}]$
$\sin \theta_{13}$	$\sqrt{0.0218}$	ρ_{56}	0.02	$[0, 2\pi]$
$\sin \theta_{23}$	$\sqrt{0.452}$	ρ_{46}	0.01	$[0, 2\pi]$
δ, β_1, β_1	0	ρ_{45}	0.03	$[0, 2\pi]$
Δm_{atm}^2	$2.457 \cdot 10^{-3} \text{ eV}^2$	γ_{56}	8	$[0.01, 2]$
Δm_{sol}^2	$7.50 \cdot 10^{-5} \text{ eV}^2$	γ_{46}	0.14	$[0.01, 2]$
$m_{\nu 1}$	$1 \cdot 10^{-7} \text{ GeV}$	γ_{45}	0.01	$[0.01, 2]$
$m_{\nu 5}$	20 GeV	$T_{e,33}$	0	$ T_{e,33} \leq 1 \text{ TeV} \frac{m_\tau}{m_w} \tan \beta$
$m_{\nu 6}$	20.001 GeV	$\tan \beta$	10	$[5, 10]$
Constants used in MSSM		$M_{\tilde{L}}^2$	$(475 \text{ GeV})^2$	$[(450 \text{ GeV})^2, (1 \text{ TeV})^2]$
Parameters	Value	$M_{\tilde{E}}^2$	$(525 \text{ GeV})^2$	$[(200 \text{ GeV})^2, (1 \text{ TeV})^2]$
M_1, M_2	$1 \cdot 10^3 \text{ GeV}$			
M_3	$1.8 \cdot 10^3 \text{ GeV}$			
M_{A^0}	$2 \cdot 10^3 \text{ GeV}$			

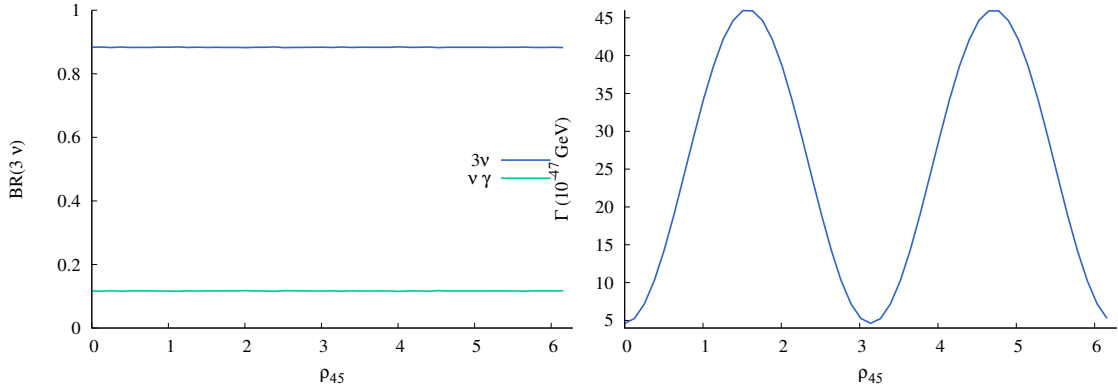
Table 7.1: The parameters and variation intervals used to generate the plots.

As can be seen from fig. 7.1b, because the mixing matrix depends on $\sinh \gamma$ and $\cosh \gamma$, the decay width increases exponentially with respect to γ_{45} . The ρ_{45} cause the decay width to oscillate sinusoidally as shown in fig. 7.1d, which confirms that ρ_{45} is an overall phase factor of the mixing matrix. The θ'_{46} component behaves the same as θ'_{45} since 5,6 components of ν_R are degenerated, the related plots are thus omitted here. Also it is shown in figs. 7.1e and 7.1f that γ_{56} and ρ_{56} does not affect the decay width of ν_4 . This is what is expected since this part controls the decay of $\nu_{R,5}$ and $\nu_{R,6}$ instead of $\nu_{R,4}$.

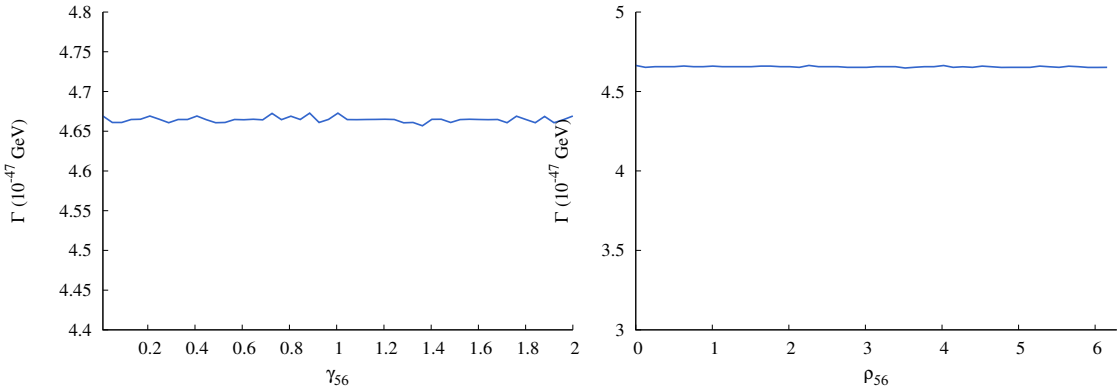
Part of the plots of varied $\tan \beta, T_e(3, 3), M_{\tilde{L}}$ and $M_{\tilde{E}}$ are shown in fig. 7.2. As can be seen from figs. 7.2a to 7.2c and 7.2e, the total decay width remains almost constant while changing these variables. The fluctuations around the constant value are caused by numerical instabilities within the loop integrals. The calculations are improved by using the approximations of loop integrals. In figs. 7.2d and 7.2f the decay widths of three-body decay increase with the increasing $M_{\tilde{L}}$ and $M_{\tilde{E}}$. This is caused by the loop correction of the coupling g . But as can be seen from the plots, this is a negligible effect.



(a) Branching ratios of three-body and radiative decays varied with γ_{45} . (b) The total decay width varied with γ_{45} .

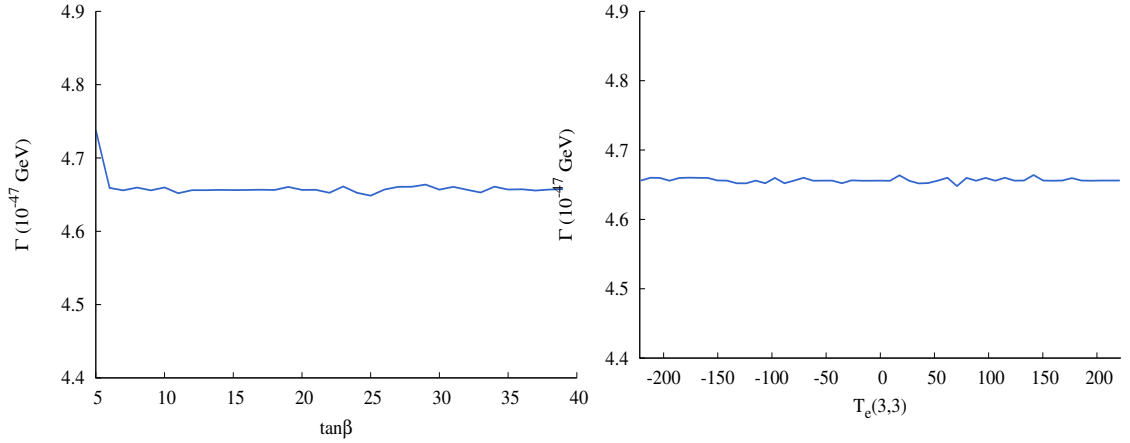


(c) Branching ratios of three-body and radiative decays varied with ρ_{45} . (d) The total decay width varied with ρ_{45} .

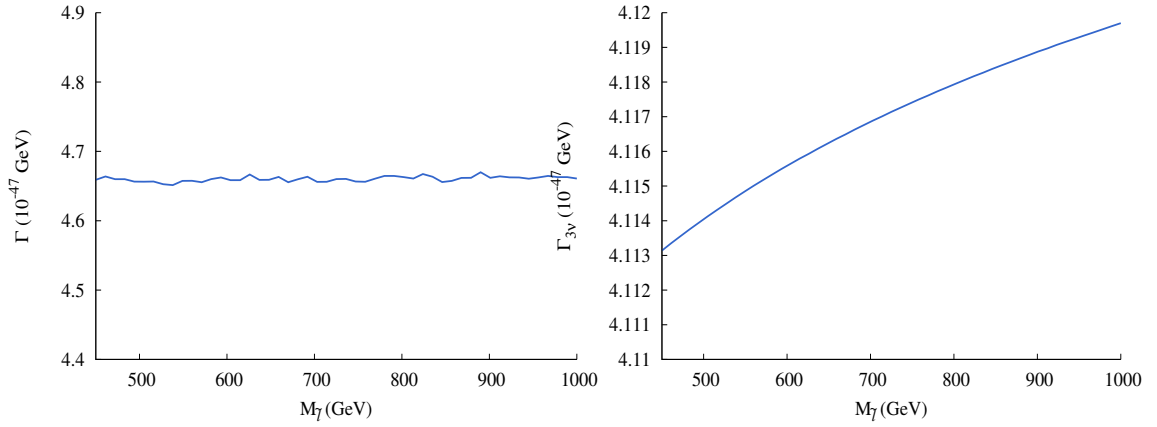


(e) The total decay width varied with γ_{56} . (f) The total decay width varied with ρ_{56} .

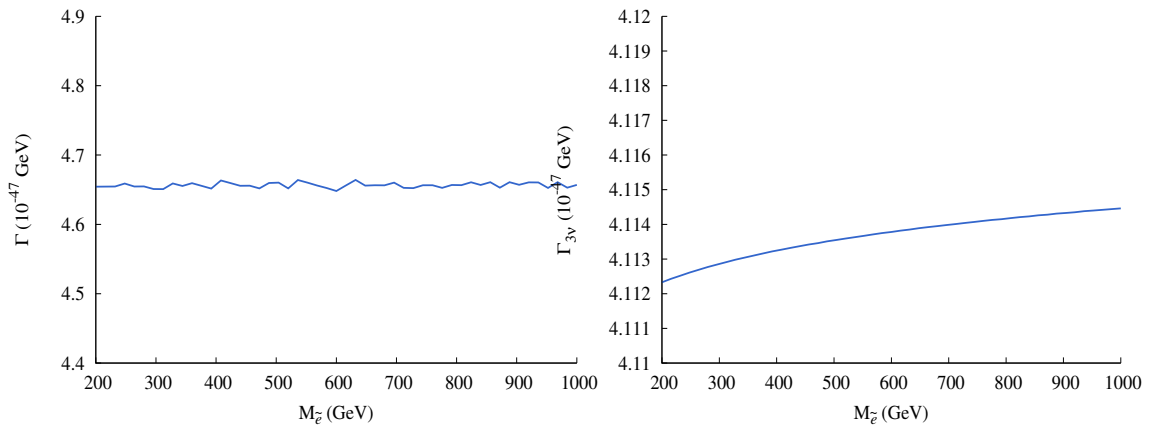
Figure 7.1: The branching ratios of three-body and radiative decays and the total decay width of ν_4 plotted against varied γ_{45} and ρ_{45} . As shown in figs. 7.1a and 7.1c, the branching ratios stay almost constant and the three-body decay is the dominate process. The decay width changes exponentially with respect to γ_{45} because the neutrino mixing matrix depends on $\sinh \gamma_{45}$ and $\cosh \gamma_{45}$. The sinusoidal variation of the decay width confirms that ρ_{45} is an overall phase factor of the neutrino mixing matrix. Figures 7.1e and 7.1f show that the decay widths of ν_4 do not depend on the 56 component of neutrino mixing matrix.



(a) The total decay width varied with $\tan\beta$. (b) The total decay width varied with $T_e(3,3)$.

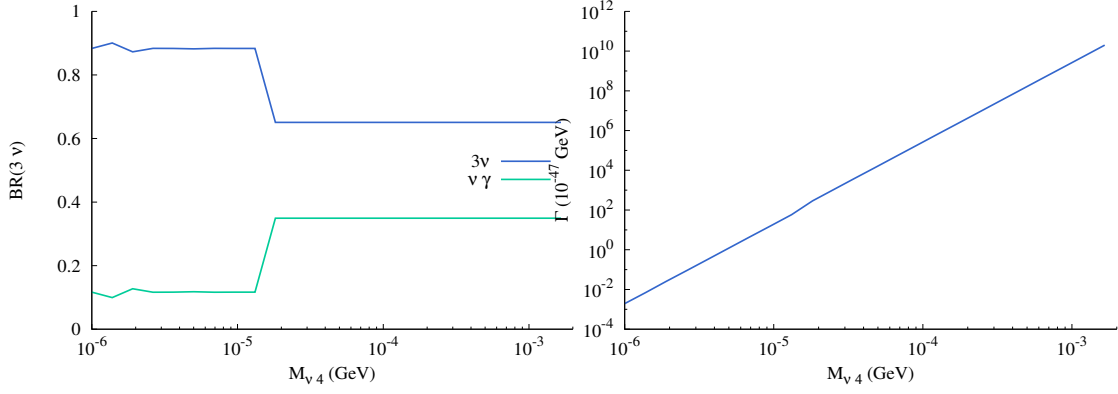


(c) The total decay width varied with $M_{\tilde{l}}$. (d) Decay width of three-body decay varied with $M_{\tilde{l}}$.

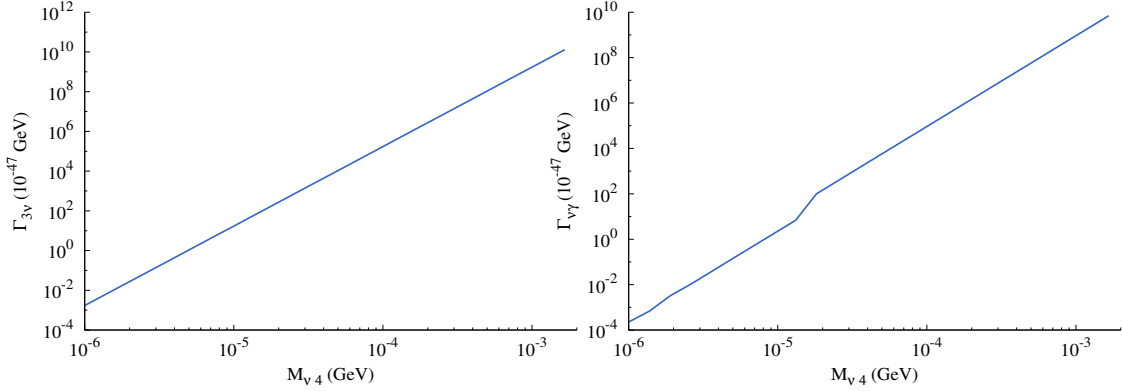


(e) The total decay width varied with $M_{\tilde{e}}$. (f) Decay width of three-body decay varied with $M_{\tilde{e}}$.

Figure 7.2: The decay widths plotted against $\tan\beta$, $M_{\tilde{l}}$, $M_{\tilde{e}}$ and $T_e(3,3)$. Figures 7.2a to 7.2c and 7.2e show that decay widths of ν_4 do not change significantly with respect to $\tan\beta$ and $T_e(3,3)$. Varying $M_{\tilde{l}}$, $M_{\tilde{e}}$ will change the coupling g and therefore cause the decay widths in figs. 7.2d and 7.2f increase slightly.



(a) The branching ratios of three-body and radiative decays. (b) The total decay width of ν_4 .



(c) The decay width of three-body decay. (d) The decay width of radiative decay.

Figure 7.3: The branching ratios and decay widths of three-body and radiative decays varied with M_{ν_4} . The little "kink" around 10^{-5} GeV is caused by the calculations of loop integrals. This is strongly suppressed by applying approximations of loop integrals. Only the variations between keV and MeV are shown, since heavier neutrinos decay too fast so that they can not be potential DM candidates any more.

According to the analytical calculations, the decay width of ν_4 is proportional to $M_{\nu_4}^5$. This describes the decay widths well. Notice that the kink shown in fig. 7.3d between $M_{\nu_4} = 10^{-5}$ and 10^{-4} GeV is caused by the calculations of loop integrals. This kink is already strongly suppressed by applying approximations of loop integrals. Note that only variations from 1 keV to 1 MeV is shown here. The decay width increases after 1 MeV which shows that the neutrinos decay too fast so that they can not be potential DM candidates any more.

$M_{4\nu}$ (keV)	min. $\sin^2 2\theta$
7	$3.38462 \cdot 10^{-9}$
20	$1.18462 \cdot 10^{-9}$
30	$7.89744 \cdot 10^{-10}$
40	$5.92308 \cdot 10^{-10}$
50	$4.73847 \cdot 10^{-10}$

Table 7.2: The mixing angles in the considered model calculated using eq. (5.2.3) by taking the smallest γ_{45} and γ_{46} value. Comparing with the bounds shown in fig. 5.2 the minimum calculated values are 3-4 magnitudes higher than the bounds. The considered model for the keV range sterile neutrino dark matter scenario is excluded.

The results are compared with the *NuSTAR* bounds[17], where both the upper limit of decay width and the mixing angle $\sin^2 2\theta$ are given assuming the DM decays 100% through radiative decay and the neutrinos are generated by Shi-Fuller mechanism. The bounds are given in fig. 5.2. The mixing angles in this model is calculated using eq. (5.2.3) and the results are listed in table 7.2. For fixed neutrino masses, only γ and ρ affects the mixing matrix. Since γ adjusts the amplitude, the minimums are achieved with the minimum values of γ_{45} and γ_{46} , i.e. 0.01. Comparing with the bounds in fig. 5.2 the calculated minimum values are 3-4 orders of magnitude higher than the given bounds. From former calculations one can see that the branching ratio of radiative decays are about 10%, even considering this factor there are still 2-3 orders of magnitude differences. Thus if all the requirements in [17] are fulfilled, the considered model for the keV range sterile neutrino dark matter is excluded.

Sneutrino Relic Density

The relic density is calculated with `micrOMEGAS-4.3.5`. At first a random point that is generated during the calculation of neutrino decays is tested. This yields $\Omega h^2 = 1.34 \cdot 10^7$. To bring down the relic density, the idea is to adjust the parameters that effect the sneutrino mass and coupling. As shown in eq. (4.1.10) this involves Y_ν , $m_{\tilde{\nu}}^2$, $m_{\tilde{L}}^2$, $\tan \beta$ and T_ν .

The μ parameter is fixed at 120 GeV, the gaugino masses are fixed at 1 TeV, 1 TeV and 1.8 TeV respectively. First Y_ν is changed. When $Y_\nu(1, i) \approx 10^{-12}$, $i = 1, 2, 3$, the relic density is $\Omega h^2 \approx 10^7$. Adjusting $\gamma_{45} = 8$ and $M_{\nu_4} = 7$ GeV to enhance $Y_\nu(1, 1)$ to 10^{-5} while keeping the masses of the lightest neutrino below the pre-

Constants					
Para.	μ	M_1	M_2	M_3	B_μ
Value	120 GeV	10^3 GeV	10^3 GeV	$1.8 \cdot 10^3$ GeV	$3.96 \cdot 10^5$ GeV
Variation					
Variable	Values				Magn. of Ωh^2
Y_ν	10^{-12}				10^7
	$\gamma_{45} = 8, M_{\nu 4} = 7 \text{ GeV} \rightarrow Y_{\nu,1} = 10^{-5}$				10^2
M_i^2	$(450 \text{ GeV})^2$				10^7
	$(750 \text{ GeV})^2$				10^7
$M_{\tilde{\nu}}^2$	$1600(\text{ GeV})^2$				10^7
	$8000(\text{ GeV})^2$				10^2
$Y_\nu, M_{\tilde{\nu}}^2$	$Y_{\nu,1} = 10^{-5}, M_{\tilde{\nu}}^2 = 8000(\text{ GeV})^2$				10
$T_{\nu,(1,2,3)}$	0				10^7
	100				10
$M_{\tilde{\nu}}^2, T_\nu$	$M_{\tilde{\nu}}^2 = 8000(\text{ GeV})^2, T_\nu = 100$				10^{-1}
$M_{\tilde{\nu}}^2, T_\nu, Y_{\nu,1}$	$M_{\tilde{\nu}}^2 = 6000(\text{ GeV})^2, T_\nu = 100, Y_{\nu,1} = 10^{-5}$				10^{-2}

Table 7.3: The variations of different parameters in changing the relic density. All the three components of $M_{\tilde{\nu}}^2$ and T_ν are set with the same value in this table. Only the magnitudes of Ωh^2 is listed. If not specified, all the other parameters are set with standard values listed in table 7.1.

dicted bounds, yields $\Omega h^2 \approx 10^2$. The soft-breaking masses are then changed. Setting $m_{\tilde{L}}^2 = (450 \text{ GeV})^2$ while keeping all the other parameters at standard values (10 keV ν_4) has almost no effect to bring down the relic density. Raising $m_{\tilde{\nu}_R}^2$ will change the relic density significantly, adjusting from $1600(\text{ GeV})^2$ to $8000(\text{ GeV})^2$ will reduce five orders of the Ωh^2 magnitude. Combining the Yukawa and $m_{\tilde{\nu}_R}^2 = 6000 \text{ GeV}^2$ gives $\Omega h^2 \sim 10^1$. Changing $\tan \beta$ does not change the magnitude of Ωh^2 , but changing T_ν does have large impact. When set all three generations of T_ν to 100 and keeping all the other parameters at standard values, Ωh^2 will change from 10^7 to 10^1 . Setting together $m_{\tilde{\nu}_R}^2 = 8000 \text{ GeV}^2$ and $T_\nu = 100$ will yield $\Omega h^2 \sim 10^{-1}$. Combining the results from Yukawa sector, $T_\nu = 100$ and $m_{\tilde{\nu}_R}^2 = 6000 \text{ GeV}^2$ yields $\Omega h^2 \sim 10^{-2}$. For the scalar potential to be stable, the global minimum is usually studied. When the trilinear coupling acquires large value, the minimum of the potential will likely become a local minimum and this local minimum might induce a charge violating effects which are not observed by experiments. Therefore the considered model with keV range sterile neutrino is for $\tilde{\nu}_R$ DM excluded. The variations are listed in table 7.3.

8 Numerical Results Model II

The BLSSM provides two additional Higgs singlets, one of them can be adjusted to around or below 125 GeV, which provides a *Higgs-Funnel* that consumes the over-produced sneutrino DM and in the meanwhile generates the sterile neutrinos non-thermally. This scenario will solve the dilemma met in the supersymmetric minimal inverse-seesaw model and make the lightest right-handed sneutrinos a potential DM candidate. The new Higgs bosons do not interact with the left-handed neutrinos and thus will not change the decay widths of ν_4 significantly. The neutrino DM scenario has the same behavior as in the first model, thus in the following discussion, the sneutrino is considered as the only DM candidate.

The setup of the Higgs-funnel in acquiring relic density ~ 0.1 requires several fine-tunings, this involves parameters shown up in the mass matrices of the Higgs boson and sneutrino, since building up a Higgs-funnel requires $m_h/2 \simeq m_{\tilde{\nu}}$. To have a rough idea of adjusting the Higgs mass m_h , it is sufficient only considering the lower-right block of eq. (4.3.5) when neglecting the gauge-kinetic mixing, i.e. $\bar{g} = 0$. Even considering the gauge-kinetic mixing, the mass eigenvalues can also be approximated in the same way. Since m_{A^0} is about several TeV, when taking first order approximation[12], the mass matrix eq. (4.3.5) can be approximated by

$$m_{h,T}^2 \approx \begin{pmatrix} m_{H_u, H_d}^2 & 0 \\ 0 & m_{\eta, \bar{\eta}}^2 \end{pmatrix}. \quad (8.0.1)$$

Each of the two blocks will contribute a light higgs eigenstate. The higgs boson of interest will then come from the lower 2×2 block. When the masses of pseudoscalar and Z' are set to be constants, the second Higgs mass only depends on $\tan \beta'$.

The Z' mass is fixed to be 4.2 TeV, the vev $v_{\bar{\eta}}$ is solved out using eq. (4.3.8) which yields

$$v_{\bar{\eta}} = \frac{M_{z'}}{g_{BL} \sqrt{1 + \tan^2 \beta'}} \quad v_{\eta} = v_{\bar{\eta}} \tan \beta'. \quad (8.0.2)$$

The vevs are set into the matrix, the gauge coupling g_{BL} is taken to be 0.55, the eigenvalues of Higgs mass matrix are then solved out by `Mathematica`. The approximated sneutrino masses in eq. (4.3.10) are set to be equal to half of the

smaller eigenvalue. Note that, the original idea is to reconstruct the same mass hierarchy as the minimal inverse-seesaw model, where the lightest two sneutrinos are almost degenerate. In the BLSSM there are 12 physical sneutrino states, the lightest real and imaginary ones are therefore the lightest sneutrinos. In the analysis, the mass of the imaginary sneutrino is set to be 0.5 GeV smaller than the real one. One can easily find out that the approximations eq. (4.3.10) has the structure

$$m_{\tilde{\nu}^S}^2 = A + B = \frac{m_h^2}{2} \quad m_{\tilde{\nu}^P}^2 = A - B = \frac{m_h^2}{2} - 2B. \quad (8.0.3)$$

The mass difference demands that $m_{\tilde{\nu}^S} - m_{\tilde{\nu}^P} = 0.5$ GeV, this means

$$B = M_{Z'} \frac{\sqrt{2}Y_x}{g_{BL}} (A_x \sin \beta' - \mu' \cos \beta') = 2\Delta \frac{m_h}{r} - \Delta^2, \quad (8.0.4)$$

where Δ is the mass difference, here it is set to be 0.5 GeV, and $r = m_h/m_{\tilde{\nu}}$ denotes the mass ratio. For Higgs-funnel r is equal to 2.

The parameter $A_x(1, 1)$, Yukawa coupling $Y_X(1, 1)$, soft-breaking term $m_{\nu^c}^2$ and $\tan \beta'$ are free parameters. Here only the first components are considered since the input matrices of the respective parameters are set to be diagonal and only the lightest sneutrinos and neutrinos are of interest. It suffices to only consider the first components. The mass difference is then fixed with eq. (8.0.4), for certain β' and $Y_x(1, 1)$ values, solving this equation gives the respective A_x value. This value is then set into the condition $m_{\tilde{\nu}^S} = m_h/2$ which solves out $m_{\nu^c}^2$. The μ' is fixed at 500 GeV, the $B\mu'$ is adjusted with respect to β' using eq. (4.3.7). Intuitively one would expect adjusting $\tan \beta'$, $Y_x(1, 1)$ and the mass ratio r will effect the decay width and further effects the relic density. These three parameters are therefore taken as variables to show the relic density dependence. The values of the related parameters are listed in table 8.1.

It should be mentioned here that all the calculations are done at tree-level. In MSSM the normal Higgs boson will receive large loop corrections (Higgs mass is around 90 GeV at tree level). To reduce the loop correction effects, the Higgs mass matrix is corrected so that the lightest MSSM Higgs boson is always fixed at 125 GeV. This is done by the follows. First the upper 2×2 block m_{H_u, H_d}^2 is diagonalized with an unitary matrix R

$$Rm_{H_u, H_d}^2 R^T = D_{H, MSSM}. \quad (8.0.5)$$

The lightest mass eigenvalue is then replaced by 125 GeV

$$D_{H, MSSM} = \begin{pmatrix} m_1^2 & 0 \\ 0 & m_2^2 \end{pmatrix} \rightarrow D'_{H, MSSM} = \begin{pmatrix} (125 \text{ GeV})^2 & 0 \\ 0 & m_2^2 \end{pmatrix}. \quad (8.0.6)$$

Constants		Varied Parameters		
Parameter	Value	var. Para.	const. Value	var. Interval
μ'	500 GeV	$\tan \beta'$	$Y_x(1, 1) \in [-5, -2, 1]$	[0.9, 1.1, 0.004]
M'_Z	4.20 TeV		$r = 2$	
m_{A^0}	6.20 TeV	$Y_x(1, 1)$	$\tan \beta' \in [0.96, 0.985, 0.005]$	[10^{-9} , 10^{-2} , 50 points]
M_1	723.95 GeV		$r = 2$	
M_2	1.19 TeV	r	$\tan \beta' \in (0.96, 0.972, 0.98)$	[1, 3, 50 points]
M_3	3.10 TeV		$Y_x(1, 1) = 10^{-5}$	
$Y_{x,2&3}$	$1.91 \cdot 10^{-2}$	Induced Variables		
$Y_{\nu,1}$	10^{-8}	$B_{\mu'} = m_{A^0}^2 \frac{\sin 2\beta'}{2}$		
$\tan \beta$	20	mass difference $m_{\tilde{\nu}_1^S} - m_{\tilde{\nu}_1^P} = 0.5$ GeV		
g_{BL}	0.55	$A_x(1, 1), m_{\nu^c}^2, T_x(1, 1) = A_x(1, 1)Y_x(1, 1)$		

Table 8.1: The values of the parameters used in the second numerical calculation. The squared bracket means [min, max, step/points] where the round bracket means (min, max, used value points).

This matrix is then transformed back to the flavor basis by the matrix R and replaced the original MSSM Higgs block

$$m_{H_u, H_d}^2 \rightarrow R^T D'_{H, MSSM} R. \quad (8.0.7)$$

The modified Higgs mass matrix is then calculated normally in `SPheno` and therefore the mixing matrices also get modified.

The variables are first solved in the `Mathematica`. The modification of Higgs mass matrix is done within `SPheno`. A program is written to change the respective parameters in the `LesHouches` file and run the `SPheno` and `micrOMEGAS` and finally generates the plots showing the dependence of relic density on the variables. Moreover, the processes that contribute to $\frac{1}{\Omega h^2}$ are also recorded and plotted. The parameters are also tested with `HiggsBounds-4.3.1`, which compares model predictions with LHC, Tevatron and LEP analyses.

Varied $\tan \beta'$

The $\tan \beta'$ is varied from 0.9 to 1.1 while keeping the mass ratio $r = 2$. Plots are generated with respect to different $Y_x(1, 1)$ which takes values from 10^{-5} to 10^{-2} and are changed one magnitude at a time. As will be seen in the next section, $Y_x(1, 1)$ does not influence the final results, thus it suffices to show only one plot here with $Y_x(1, 1) = 10^{-5}$, as illustrated in fig. 8.1.

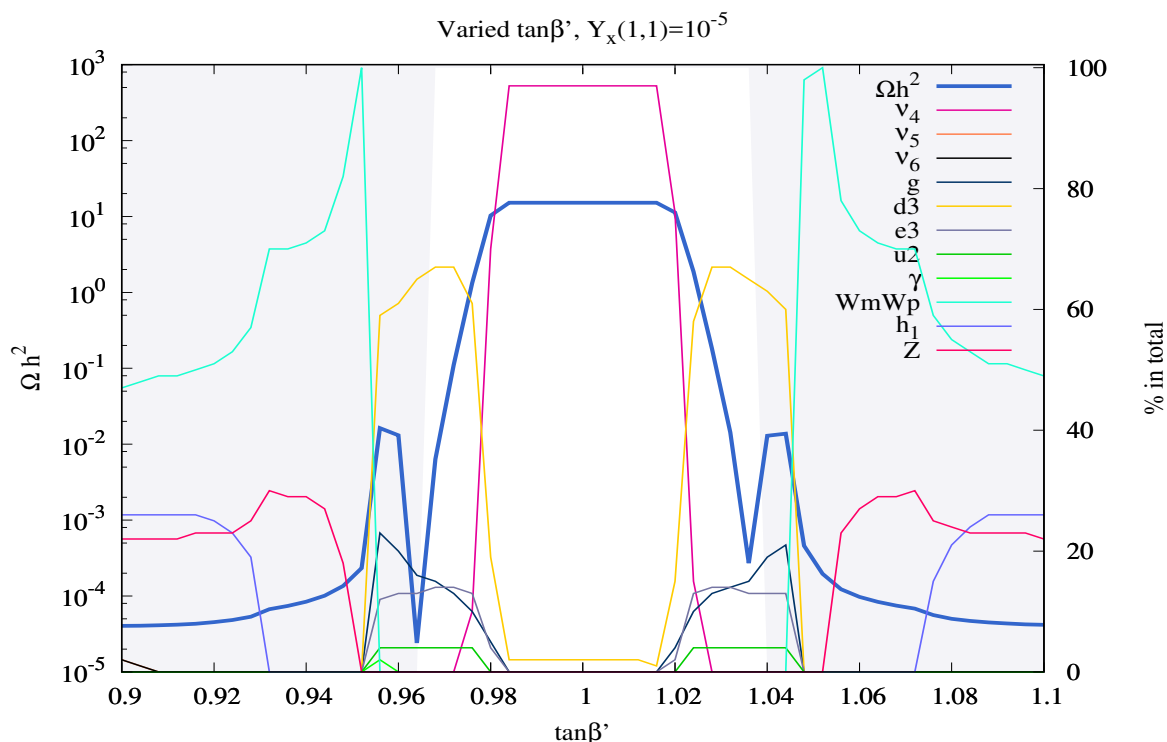


Figure 8.1: The relic density of the sneutrino dark matter and the respective contributions of decay final states. $\tan \beta'$ is varied from 0.9 to 1.1 with 0.004 as step, mass ratio $r = 2$ and $Y_x(1,1) = 10^{-5}$. The shaded area is excluded by `HiggsBounds` while the white area is allowed. The plateau around $\tan \beta = 1$ is caused by the break down of Higgs funnel. This plot shows that there is a region in the parameter space where the relic density agrees with the astronomical observations and in the meanwhile is allowed by `HiggsBounds`.

In fig. 8.1, the relic density is shown with the thick blue curve, which is symmetric with respect to $\tan \beta'$. Therefore in the following, if not mentioned, only the left half is discussed. The plateau around $\tan \beta' = 1$ should not be considered as data points, because around $\tan \beta' = 1$ the Higgs and sneutrino masses are close to 0, the lightest sneutrinos become tachyonic. For the rest points, one might notice at first glance that two dips are present at around $\tan \beta' = 0.96$ and 1.04. This is caused by the level-crossing of the lightest Higgs bosons. To show it more in detail, the lightest two Higgs masses and related mixing matrix contributions are plotted in fig. 8.2. As can be seen from the plot, the two dips lie exactly at the position where the level-crossing happens. The Higgs boson of interest is mainly bilepton-like with about 1% mixing from the MSSM-like Higgs. At smaller $\tan \beta'$ the Higgs of interest has larger mass (about 2 times of the normal Higgs mass),

the decay into ν_4 is suppressed by the small Yukawa, which results in quark and boson final states. In principle the averaged cross-section is inverse proportional to the relic density. The annihilation into different particles results in the suppressed relic density. As the Higgs mass decreases, the annihilation into heavy particles is not possible any more. The relic density therefore increases with decreasing Higgs mass. At the level-crossing point, the Higgs of interest is a maximally mixture of normal Higgs and bilepton. This causes the reduce of relic density. After the level-crossing point, annihilation into quarks and especially ν_4 s start to dominate.

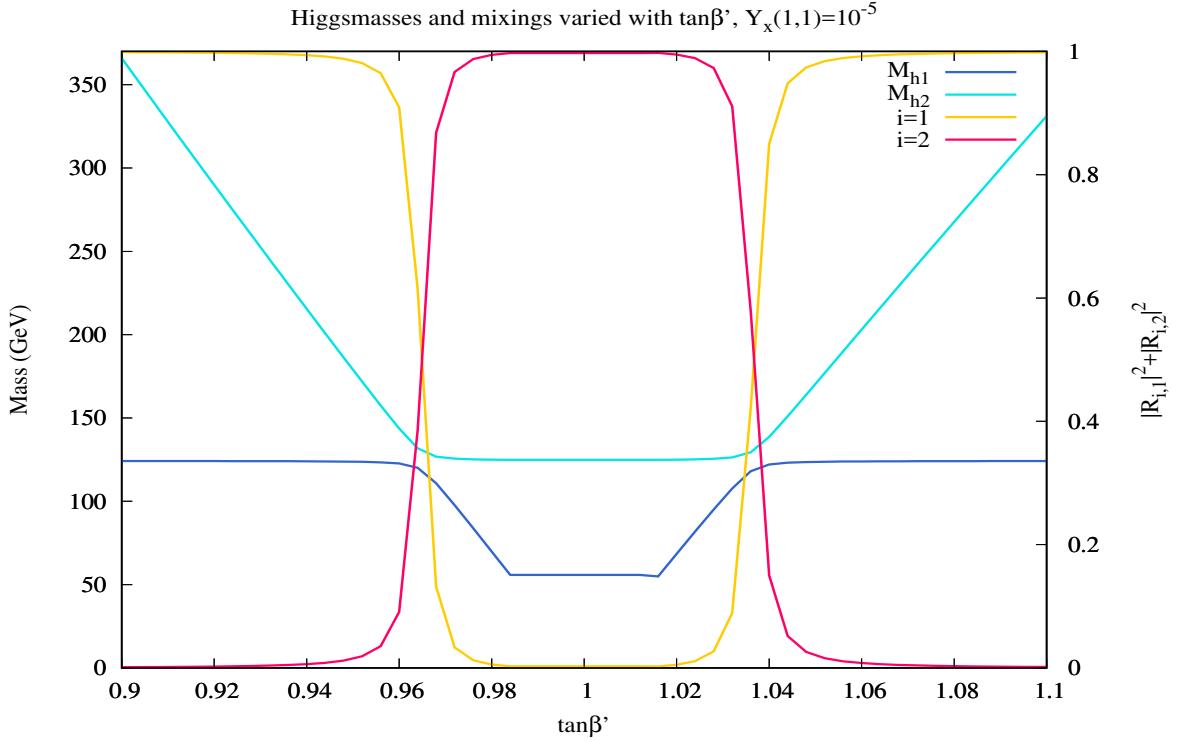


Figure 8.2: The masses of the lightest two Higgs bosons and their mixing matrix contributions. The mixing matrix R is defined as $H_{mass} = RH_{flavor}$. The level-crossing happens at the position $\tan\beta'$ about 0.96 and 1.04 which explains the dips shown in fig. 8.1.

The ν_4 dominance also explains the increase of the relic density after the level-crossing. Since the total cross-section is now only determined by $\tilde{\nu}_{R/I,1}\tilde{\nu}_{R/I,1} \rightarrow \nu_4\nu_4$, it is suppressed by the small Yukawa. Therefore the ν_4 dominance will increase the relic density. The upshot is, between the overproduced region and the level-crossing point, there exist two regions that can provide lower relic density (lower or around 0.1) and are allowed by collider experiments.

Varied $Y_x(1, 1)$

To see whether $Y_x(1, 1)$ effects the relic density, the $\tan \beta'$ is fixed at points varying from 0.96 to 0.985 with 0.005 as step, r is fixed at 2, while letting $Y_x(1, 1)$ vary from 10^{-9} to 10^{-2} at each point. This corresponds to ν_4 mass spans from 8 keV to 75 GeV. The plots are shown in fig. 8.3. As shown in the figure, the relic density shows no dependence on singlet Yukawa coupling $Y_x(1, 1)$ unless it exceeds 10^{-3} . If only consider the keV range sterile neutrino which corresponds to $Y_x(1, 1) = 10^{-9} - 10^{-8}$, then changing the Yukawa coupling does not effect the relic density. One thing to notice is that the annihilation processes into neutrinos are highly suppressed at lower Yukawa values, this might open a window to the scenario where sneutrinos have relic density that fits the observation with the lightest sterile neutrino a good DM candidate.

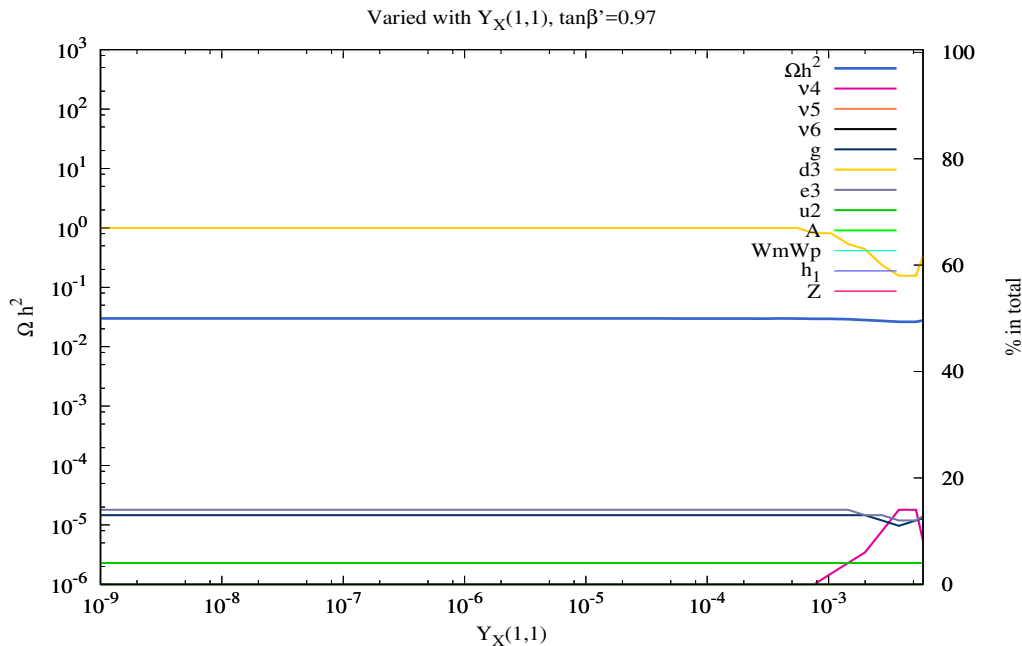
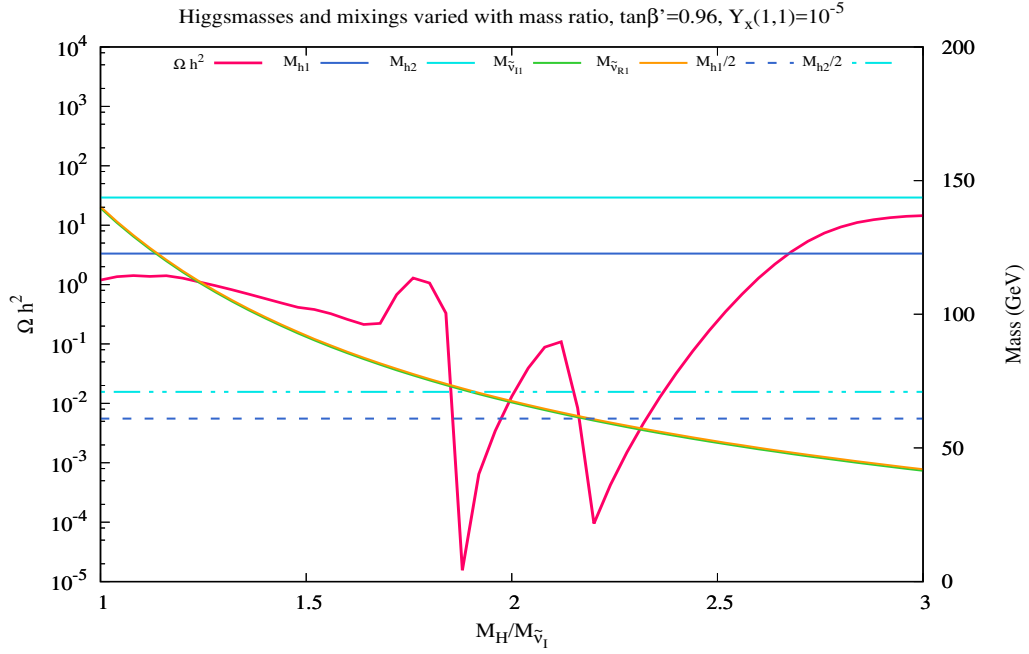
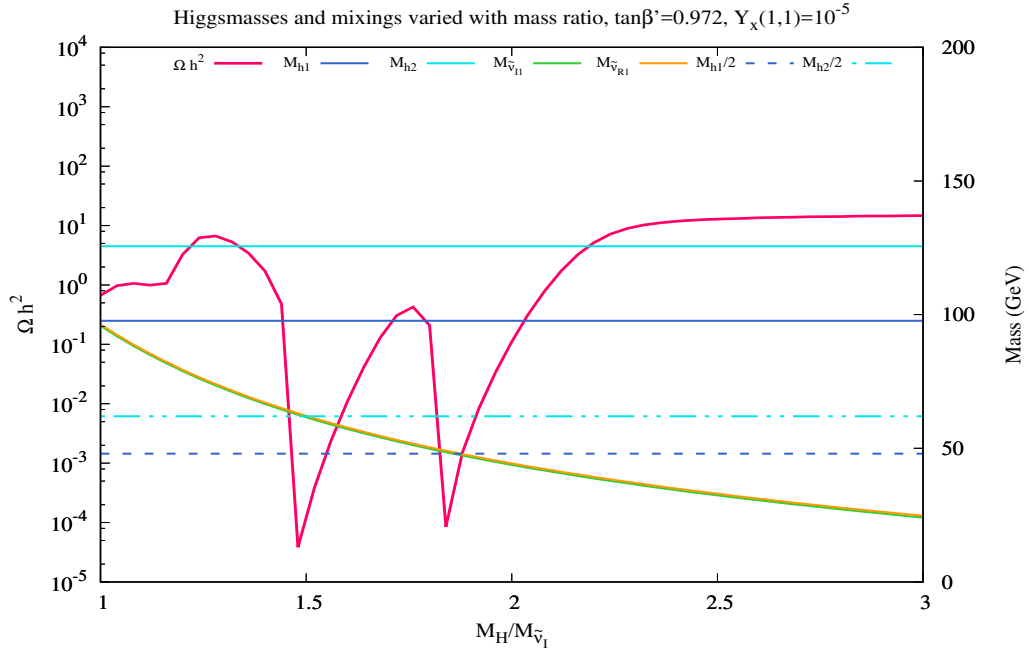


Figure 8.3: The relic density varied with $Y_x(1, 1)$ while $\tan \beta' = 0.97$ and $r = 2$. The plot show no dependency of relic density on $Y_x(1, 1)$ unless $Y_x(1, 1)$ is larger than 10^{-3} . For the keV range sterile neutrinos (corresponds to $Y_x(1, 1) = 10^{-9} - 10^{-8}$), changing Yukawa coupling of the singlets does not influence the relic density.

Varied Mass Ratio



(a) $\tan\beta' = 0.96$



(b) $\tan\beta' = 0.972$

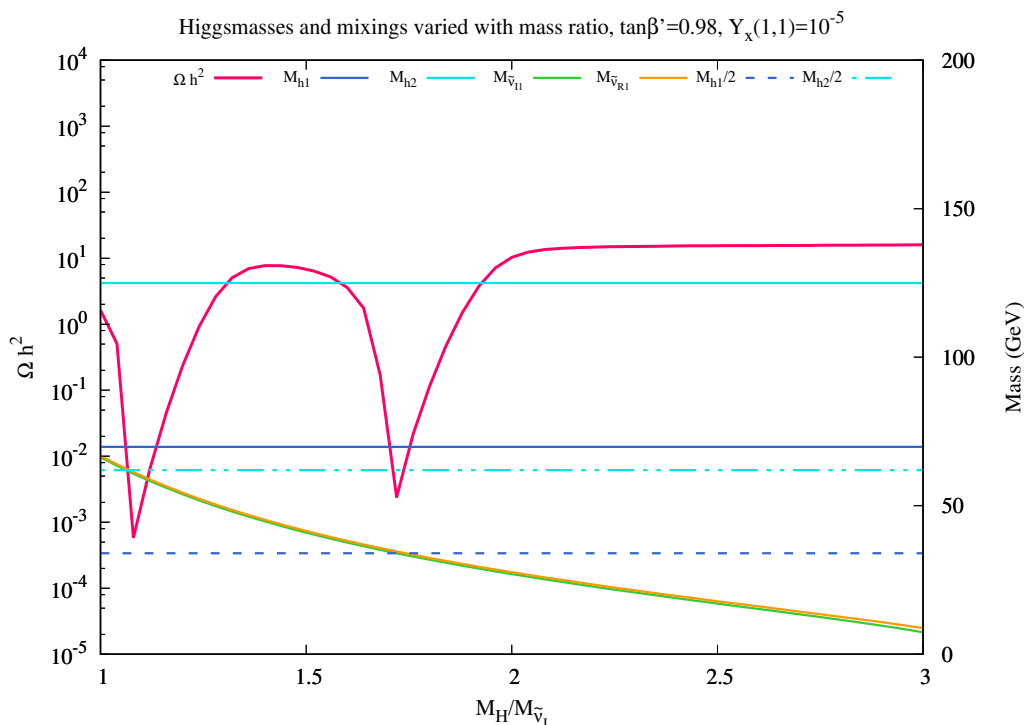

 (c) $\tan \beta' = 0.98$

Figure 8.4: The relic density plotted with respect to mass ratio varies from 1 to 3. Three $\tan \beta'$ values are used in the plots while $Y_x(1,1)$ is fixed at 10^{-5} . All the three plots show two dips instead of one. This is caused by the other lightest Higgs boson which is mainly MSSM-like. Also the dip of the Higgs funnel does not show up at exactly $M_h/M_{\tilde{\nu}}$ = 2 as set manually in *Mathematica*. As $\tan \beta'$ decreases the deviation gets larger. It is because the Higgs and sneutrino masses decreases with the increasing $\tan \beta'$ and the off-diagonal contribution of the sneutrino mass sets in. But compare with the dashed lines which marks half of the Higgs masses, the funnels happen exactly at the point where $m_{\tilde{\nu}} = m_h/2$.

To show the existence of Higgs funnel, the relic density is plotted with respect to the mass ratio which vary from 1 to 3. In the meanwhile the $\tan \beta'$ is set at 0.96, 0.972 and 0.98 and $Y_x(1,1) = 10^{-5}$. The plots are shown in fig. 8.4. The red line marks the relic density, the blue lines and dashed blue lines show the masses and half of the masses of the lightest two Higgs bosons. The yellow and green lines show the masses of the lightest two sneutrinos. Since the masses are set to be degenerate, these two lines overlap with each other.

At first sight one may notice that two dips instead of one show up in all the three plots. As shown by the intersection of the dashed lines and the relic density curve, one of the dips is caused by the MSSM-like Higgs funnel. Also the Higgs funnel of interest does not seem to happen exactly at $M_H/M_{\tilde{\nu}_I} = 2$ as expected, and the deviation varies with the increasing $\tan \beta'$. It is because the x-axis is set manually as an initial condition in the `Mathematica`. When $\tan \beta'$ is smaller, M_H is larger and the neutrino mass does not receive large corrections from the off-diagonal terms of the mass matrices. As $\tan \beta'$ increases the sneutrino mass decreases, the off-diagonal effects start to set in. Therefore the position where Higgs funnels appear is marked by the intersection of the sneutrino mass and $M_H/2$ curves.

9 Conclusion and Outlook

The neutrino and sneutrino sectors of supersymmetric minimal inverse-seesaw model and BLSSM are discussed in this work. The decay width of the lightest right-handed neutrino is calculated both analytically and numerically. In the numerical calculations approximations of loop integrals are implemented. In the minimal inverse-seesaw model, the decay widths and mixing angle of the lightest right-handed neutrino is calculated numerically. The results are compared with the data of *NuSTAR* collaboration, it shows that if one assumes the sterile neutrinos are produced by Shi-Fuller mechanism, then the model is excluded for keV range sterile neutrino DM. The numerical tests of the lightest right-handed sneutrino shows that, when assuming keV range sterile neutrino, the sneutrino is overproduced. The relic density can be bring down to the order 0.1 using large trilinear coupling, but this might induce violation of charge conservation. In general, the minimal inverse-seesaw model is excluded for lightest right-handed sneutrino DM with keV range sterile neutrino scenario.

The model BLSSM is then studied. A $U(1)_{B-L}$ gauge group is added to the MSSM gauge groups. This model includes twelve sneutrinos (imaginary and real, six for each) and two additional gauge singlet Higgs bosons. The lightest singlet Higgs boson is used to build up the Higgs-funnel. The sneutrinos are taken to be degenerated, the lightest state is the imaginary one with a mass difference of $m_{\tilde{\nu},re} - m_{\tilde{\nu},im} = 0.5$ GeV. The lightest right-handed sneutrinos annihilate through this Higgs-funnel and produce sterile neutrinos, which solves the overproduction problem in the first model. In the numerical calculations $\tan \beta'$ and $Y_\nu(1,1)$ are taken as variables. The results show that Yukawa coupling does not change the magnitude of relic density unless it exceeds 10^{-3} . The relic density depends largely on $\tan \beta'$ which modifies the mass of the Higgs-funnel and thus sneutrino masses. The numerical calculations show that there exist regions that are allowed by collider experiments where the relic density is reduced to below 0.1 and in the meanwhile sterile neutrinos are produced non-thermally.

In this thesis only the parameters that are related to the DM of interest are studied. Fine-tunings of other parameters are also possible to maintain the observed relic density. In the ongoing work it is already shown that increasing the left-right mixing in the sneutrino sector can significantly reduce the relic density to 10^{-4} ,

where the large trilinear coupling is avoided. In the BLSSM other parameter ranges might also be possible to have sneutrino and/or neutrino DM that fits the observed relic density. Beside neutrino and sneutrino, in BLSSM the lightest neutralino can also be a good DM candidate[19]. Other supersymmetric and inverse-seesaw (-like) models that have similar structure as BLSSM, also offer opportunities where other funnels are possible to consume the relic density and make sneutrino good DM candidate[15].

Bibliography

- [1] I.J.R. Aitchison. Supersymmetry and the mssm: An elementary introduction. [arxiv:hep-ph/0505105v1](https://arxiv.org/abs/hep-ph/0505105v1), 2005.
- [2] A. Aste. A direct road to majorana fields. *Symmetry*, 2(4):1776–1809, 2010.
- [3] H. Baer and X. Tata. *Weak Scale Supersymmetry: From Superfields to Scattering Events*. Cambridge University Press, 2006.
- [4] D. Bailin and A. Love. *Supersymmetric Gauge Field Theory and String Theory*. Institute of Physics Publishing, Bristol and Philadelphia, 1994.
- [5] L. Basso, B. O’Leary, and W. Porod. Dark matter scenarios in the minimal susy b - l model. *Journal of High Energy Physics*, 2012:54, 2012.
- [6] G. Bélanger, F. Boudjema, and A. Pukhov. Micromegas a package for calculation of dark matter properties in generic model of particle interaction. <https://laph.cnrs.fr/micromegas/>, 2012.
- [7] L. Berström and A. Goobar. *Cosmology and Particle Astrophysics, Second Edition*. Springer, 2004.
- [8] G. Bertone and J. Silk. *Particle Dark Matter: Observations, Models and Searches*. Cambridge University Press, 2010.
- [9] N. Cerna-Velazco, T. Faber, J. Jones-Pérez, and W. Porod. Constraining sleptons at the lhc in a supersymmetric low-scale seesaw scenario. *Eur. Phys. J. C*, 77:661, 2017.
- [10] S. Dodelson and L.M. Widrow. Sterile neutrinos as dark matter. *Phys. Rev. Lett.*, 72:17, 1994.
- [11] M. Drees, R.M. Godbole, and P. Roy. *Theory and Phenomenology of Sparticles: An account of four-dimensional N=1 supersymmetry in High Energy Physics*. World Scientific, 2004.
- [12] B. O’Leary et al. Mass spectrum of the minimal SUSY B - L model. *Journal of High Energy Physics*, 2012:42, 2012.

- [13] D.J.H. Chung et al. The soft supersymmetry breaking lagrangian: Theory and applications. *Phys. Rept.*, 407:1–203, 2005.
- [14] F. Simpson et al. Strong bayesian evidence for the normal neutrino hierarchy. *Journal of Cosmology and Astroparticle Physics*, 2017(06):029, 2017.
- [15] J. Chang et al. Sneutrino dark matter via pseudoscalar x-funnel meets inverse seesaw. [arxiv:1806.04468v1](#), 2018.
- [16] J. Lesgourgues et al. *Neutrino Cosmology*. Cambridge University Press, 2013.
- [17] K. Perez et al. (almost) closing the ν msm sterile neutrino dark matter window with *NuSTAR*. *Phys. Rev. D.*, 95:123002, 2017.
- [18] L. Canetti et al. Dark matter, baryogenesis and neutrino oscillations from right-handed neutrinos. *Phys. Rev. D*, 87:093006, 2013.
- [19] L.D. Rose et al. Prospects for sneutrino dark matter in the blssm. [arxiv:1804.09470v1](#), 2018.
- [20] R. Adhikari et al. A White Paper on keV sterile neutrino Dark Matter. *Journal of Cosmology and Astroparticle Physics*, 2017(01):025, 2017.
- [21] M. Tababashi et al (Particle Data Group). Neutrino mixing. *Phys. Rev. D*, 98:030001, 2018.
- [22] K. Garrett and G. Dūda. Dark matter: A primer. *Advances in Astronomy*, 2011, 2011.
- [23] H.E. Haber and D. Wyler. Radiative neutralino decay. *Nuclear Physics*, B323:267–310, 1989.
- [24] H.E.Haber and G.L. Kane. The search for supersymmetry: Probing physics beyond the standard model. *Physics Reports*, 117:75–236, 1985.
- [25] S.F. King. Neutrino mass models. [arxiv:1006.1718v2](#), 2003.
- [26] S. Law and K.L. McDonald. Generalized inverse seesaws. *Phys. Rev. D.*, 87:113003, 2013.
- [27] F. Mandl and G. Shaw. *Quantum Field Theory: Revised Edition*. John Wiley & Sons, 1995.
- [28] S.P. Martin. A supersymmetry primer. [arxiv:hep-ph/9709356v7](#), 2016.

- [29] R.N. Mohapatra. Mechanism for understanding small neutrino mass in superstring theories. *Phys. Rev. Lett.*, 56:561, 1986.
- [30] R.N. Mohapatra and P. Pal. *Massive Neutrinos in Physics and Astrophysics*. World Scientific, 1991.
- [31] P.B. Pal. Dirac, Majorana and Weyl fermions. *American Journal of Physics*, 79:485–498, 2011.
- [32] V. Rubin and W.K. Ford. Rotation of the andromeda nebula from a spectroscopic survey of emission regions. *The Astrophysical Journal*, 159:379, 1970.
- [33] X. Shi and G.M. Fuller. New dark matter candidate: Nonthermal sterile neutrinos. *Phys. Rev. Lett.*, 82:2832, 1999.
- [34] P. Stockinger. *Effects of Neutrino Oscillations and Neutrino Magnetic Moments on Elastic Electron-Neutrino Scattering*. Dissertation zur Erlangung des akademischen Grades des Doktors der Naturwissenschaften an der Formel-und Naturwissenschaftlichen Fakultät der Universität Wien, 1997.
- [35] F. Zwicky. Die rotverschiebung von extragalaktischen nebeln. *Helvetica Physica Acta*, 6:110–127, 1933.

Declaration

I declare that this thesis has been composed solely by myself, no other literatures/materials except the ones listed in this thesis are used. This thesis is until now neither handed in nor will be used to apply for any other degrees.

.....

Würzburg, 1. September 2018.

Acknowledgement

I want to thank Prof. Dr. Werner Porod who took great effort teaching and helping me to finish this thesis. I also want to thank Thomas Faber, who kindly corrected my terrible Zusammenfassung written in German.